EXPERIMENTAL INVESTIGATION OF DYNAMIC INTERLAMINAR CRACK PROPAGATION IN DCB SPECIMEN

by

AJAY KUMAR RAY
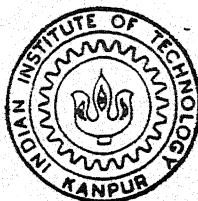
DEPARTMENT OF MECHANICAL ENGINEERING

INDIAN INSTITUTE OF TECHNOLOGY KANPUR

JUNE, 1994

EXPERIMENTAL INVESTIGATION OF DYNAMIC INTERLAMINAR CRACK PROPAGATION IN DCB SPECIMEN

A Thesis Submitted
in Partial Fulfilment of the Requirements
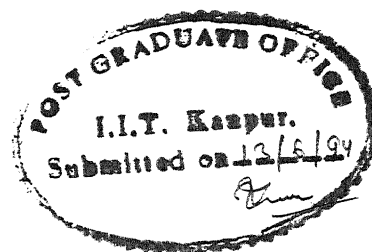for the Degree of

MASTER OF TECHNOLOGY

by

AJAY KUMAR RAY

to the

DEPARTMENT OF MECHANICAL ENGINEERING

INDIAN INSTITUTE OF TECHNOLOGY

JUNE, 1994

CERTIFICATE

It is certified that the work contained in the thesis entitled 'EXPERIMENTAL INVESTIGATION OF DYNAMIC INTERLAMINAR CRACK PROPAGATION IN DCB SPECIMEN', by `AJAY KUMAR RAY' has been carried out under our supervision and that this work has not been submitted elsewhere for a degree.

P Kumar
13-6-94

Dr. Prashant Kumar

Professor

Department of Mechanical Engg.

Indian Institute of technology

Kanpur — 208 016

Dr N. N. Kishore

Professor

Department of Mechanical Engg.

Indian Institute of technology

Kanpur — 208 016

June, 1994.

ACKNOWLEDGEMENTS

CONTENTS

LIST OF FIGURES

LIST OF TABLES

NOMENCLATURE

M	Mass matrix
K	Stiffness matrix
R	External load matrix
u	Displacement vector of finite element assemblage
$\ddot{u}$	Acceleration vector of finite element assemblage
a	Crack length
P	Load
K_d	Dynamic stress intensity factor
σ_1	Incident stress
σ_3	Reflected stress
σ_2	Stress imparted to the DCB specimen
ρ	Mass density
c	Longitudinal stress wave velocity
v	Partical velocity
E	Energy / DC Voltage
e	Output voltage from the bridge
V_c	Calibration voltage
ε	strain

ABSTRACT

An experimental-cum-numerical technique has been developed to determine dynamic interlaminar fracture toughness for slender laminates. The experiments provide crack initiation time, crack velocity and the corresponding dynamic load pulse applied to one of the cantilevers of a slender DCB specimen. To obtain the dynamic interlaminar fracture toughness parameter these experimental data are later used in the numerical program developed by Kishore, kumar and Verma [16].

A load bar technique has been developed to apply dynamic load pulse to the cantilever of the DCB specimen and propagation gauges monitor the crack velocity. The load pulse applied to the specimen has a duration of 40 to 60 μs and and a peak value of 6 to 30 kN. The crack velocity achieved is very high. It ranges from 100 to 600 m/s. The crack initiation time has been obtained by extrapolating the experimental data of propagation gauges towards the crack tip. The crack initiation time for different experiment range from 80 μs to 150 μs. This is much larger value as compared to that predicted by finite element analysis (within 30 μs).

The explanation for late initiation of crack requires further theoretical and experimental studies. A possible reason for late initiation of crack might be that the crack propagation is not directly initiated by the applied direct load pulse but by the pulses reflected from the ends of the DCB cantilever. Other possible reason might be a time lag in the shearing of propagation gauges.

1 INTRODUCTION

1.1 BACKGROUND

Laminates fabricated by bonding slender sheets together are known to be susceptible to interlaminar crack propagation. In fact the critical energy release rate of interlaminar crack in laminates of fiber reinforced plastics (FRP) is found to be considerably less than that for a through the thickness crack for the same laminates. For example, in a typical angle ply laminate of carbon-epoxy the critical energy release rate is of the order of several hundred J/m^2 [1], while for a through the thickness crack for similar laminate the critical energy rate is of the order of several thousand J/m^2 [2]. It is therefore important to characterize the toughness of interlaminar crack growth.

A laminate shows considerable delamination damage when it is impacted by a stone, projectile or dropped hammers. Under dynamic loading the interlaminar cracks can propagate at high velocities exceeding 300 m/s. Because of this reason the dynamic fracture is of special interest in the case of composite materials and laminates of slender sheets. In the case of dynamic fracture role of material inertia becomes significant. The inertia effect may arise due to two reasons (i) rapidly applied loading on a cracked solid and (ii) rapid crack propagation. In the first case the influence of load is transferred to the crack by stress wave through the material. In the second case the material particle on opposite crack faces displace with respect to each other once the crack has advanced. The inertia effect, in the first case, is considered significant when the time taken to load the specimen to maximum value is small compared to time required for the stress wave to travel at a characteristic wave speed of the material over a characteristic dimension of the body. In the second case the inertia effect should be accounted for whenever the crack velocity is a significant

fraction of the characteristic velocity (e.g. Rayleigh wave velocity).

Dynamic fracture phenomena has several important features. The mathematical models are more complex than static models. The boundaries of body change with time. From experimental point of view, many transient parameters have to be measured accurately within a very short period.

1.2 LITERATURE SURVEY

In the current study a double cantilever beam (DCB) specimen of slender strips is used. In the specimen the free lateral surfaces are very close to the crack tip (<3mm) and therefore the reflection of stress waves become prominent. There is no literature available for the dynamic interlaminar crack propagation in laminates made of thin sheets of similar material, to the best of author's knowledge. The survey of literature is presented on related fields.

Considerable work has been done to study the dynamic fracture phenomena. Transparent polymeric material drew maximum attention whose dynamic behavior can be studied using shadow spot (caustic) technique. Ravi Chander and Knauss [3-7] have done a detailed study of crack tip stress, initiation, propagation, branching and stress wave interaction on Homalite 100 using shadow spot technique.

Rosakis, Duffy and Freund [8] performed dynamic crack propagation experiments using wedge loaded double cantilever beam specimens of an austenitized, quenched and tempered 4340 steel. They measured the dynamic stress intensity factor by means of optical method of caustics. The experimental data was obtained from the shadow spot patterns photographed with a Cranz-Schardin high speed camera. The interpretation of the data was based on an elastodynamic analysis. They obtained the instantaneous value of the dynamic stress intensity factor K_{Id} as a function of crack tip velocity. It is

observed that the fracture toughness increases with increase in crack velocity. The specimen used by them was large in size and therefore the technique cannot be used for DCB specimen with thin cantilevers.

Stress Intensity Factor of a crack in a large orthotropic composite material was measured using strain gauges by Shukla, Agarwal and Bharat Bhushan [9]. They developed theoretical equations for the strain field in the vicinity of the crack tip in an orthotropic material. These equations were then critically evaluated to obtain the optimum location and orientation of the strain gauges to be used for strain measurements. They then verified the applicability of the procedure using a glass epoxy specimen. This work deals with large plate under quasi-static loading conditions.

Ravichandran and Clifton [10] developed a new plate impact experiments to study the fracture process under sub-micro second loading. A 4340 VAR steel disc containing mid plane edge crack is impacted by a thin flyer plate of same material. The motion of the rear surface is monitored using a laser interferometer system. The experiments were conducted at different temperatures.

Strain gauges were used by Berger and Dally to measure the dynamic fracture toughness of steel [11]. They recorded a sequence of strain time traces during the passage of crack beneath a line of strain gauges. The data analysis uses the spatial distribution of strains along the gauge line at a specified time. They developed an overdetermined system of equations which are solved to determine K_{ID} as a function of time and position during crack propagation. In this study also, only large plates are dealt with.

Nishioka et. al. [12] studied the specimen size effects on dynamic crack propagation and arrest in DCB specimens using laser caustic method. They worked on polymethyl methacrylate (PMMA) made specimens in mode I. Dynamic condition was obtained using the conventional technique of storing energy through a blunt crack.

They worked with maximum crack velocities of the order of 200 m/s. The specimen length was changed in order to study the specimen size effects on dynamic crack propagation and arrest. They found that dynamic stress intensity factor decreases as the crack moves forward. They also observed that K_{ID} increases with crack velocity. However the studies were conducted on large specimens.

Kolednik in his theoretical study [13] gave a physical interpretation of the J-R curves for elastic-plastic fracture. He derived the difference between the crack-initiation toughness and crack-growth toughness using energy balance under quasi-static conditions. He considered three point bend specimens each of which consists of two parts glued together along the ligament. Here also large specimens were analyzed.

Potty [14] investigated SIF in a DCB specimen with thin cantilevers through a combined scheme of experimentally measureing the strain near the crack tip and analyzing this data by using FEM. In the finite element program he developed a relationship between stress intensity factor and strain near the crack tip. The strain measured near the crack tip with the help of a very small strain gauge (gauge length 0.2 mm) is used in the FEM program to obtain the SIF of the DCB specimen. Lovi [15] improved upon Potty's method by using two strain gauges one on each cantilever to neutralize the possibility of the recording of bending strains in the cantilevers which might develop during specimen preparation.

1.3 PRESENT WORK

A technique has been developed to determine the dynamic interlaminar fracture toughness for slender laminates. This technique employs a combined experimental and numerical work. For numerical work a finite element code has been developed by Kishore, Kumar and Verma [16].

The aim of the present work has been to experimentally determine the

crack initiation time, crack velocity and the corresponding dynamic load pulse applied to a slender double cantilever beam (DCB) specimen for interlaminar crack propagation. These experimental data can be used as input by the finite element code to obtain the dynamic interlaminar fracture toughness parameter for slender laminates.

The outline of finite element code is given in chapter II. Chapter III deals with the experimental technique and results are discussed in chapter IV.

2. NUMERICAL MODELLING OF CRACK PROPAGATION

2.1 INTRODUCTION

As a part of combined experimental and numerical technique to determine the interlaminar dynamic fracture toughness of DCB specimen in mode I, the experimental data of load profile and crack velocity history are used in the finite element code simulating the dynamic fracture behavior of the DCB specimen. A brief outline of the finite element formulation as developed by Kishore, Kumar and Verma [16] is given here.

2.2 FINITE ELEMENT FORMULATION

The following finite element equations [17] represent dynamic equilibrium governing of a linear system.

$$M \ddot{u} + K u = R \qquad (1)$$

where M and K are the mass and stiffness matrices respectively and R is the external load vector; u, $\ddot{u}$ are displacement and acceleration vectors of finite element assemblage. A computer code has been developed for 2-D using finite element discretization in space analysis and Newmark integration method for time variable [18]. The problem of DCB specimen is regarded a case of plane strain.

A computer code was developed to generate mesh of four noded elements. Very fine mesh is generated around the crack tip and coarse mesh away from the crack tip as shown in Fig. 2.1. The mesh is drawn for the DCB specimen of Fig. 2.2.

2.3 FLOW CHART

The flow chart of the finite element code is as shown in Fig 2.3.
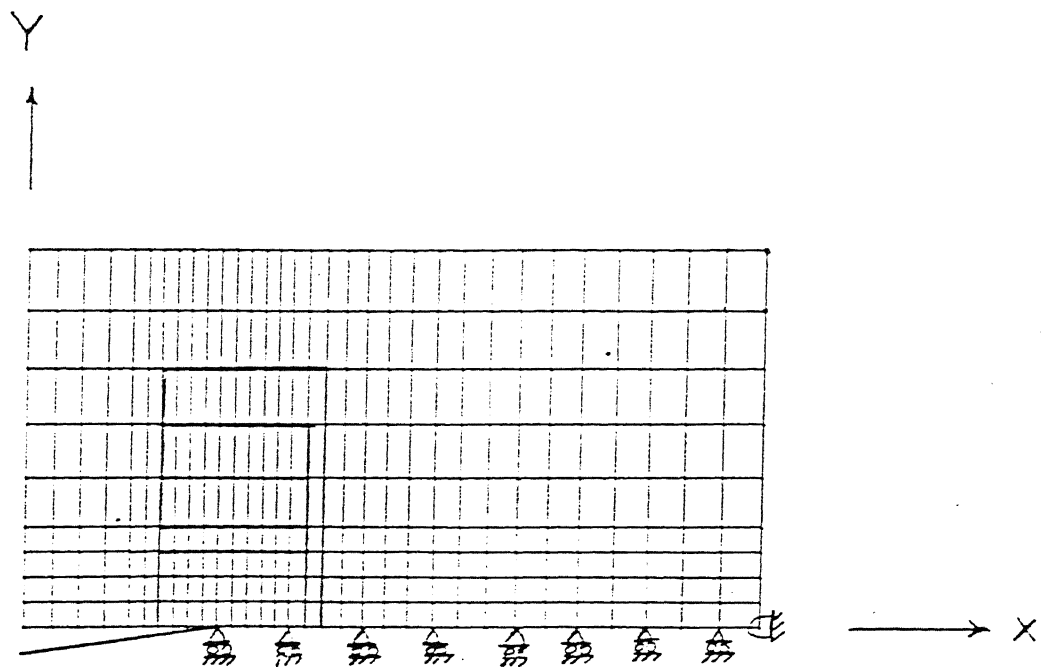
FIG. 2.1   MESH FOR DCB SPECIMEN

7

FIG. 2.2   DCB SPECIMEN

```
          ┌─────────────┐
          │    Input    │
          └─────────────┘
          ┌─────────────────────┐
          │      Assemble       │────────────────────┐
          └─────────────────────┘                    │
                                          ┌───────────────────────┐
                                          │      Elemental        │
                                          │      Stiffness        │
          ┌─────────────────────┐         │      Matrix.          │
          │       Apply         │         └───────────────────────┘
          │     Boundary        │     ┌─────────┐ ┌─────────┐ ┌─────────┐
          │    Conditions.      │     │  D mat  │ │  B mat  │ │ Mat Mul │
          └─────────────────────┘     └─────────┘ └─────────┘ └─────────┘
          ┌─────────────┐
          │    Solve     │
          └─────────────┘
          ┌─────────────────────┐
          │    Displacement     │
          └─────────────────────┘
   ┌─────────────────┐  ┌─────────────┐  ┌─────────────┐
   │  Derivatives    │  │   Strain    │  │   Sterss    │
   │   ∂v/∂x etc.    │  └─────────────┘  └─────────────┘
   └─────────────────┘
              ┌───────────────────────┐
              │    J — Integral       │
              └───────────────────────┘
```
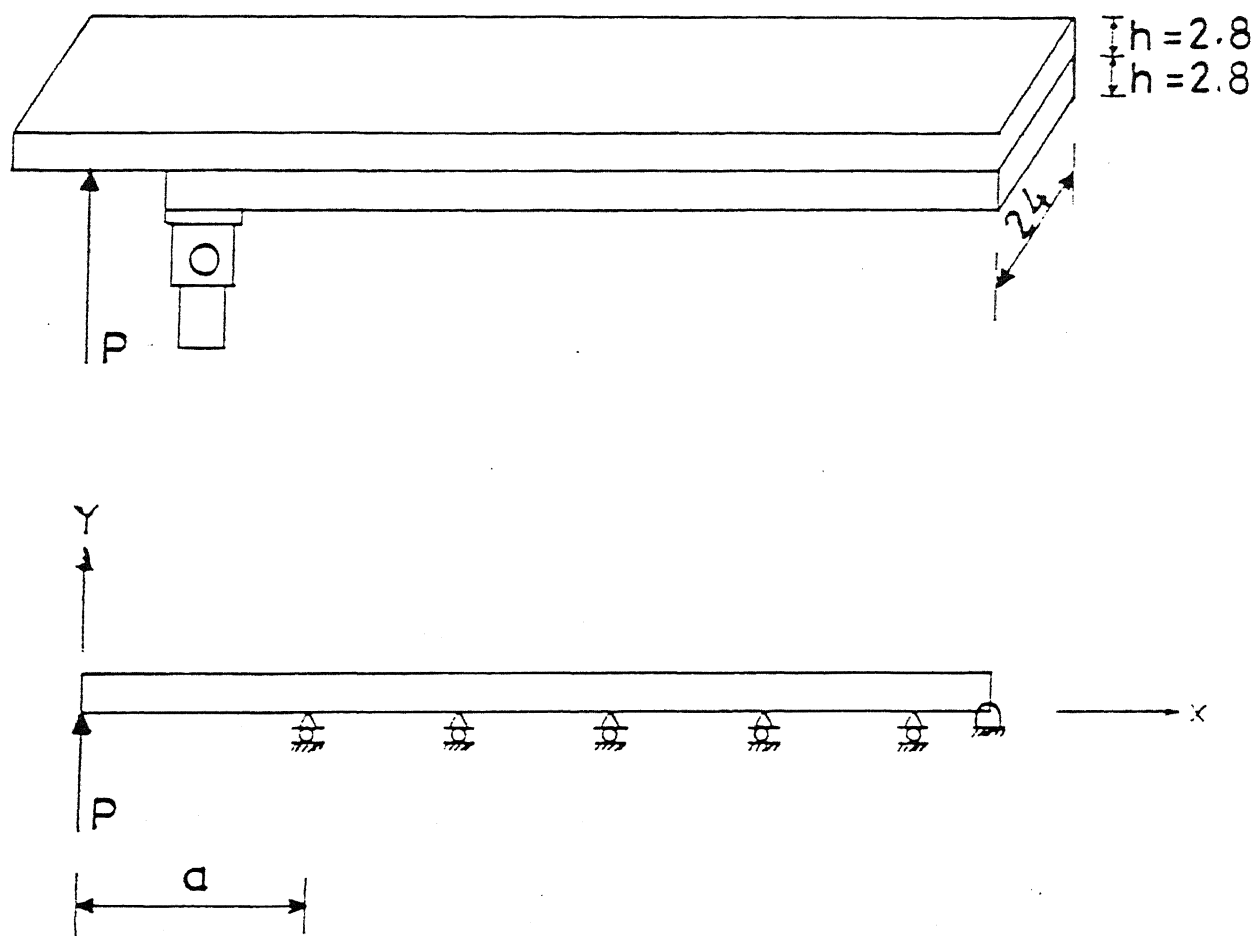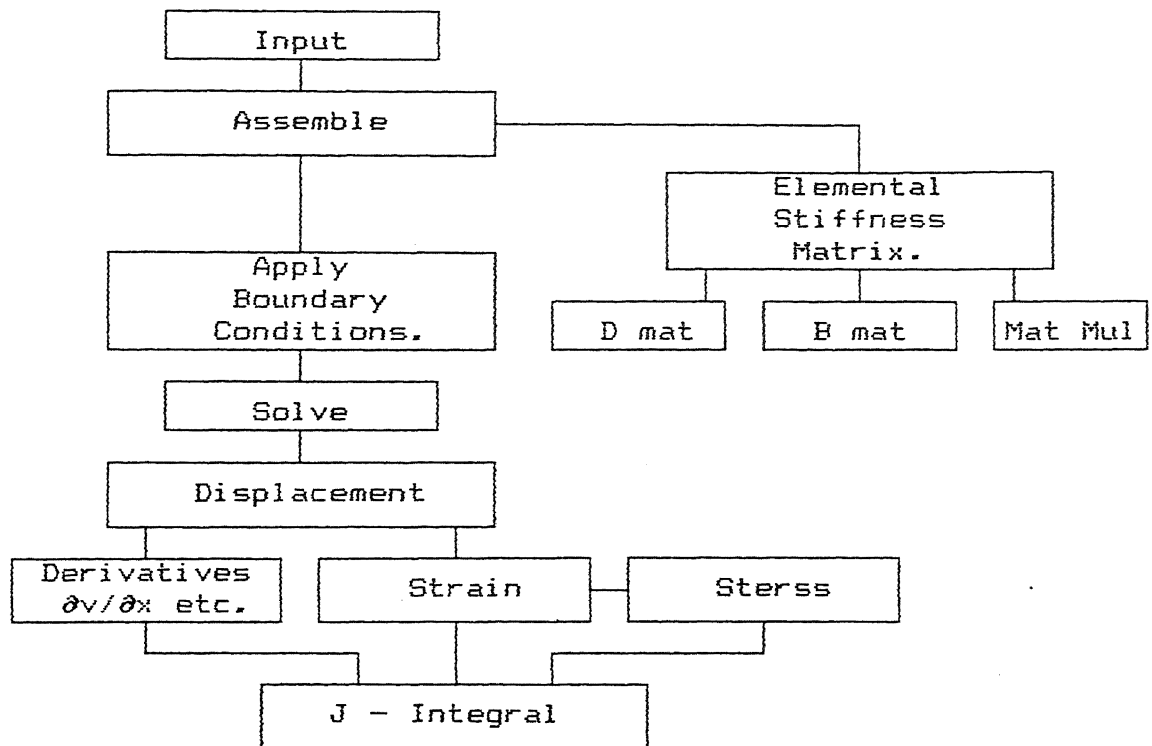
FIG. 2.3 FLOW CHART OF THE FINITE ELEMENT CODE.

Input required for the program are material properties, mesh size, time step, load pulse, crack propagation rate, time of crack initiation and force/displacement boundary condition.

2.4 CRACK PROPAGATION SIMULATION

To propagate the crack the gradual nodal release method was used. Suppose that the actual crack tip is located at C in between the nodes B and D as shown in the Fig. 2.4 ; b and d are the length of segment BC and BD respectively. The holding back force F at node B is gradually reduced to zero as the crack tip reaches the node D. The various scheme available to decrease the force to zero are as follows :

(i) Kobayashi and King [19] suggested the release rate based on constant stress intensity factor.

9

$$F/F_o = (1 - b/d)^{1/2} \qquad\qquad (2)$$

where F_o is the original reaction force when the crack tip was located at node B.

(ii) Rydhom et. al. [20] suggested the release rate based on constant energy release rate.

$$F/F_o = (1 - b/d)^{3/2} \qquad\qquad (3)$$

(iii) Kobayashi et. al. [21] suggested the linear release rate based on no physical argument other than pure intuition.

$$F/F_o = (1 - b/d) \qquad\qquad (4)$$

To have a more gradual and smooth opening of crack the authors tried an alternate method. The holding back force at the crack tip B is not decreased to zero until the crack has reached the end of the next element and the force is decreased linearly. When the crack tip opens at node B,

$$\frac{F_B}{F} = \left(1 - \frac{b}{d + d_1} \right) \qquad\qquad (5)$$

where F_{HB} is the reaction at the node B when it is opened. And when the crack moves beyond node D to a point D_1

$$\frac{F_B}{F_{HB}} = \left(1 - \frac{b_1}{d + d_1} \right) \qquad\qquad (6)$$

$$\frac{F_D}{F_{HD}} = \left(1 - \frac{b_2}{d_1 + d_2} \right) \qquad\qquad (7)$$

F_{HD} is the reaction at node D when it is opened ; b, b_1, b_2 are the crack extension and d, d_1, d_2 are the element lengths as shown in the Fig.2.4.

2.5 $\hat{J}$-INTEGRAL

Atluri [22] and Nishioka and Atluri [23] have undertaken the study of several path independent integrals in the analysis of crack

10

growth initiation and propagation of cracks in elastic or inelastic material under quasistatic and dynamic conditions. In the present work $\hat{J}_k$ given by Kishimoto, Aoki and Sakata [24] is used. $\hat{J}_k$ is defined as follows

$$\hat{J}_k = \lim_{\epsilon \to 0} \int_{\Gamma_\epsilon} [W n_k - T_i u_{i,k}] \, ds$$

$$= \lim_{\epsilon \to 0} \int_{\Gamma + \Gamma_c} [W n_k - t_i u_{i,k}] \, ds + \int_{V-V_\epsilon} \rho \, \ddot{u}_i u_{i,k} \, dV \qquad (8)$$

where J_1, J_2 represent two fracture modes, W and T are strain energy density and kinetic energy density respectively, n_j are direction cosines of unit outward normal, t_i are the surface traction and the definition of the paths Γ_ϵ, Γ, Γ_c and the volume V, V_ϵ are shown in Fig.2.5. $\hat{J}_1$ is more relevant for the DCB specimen and is given by,

$$\hat{J}_1 = \lim_{\epsilon \to 0} \int_{\Gamma + \Gamma_c} [W n_1 - t_i u_{i,1}] \cdot ds + \int_{V-V_\epsilon} \rho \, \ddot{u}_i u_{i,1} \cdot dV \qquad (9)$$

For the case of plane strain, neglecting a speed dependent correction very close to unity for the range of crack speeds of interest, the relation between the $\hat{J}$ and the dynamic SIF (K_d) is given by [25].

$$K_d = \left(\frac{E \hat{J}_1}{1-\nu^2} \right)^{1/2} \qquad (10)$$

The value of $\hat{J}_1$ is independent of the choice of Γ only under stringent ideal conditions (e.g.steady state crack growth). In many cases, though these conditions are obviously not met the path independence of $\hat{J}$-Integral can still be established within certain allowable error. The path is held stationary as the crack tip extends in a self similar manner.

11
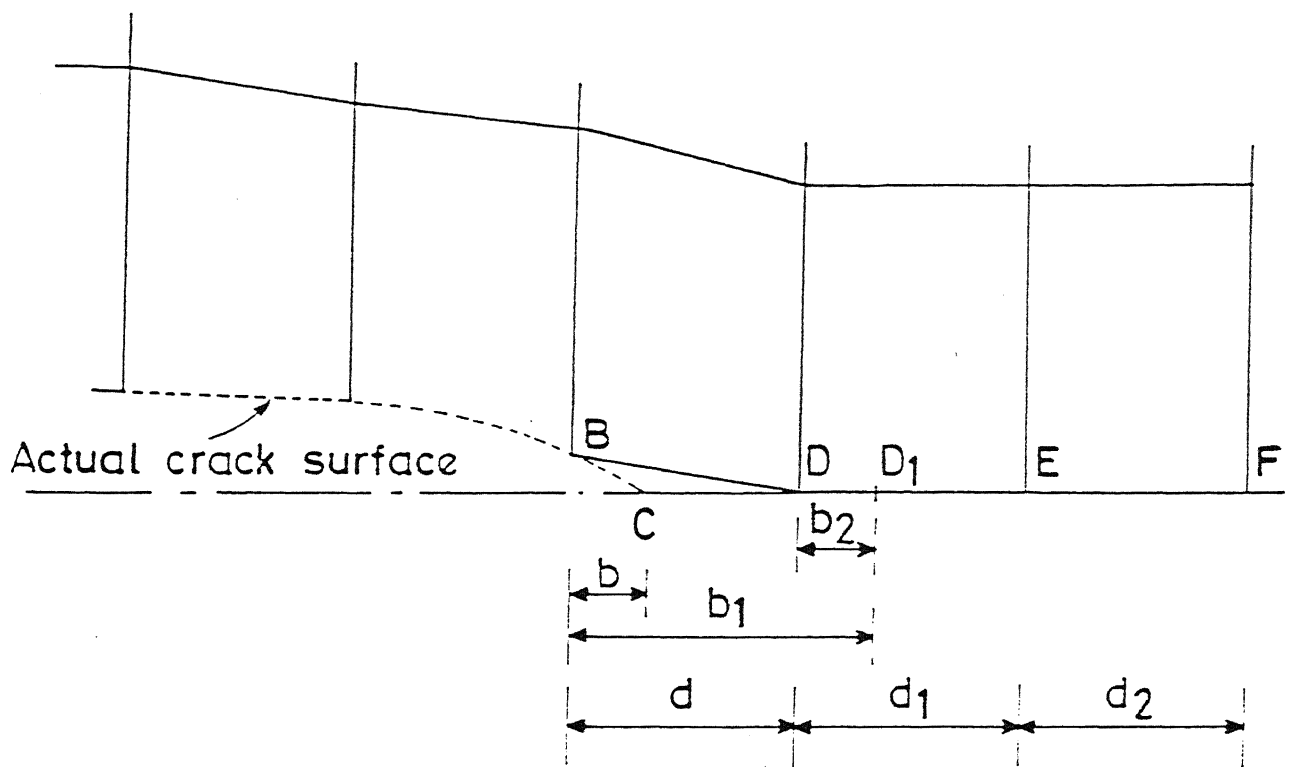
FIG. 2.4   CRACK OPENING SCHEME

$$\Gamma_C = \Gamma_C^+ + \Gamma_C^-$$

$$o\,(V - V_\epsilon) = \Gamma + \Gamma_C - \Gamma_\epsilon$$
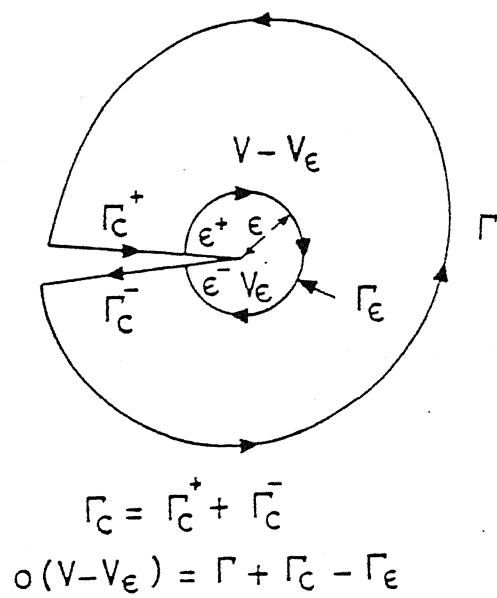
FIG. 2.5   CONTOUR FOR $\hat{J}_1$ INTEGRAL

12

3. EXPERIMENTAL TECHNIQUE

3.1 INTRODUCTION

Experiments are conducted to get the crack history of a double cantilever beam (DCB) specimen for a known load pulse. This chapter deals with experimental details of specimen preparation, experimental set up, experimental measurements and data processing.

In the technique a stress pulse is generated in a load bar which in turn applies dynamic load to a cantilever of the DCB specimen. Propagation gauges are bonded slightly ahead of the crack tip on the side face of the specimen to determine the crack velocity. The propagation gauges use a electronic circuit unit to give a voltage drop on the oscilloscope corresponding to the shearing of the gauges. A dual beam digital oscilloscopes monitors these voltage drops as well as the stress pulses in the load bar. These experimental records are analyzed to get the load pulse and energy imparted to the specimen and the crack velocity. Also, two experiments were conducted using strain gauges, instead of propagating gauges to monitor the stress pulse in the specimen.

3.2. SPECIMEN DETAIL

Two kinds of DCB specimen were used. The first kind of DCB specimen is made of thin strips of hardened alloy steel bonded together with epoxy and the second kind was made up of glass fiber reinforced plastic (GFRP). The geometry and material of both kinds of specimen have been discussed in detail in subsequent sections.

3.2.1. Steel DCB Specimen

Most of the experiments were done on steel DCB specimen. In this section the geometry of the specimen, specifications of material and

the binding technique of the cantilever of steel DCB specimen are discussed.

Geometry

Each cantilever of the DCB is 2.78 mm thick and 24mm wide. Their length is 170 mm each. The cantilevers are bonded together by epoxy with an offset of 20 mm (Fig.3.1) so that the rear cantilever can be impacted by the load bar. With the help of a tapped hole near the end of the front cantilever a hinge is mounted. A pre-crack is introduced by placing a thin sheet of bi-axially oriented poly-propylene (BOPP) between the cantilever strips during bonding process.

Material

The material of the cantilever of the DCB specimen is alloy steel 40Ni2Cr1Mo28[*] [EN 24], which is hardened to achieve a yield stress value higher than 1000 Mpa. Hardening was performed by keeping the metal strips at $830°$ to $850°$ C for one hour and then ahenching in oil. This was followed by annealing to relieve residual stresses, which was done by heating the strips at $310°$ C for a period of 20 minutes accompanied by furnace cooling. Average hardness of the strips on Rockwell C-scale is 33. Each strips was grounded that and polished with alumina powder.

Bonding

The faces of the metal strips to be bonded are etched to give better interfacial strength. The etching is done by dilute nitric acid. For bonding, epoxy LY 556 and hardener HY 1907IN in the ratio of 100:85 by weight are used. To this mixture, accelerator DY 062 is added at the rate of 1.5 ml per 100 gm of epoxy. The resin, the hardener and the accelerator are supplied by Ciba-Geigy Limited , Bombay. During bonding, the faces to be bonded are cleaned with AR grade acetone and all other faces are covered with a layer of wax to prevent them from getting coated with epoxy The mixture is then

14

REAR CANTILEVER

160

20

2.78
2.78

FRONT CANTILEVER

LOAD
APPLICATION
POINT

10

TAPPED HOLE
FOR SCRENG
TO THE HINGE

TOP VIEW

12   12

10   10

13

$\phi 4$

24

FRONT VIEW
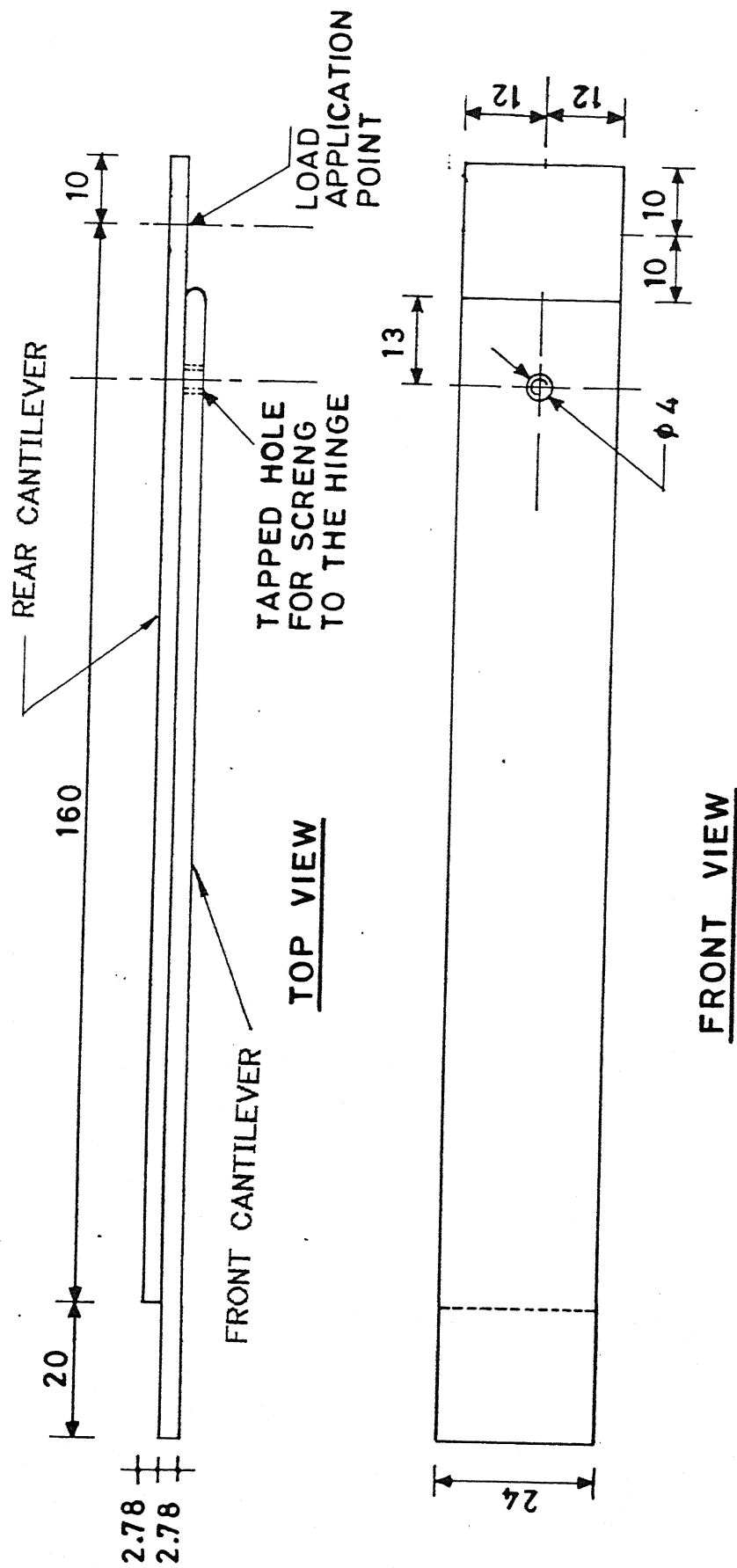
FIG. 3.1 STEEL DCB TEST SPECIMEN

applied to the cleaned faces of the DCB specimen. Two strips are
then put together with an offset of 20 mm and pressed in specially
built fixture made of two steel plates (each 25 mm thick) with ground
flat faces (Fig. 3.2). Between the strips and the flats of the
fixture plate a sheet of BOPP film is placed on each side to work as
a release film.

Provisions are made in the fixture for keeping the two strips in
position while curing. The base plate of the fixture has four
cylindrical stops and two adjustable buttons. Two cylindrical stops
are placed at a distance of 190 mm from each other. This is done to
allow for an off set of 20 mm for 170 mm long specimens. Each
specimen is butted against three of the four stops and kept in place
with the help of adjustable buttons. Both the adjustable buttons
have a slot of 4X7 mm^2, so that they can be tightened to the base at
the desired location. Also, they are of different heights so as to
hold each strips in its place. Fig. 3.3 shows the photograph of the
plates of the fixture.

The fixture along with the specimen is placed between two plates of a
hydraulic press. The plates are heated by inbuilt heating pads and
the temperature of the specimen is monitored by placing a
chromel-alumel thermo-couple between the plates. The specimen is
kept at 130° C (corresponding to a potential differences of 3.8 mv
between the two ends of the thermo-couple), and a pressure of 1.2
Mpa, for one hour. It is then cooled to room temperature at the same
pressure.

3.2.2 DCB Specimen of GFRP

Two kinds of GFRP specimen were used ; one using unidirectional glass
fibers and other using glass fiber fabrics. The geometry,
orientation of fiber layers (laminae) and the preparation of the
specimen is as follows :

RELEASE FILMS (BOPP)

FIXTURE

25 mm

HEATED PLATENS

SPECIMEN

BOPP FILM FOR PRECRACK
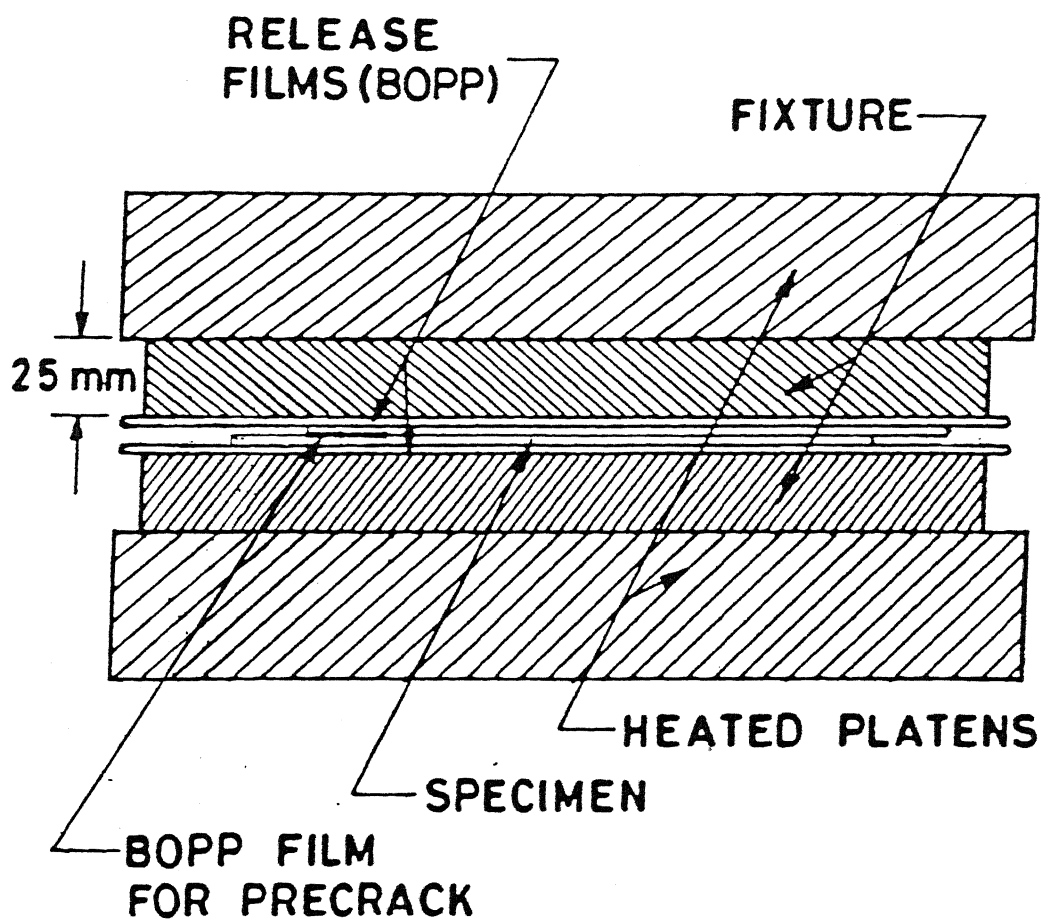
FIG. 3.2   FIXTURE FOR HEATING AND PRESSING THE CANTILEVERS OF THE SPECIMEN
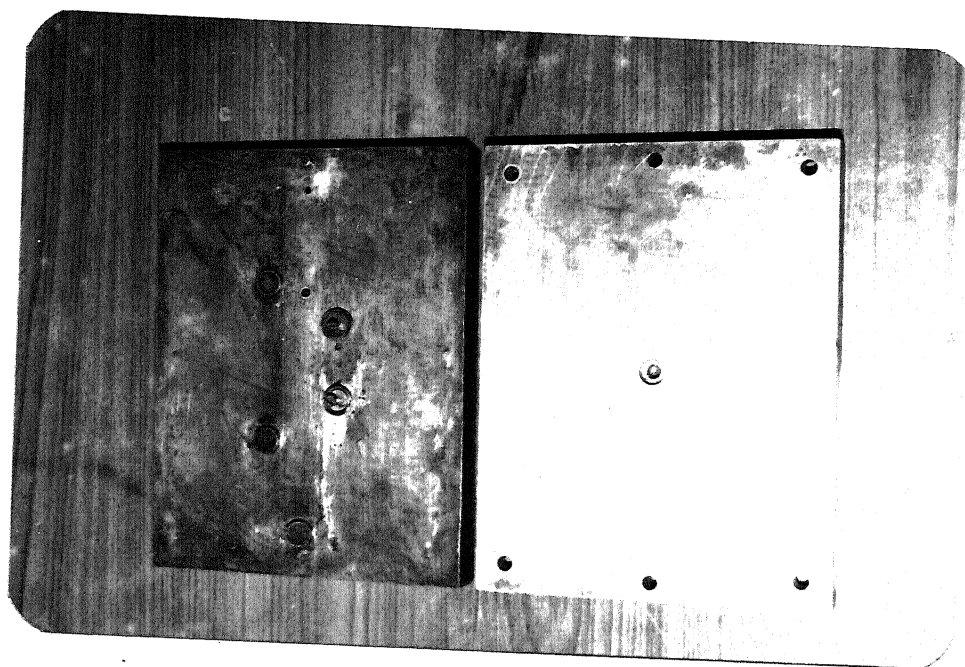
FIG. 3.3   PHOTOGRAPH OF BASE FIXTURE USED IN CASTING

Geometry

The geometry of these specimens were same as that of steel DCB except the thickness of cantilevers. Each cantilever was 2.37 mm thick in the case of unidirectional glass fiber reinforcement and 1.54 mm in the case of glass fabric reinforcement. To fix the hinge to the specimen the hinge bracket was screwed to the front cantilever with an M4 cap screw (Fig. 3.4)

Fiber Orientation

Both kinds of GFRP specimen were reinforced by sixteen layers of glass fibers. The glass fibers, of GFRP reinforced with unidirectional fibers, and the warp fibers, of GFRP reinforced with glass fiber fabric, were stacked in the sequence of $(0/+45/-45/90/90/-45/+45/0)_s$. Each cantilever strip of the DCB specimen consisted of 8 layers.

Specimen Preparation

The hand lay up technique is employed to make a laminate OF GFRP of dimension 190 X 190 mm^2. The resin used is same as that used for binding the strips of steel DCB specimen. Each lamina of the glass fiber was wetted with the resin and was placed over each other in the above mentioned orientation. To introduce a pre-crack a BOPP sheet was placed after 8 layers. All the sixteen laminae put together were then pressed between two steel plates. Between the GFRP sheet and the flats of the steel plate, a BOPP sheets was placed on each side to act as a release film. The pressure and temperature of the sheet was maintained at 1.2 Mpa and 130° C for one hour. And then it was allowed to cool to room temperature at the same pressure. The DCB specimen of required dimension were cut from this sheet.

3.2.3 Crack Sharpening

The pre-crack introduced in the DCB specimen by placing a BOPP sheet needs further preparation before the specimen is impacted. The tip

REAR CANTILEVER

FRONT CANTILEVER
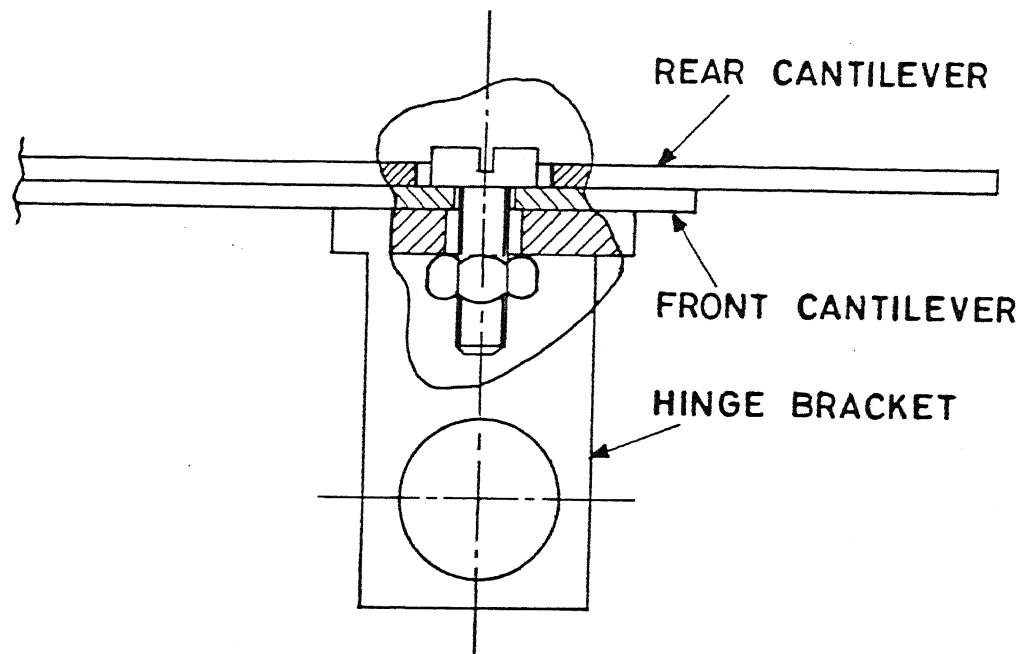
HINGE BRACKET

FIG. 3.4   GFRP SPECIMEN SCREWED TO THE HINGE BRACKET

of the pre-crack is not very sharp due to the BOPP sheet's finite thickness. Therefore the pre-crack should be grown further by a few millimeters to sharpen the crack. Furthermore, although the BOPP sheet does not bond well to the steel faces, it does stick weakly to the steel faces at many points. The cantilevers of the DCB are therefore pulled to snap off these weak stickings.

A fixture is designed to sharpen the crack. It consists of three plates. The specimen is clamped between two thick plates (20 mm). The inner faces of the thick plates are ground flat so as to have uniform pressure on the specimen. Before the plates are tightened between the two jaws of a vice, all three of them are placed on their side faces over the third plate of the fixture whose top surface is also grounded flat. This ensures that the edges of the thick plates are parallel to the crack front. The specimen is placed between thick plates in such a way that the tip of the pre-crack is projected out by 2-3 mm beyond the edges of the plates. The specimen between the thick plates is pressed properly between the jaws of a vice (Fig. 3.5). Before opening the crack of the DCB specimen with a wedge (sharp chisel), a layer of white ink is applied at the side faces of specimen and allowed to dry. The sharp chisel is, then cautiously and gently pressed to open the crack. The dry white ink cracks with opening of the pre-crack of the specimen and thus gives the location of the tip of the sharpened crack.

3.3 OVERALL EXPERIMENTAL SETUP

Load bar technique is used to apply dynamic load to the DCB specimen and the propagation gauges are used to measure the crack velocity. Figure 3.6 shows the schematic diagram and Fig. 3.7 the photograph of the complete experimental setup which includes specimen, load bar, striker, propagation gauges, bridge circuit for pulses in the load bar, logic circuit unit for the propagation gauges and the oscilloscope. A phonographic needle is used to trigger the oscilloscope after the striker, shot by the air gun, hits the load bar. The oscilloscope records the strain pulses in the load bar, picked by strain gauges, through a bridge circuit and the shearing of
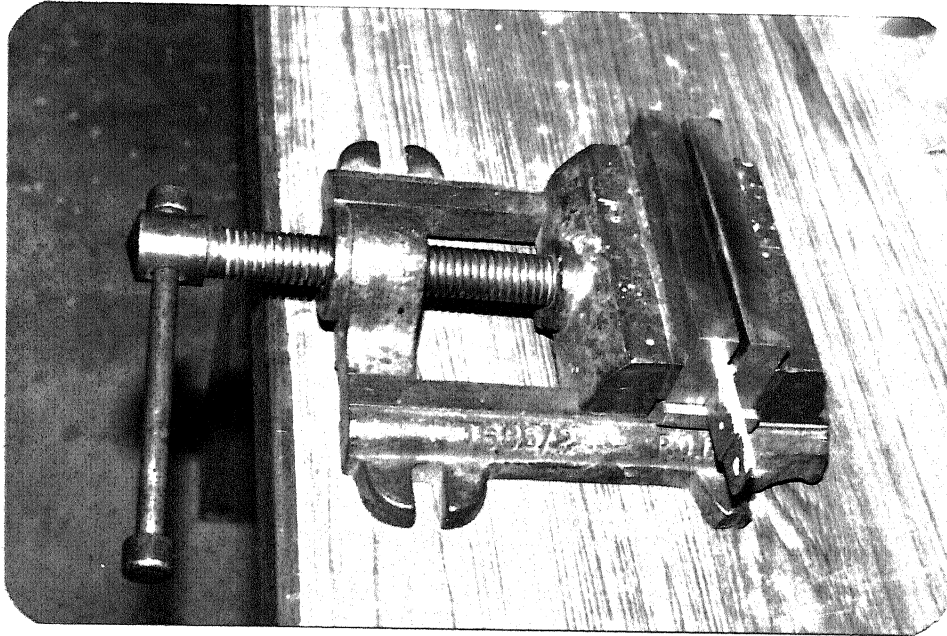
FIG. 3.5   PHOTOGRAPH OF CRACK SHARPENNING FIXTURE ALONG WITH THE DCB SPECIMEN

22

FIG. 3.6 OVERALL EXPERIMENTAL SETUP.

DCB SPECIMEN

ELECTRONIC CIRCUIT UNIT

OSCILLOSCOPE

V_1 V_2 T

TEFLON STOPPER

PROPAGATION GAUGES

HINGE

STRAIN GAUGES

LOAD BAR

BRIDGE CIRCUIT

PHONOGRAPHIC NEEDLE

F   F

BARREL OF AIR GUN

V

STRIKER

CORD AND PULLEY ARRANGEMENT FOR APPLYING STATIC LOAD
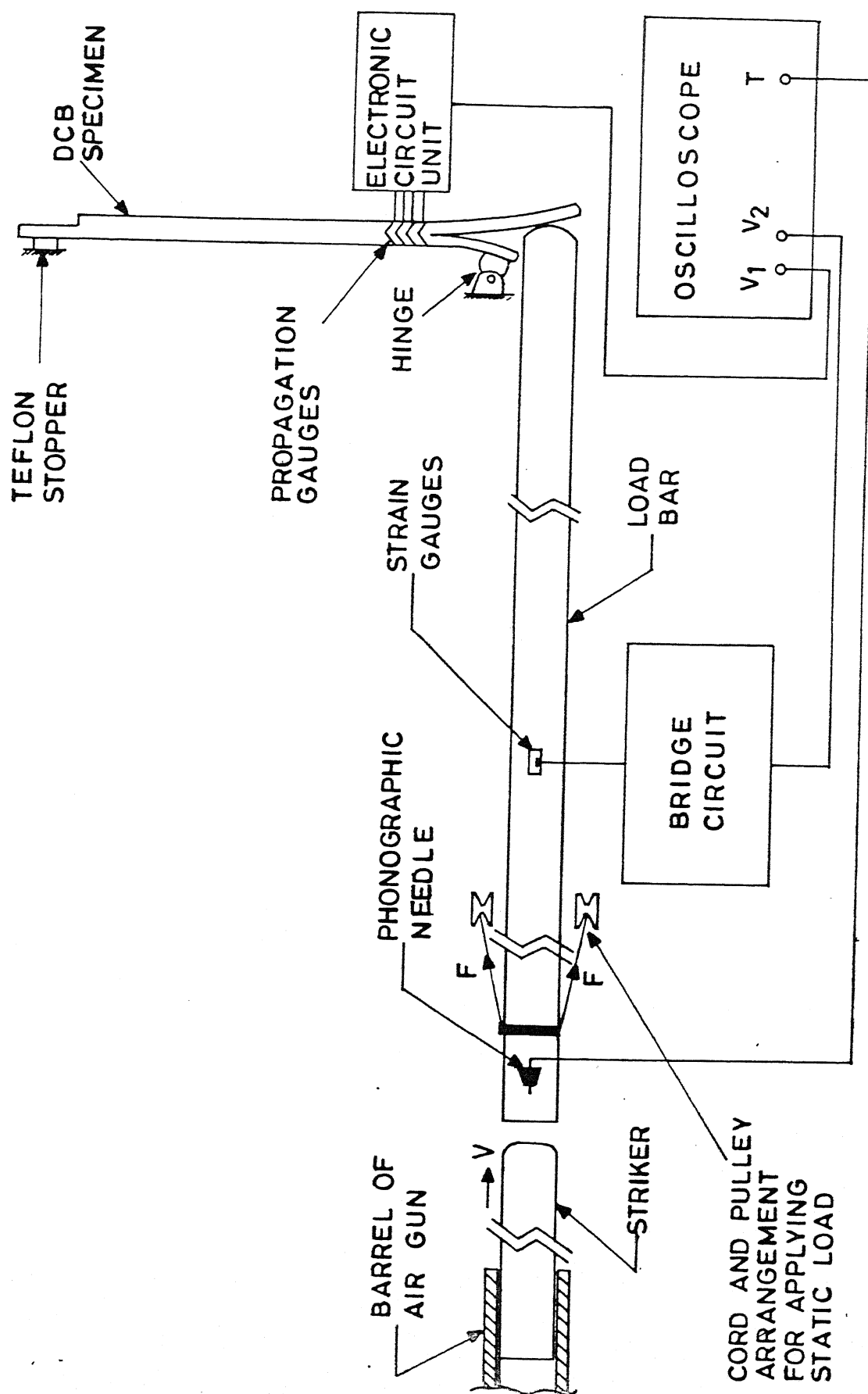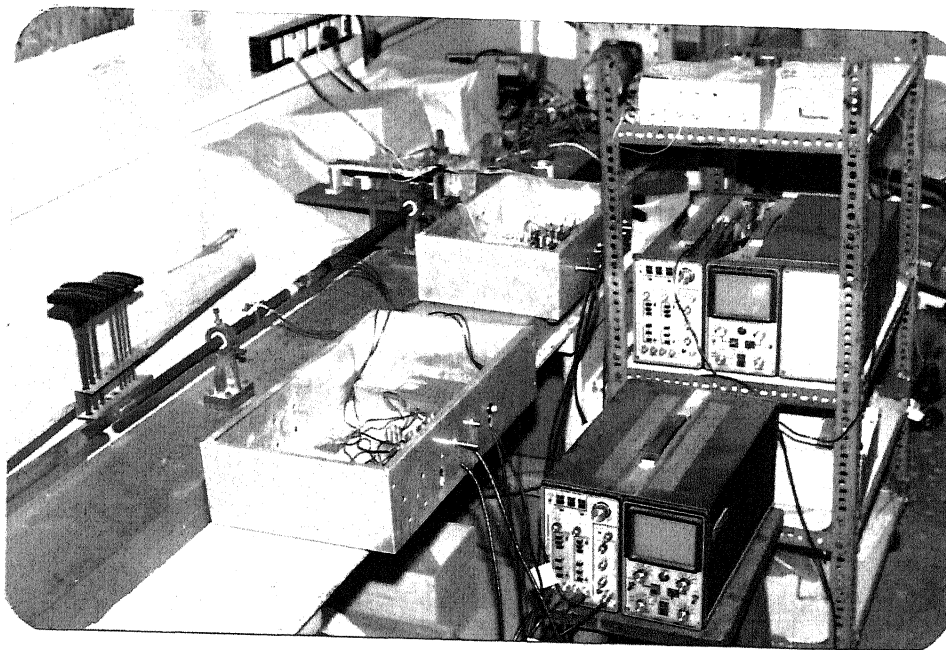
FIG. 3.7   PHOTOGRAPH OF OVERALL EXPERIMENTAL SETUP

propagation gauges as voltage drops, with the help of an electronic circuit unit.

3.4 EXPERIMENTAL SETUP FOR IMPACT LOADING

As mentioned earlier, the load bar technique is used for applying a dynamic load pulse on the DCB specimen. The specimen is held in its position by a hinged support tied to the front cantilever of the DCB specimen. The load bar is kept in contact with the rear cantilever. When the striker, from the air gun, hits the load bar a stress pulse is generated. This pulse is partly transmitted to the cantilever, thus dynamically loading the specimen.

3.4.1 Fixture for Holding the Specimen

A specially designed fixture (Fig. 3.8) is used for holding the specimen when the load is applied. The fixture consisted of a base, a hinge holderand a hinge assembly. The base of the fixture, with details shown in Fig. 3.9 is screwed to the channel on which the gun barrel is mounted. The hinge holder (Fig. 3.10) is screwed to the base with the help of the tapped holes provided on the base. The hinge assembly consistes of a hinge support, a bracket, a pin and a T (Fig 3.11).

The hinge holder has a specially made hole and slot arrangement for gripping the hinge support. The hinge support is attached to the hinge bracket with the help of the pin. The hinge bracket is screwed to the T through two tapped holes provided on the T. The T in turn is screwed to the front cantilever of the DCB specimen with the help of a tapped hole at the end of the cantilever. The T is used only with the steel DCB specimen and not with the GFRP specimen. The GFRP specimen is directly attached to the hinge bracket (Fig. 3.4).

The other end of the specimen is supported by an end stopper (Fig 3.12) which is screwed to the base of the fixture.
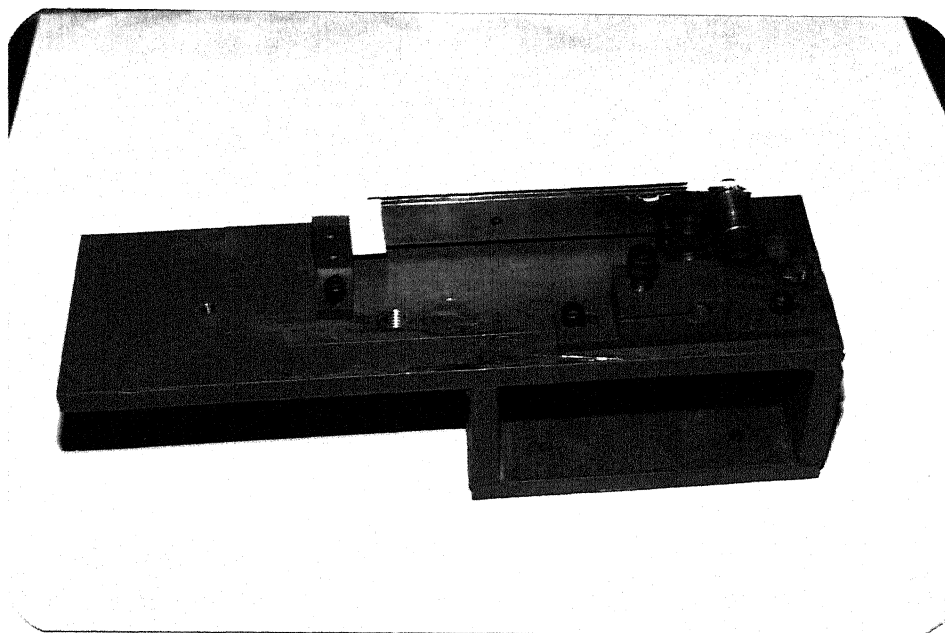
FIG. 3.8   FIXTURE FOR HOLDING THE SPECIMEN ALONG WITH THE SPECIMEN

TAPPED HOLES FOR
STOPPER

TAPPED HOLES FOR
HINGE HOLDER

100

TOP VIEW

10

90

160

FRONT VIEW
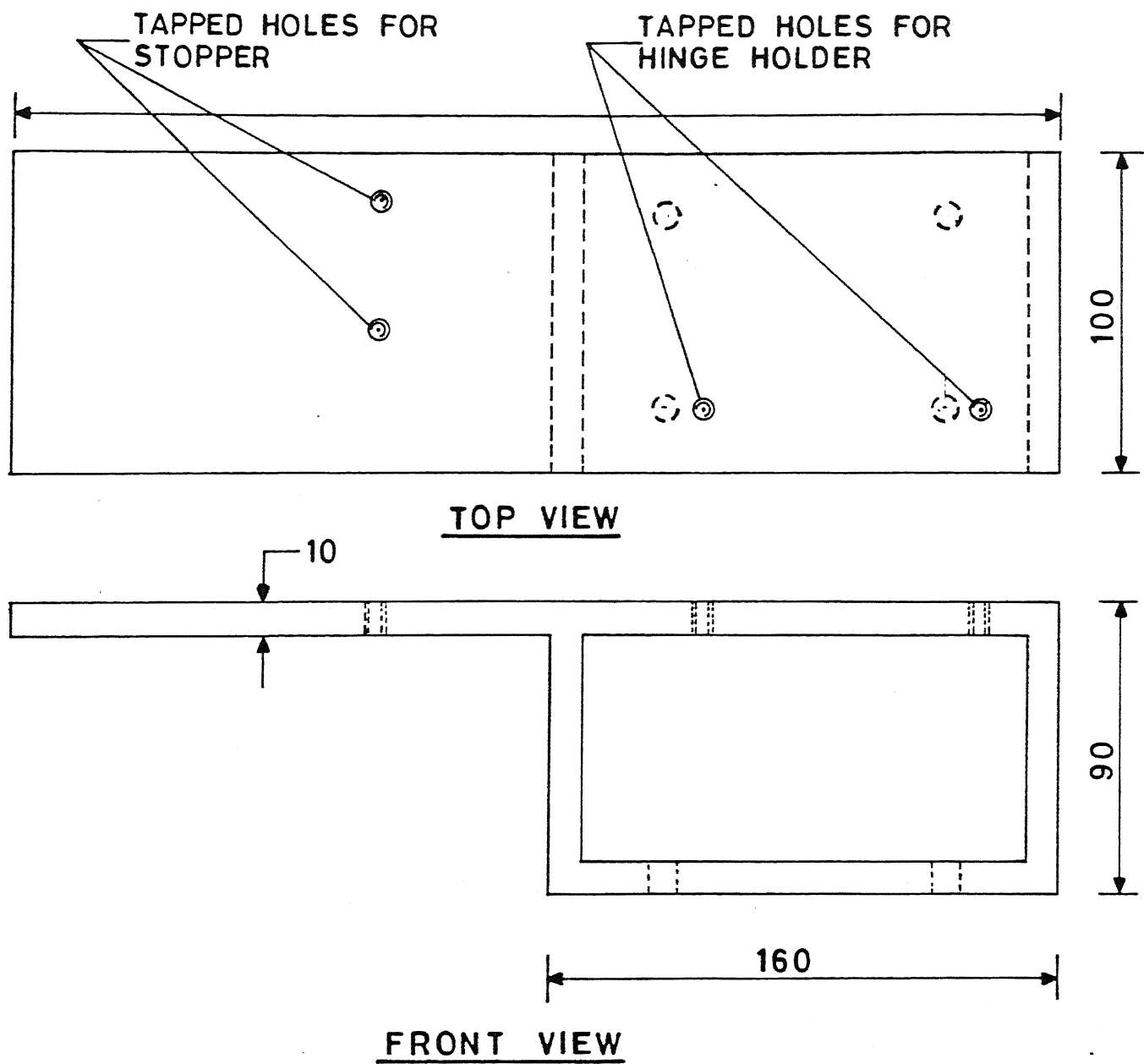
FIG. 3.9   BASE OF FIXTURE FOR HOLDING THE
SPECIMEN.

110

25   45

SLOTS FOR
TIGHTENING
TO THE BASE

φ8

7

12

24

4   15

4

TOP VIEW

10

φ10

HOLE FOR
HING SUPPORT

7.5

33

1.5

25

6

φ7

FRONT VIEW

FIG. 3.10   HINGE   HOLDER

28

Ø10

Hole for
the pin

15

15

45

TOP

Ø10

15

FRONT

ⓓ SUPPORT

Ø11

TOP

3

Ø10

33

FRONT

ⓒ PIN

Ø10

20

Hole for
the pin

TOP

Ø4

4

15

FRONT

ⓑ BRACKET

Hole for Screwing
to the specimen

Ø4

6.5

Ø6

Ø3

TOP

3

5

24

8

24

FRONT

ⓐ T
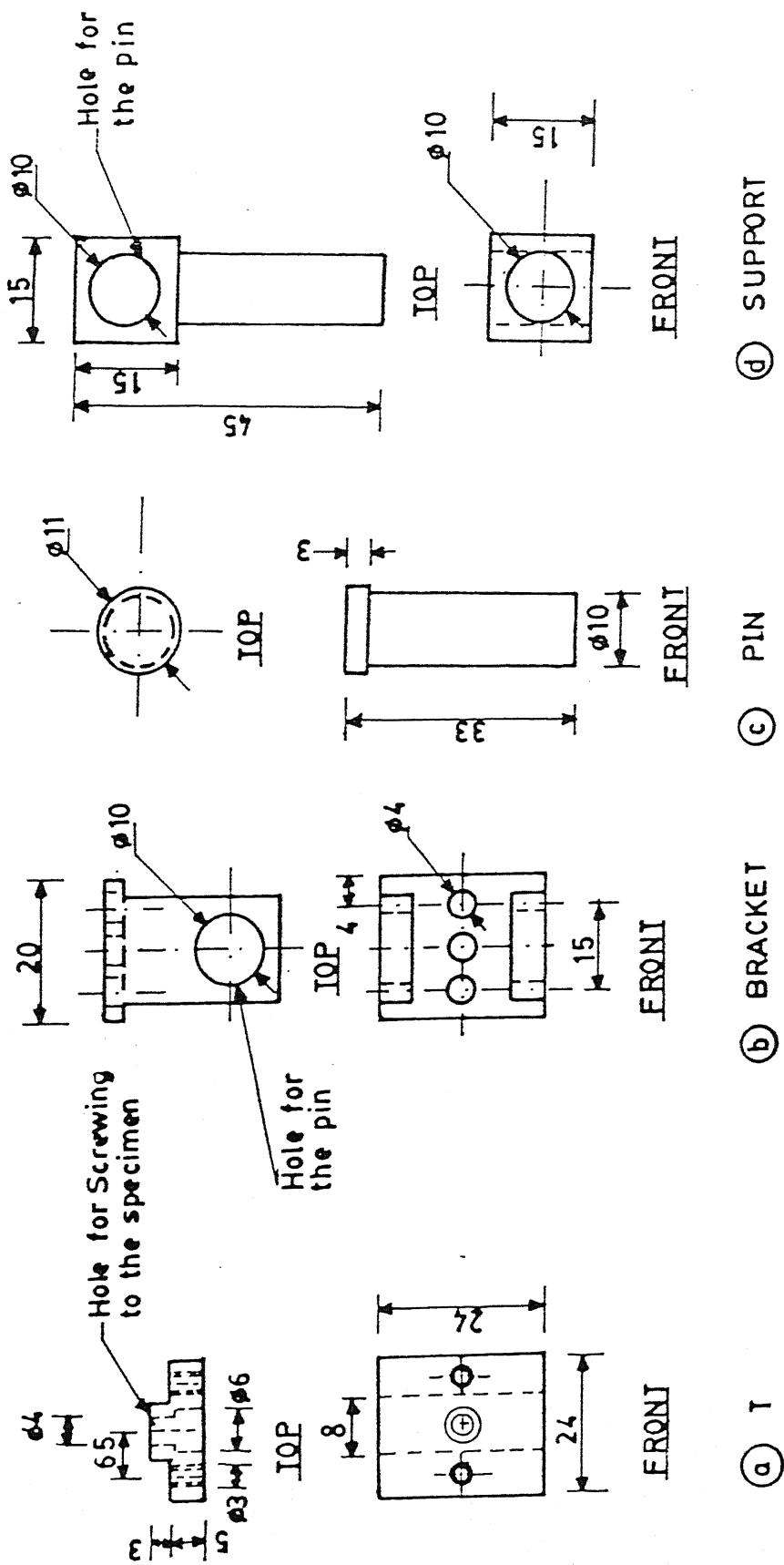
FIG. 3.11   DIFFERENT PARTS OF THE HINGE ASSEMBLY

29

TOP VIEW

16
61
6.6
6.6
25
3
3
7

SLOTS FOR
TIGHTENING
TO THE BASE

SIDE VIEW

31
$\phi 4$
$\phi 3$
6

TEFLON
CUSHIONING
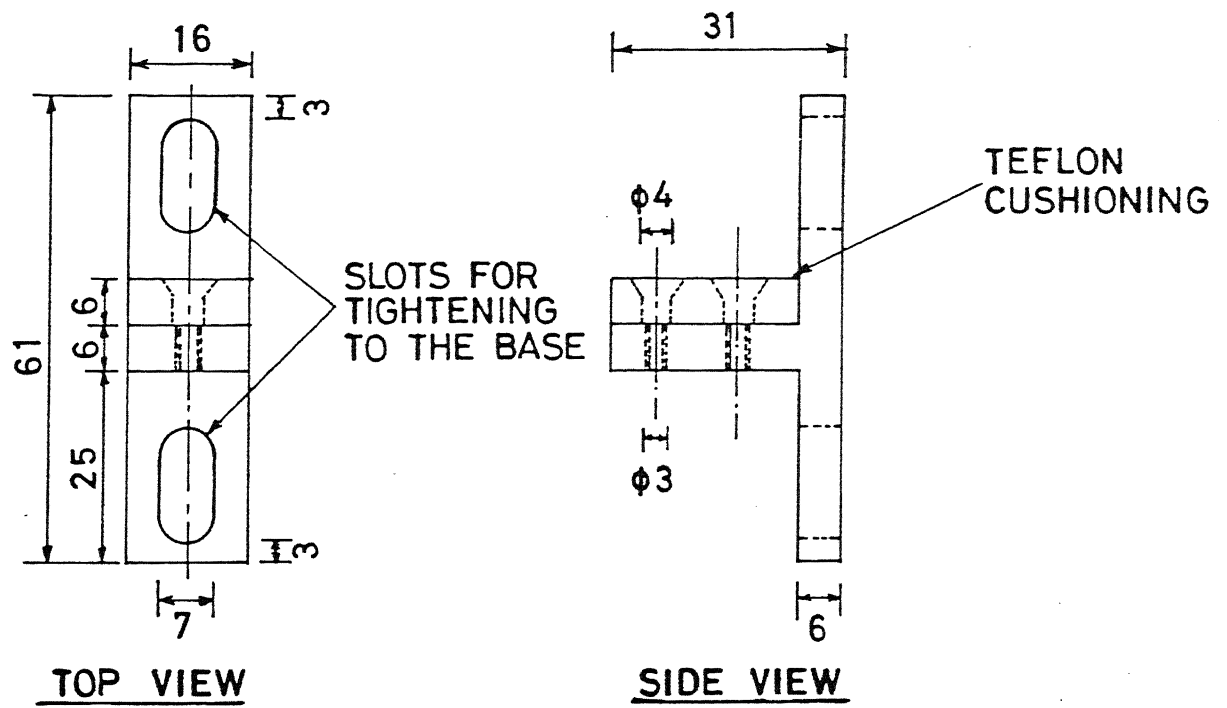
FIG. 3.12   END STOPPER

3.4.2 Striker and the Load Bar

Applying a dynamic load pulse to the DCB specimen include an air gun and a load bar. The load bar is properly aligned with the center-line of the barrel of the air gun. When the striker, from the air gun, impacts the load bar, a longitudinal compressive stress pulse is generated in the load bar. As this compressive stress pulse reaches the specimen end of the load bar, part of it is transmitted to the specimen and remaining is reflected back as a tensile pulse. Two strain gauges bonded at diametrically opposite locations on the load bar (Fig. 3.6) connected in a bridge circuit pick up these stress pulses and are recorded in a storage oscilloscope. The oscilloscope is triggered by a phonographic needle, kept in contact with the surface of the load bar, with the help of a rubber band.

3.4.3 Stress Pulses

Atypical record of the incicent and reflected pulses in the load bar is shown in Fig. 3.13. From this experimental record the load pulse imparted to the specimen can be obtained using one dimensional wave propagation theory. Fig. 3.14 shows the time distance (t-x) diagram for propagation of stress pulse in the load bar. When the striker bar impacts the load bar, the compressive incident pulse propagates towards the DCB specimen and is recorded at the location 1. The reflected tensile pulse is recorded at the same location but at a different time and is depicted by point 3 in the t-x diagram. The aim is to express stress σ_2 in terms of experimentally recorded σ_1 and σ_3.

One dimensional wave equation along the characterstic with the acoustic impedance, ρc, is expressed as

$$d\sigma - \rho c dv = 0 \qquad (\text{Along +ve characterstic})$$

$$d\sigma + \rho c dv = 0 \qquad (\text{Along -ve characterstic})$$

Using above eqations the relation along characterstic 1-2 simplifies

31
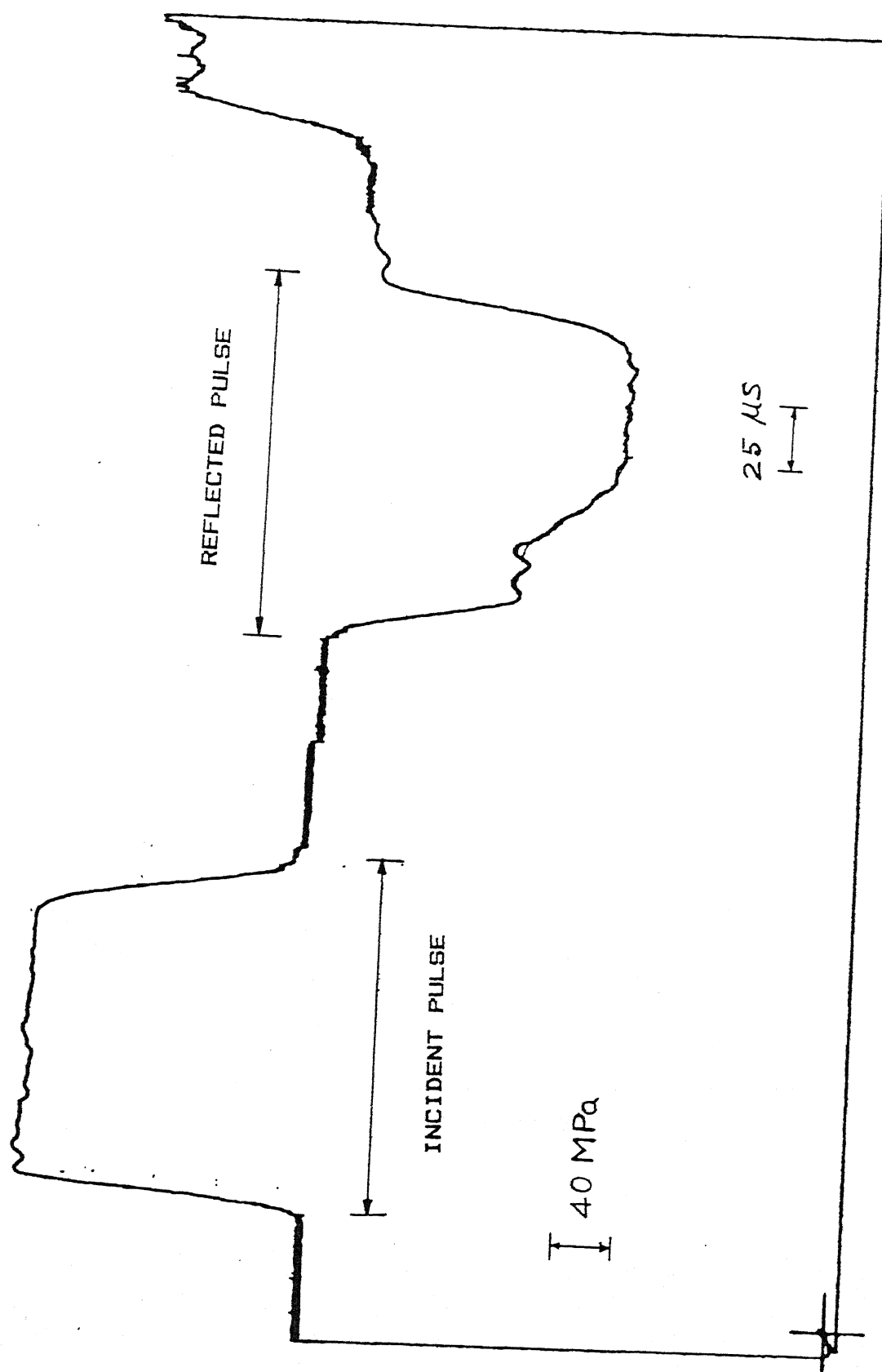
FIG. 3.13   A TYPICAL RECORD OF STRESS PULSES IN THE LOAD BAR

REFLECTED PULSE

INCIDENT PULSE

25 μS

4.0 MPa
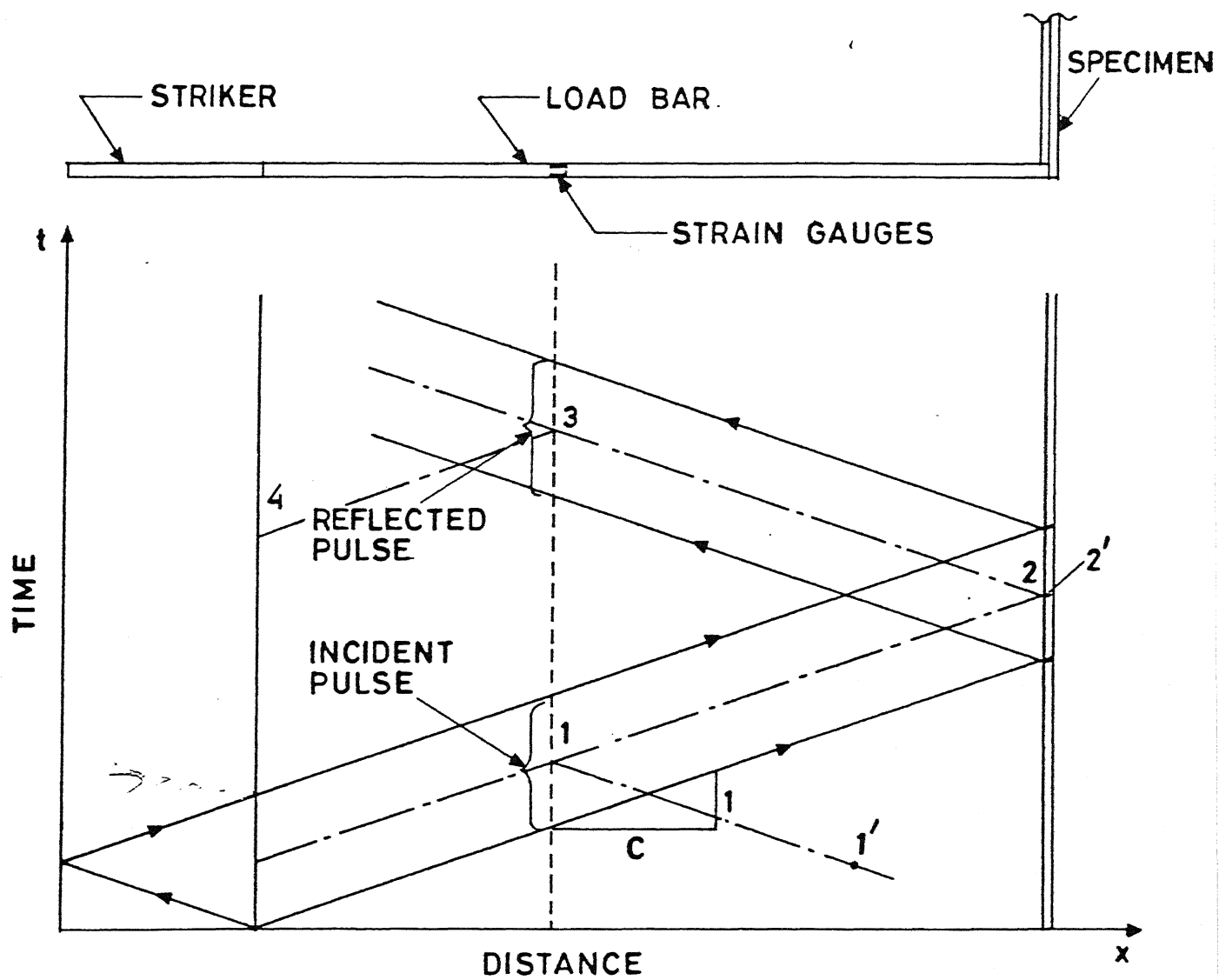
FIG. 3.14   TIME-DISTANCE (t-x) DIAGRAM

33

$$\sigma_2 - \rho c v_2 = \sigma_1 - \rho c v_1 \qquad (1)$$

Along the characterstic 1-1'

$$\sigma_1 + \rho c v_1 = \sigma_{1'} + \rho c v_{1'} \qquad (2)$$

But $\sigma_{1'} = 0$ and $v_{1'} = 0$ because the load bar is initially at rest and stress waves does not reach at point 1'. Then the above equation gives

$$\sigma_1 = -\rho c v_1 \qquad (3)$$

Using Eqn. 1 and Eqn. 3

$$\sigma_2 - \rho c v_2 = 2\sigma_1 \qquad (4)$$

Relations along characterstics 2-3 and 3-4 are

$$\sigma_2 + \rho c v_2 = \sigma_3 + \rho c v_3 \qquad (5)$$
$$\sigma_3 - \rho c v_3 = \sigma_4 - \rho d v_4 \qquad (6)$$

At point 4 $\sigma_4 = 0$ and $v_4 = 0$ because the striker and the load bar are of same material and diameter and the striker comes to rest. The above two equations yield

$$\sigma_2 + \rho c v_2 = 2\sigma_3 \qquad (7)$$

Eqn. 4 and Eqn. 7 give

$$\sigma_2 = \sigma_1 + \sigma_3 \qquad (8)$$
and $$v_2 = (\sigma_3 - \sigma_1)/(\rho c) \qquad (9)$$

Note that σ_2 in Eqn. 8 gives the stress pulse imparted to the specimen and v_2 the partical velocity in the load bar. Since σ_1 is compressive and σ_3 is tensile in nature, the pulse transmitted to the

specimen is actually the difference in magnitude of incident and reflected pulse. Thus the load pulse transmitted to the specimen can be obtained by superposing the incident stress pulse with the inverted reflected pulse. Figure. 3.15 shows the load pulse imparted to the specimen corresponding to the incident and reflected stress pulses of Fig. 3.12.

The load imparted to the end of the cantilever, P_2 can be given by

$$P_2 = \sigma_2 . A = (\sigma_1 + \sigma_3) . A \qquad\qquad (10)$$

where A is the area of cross-section of the load bar. The energy corresponding to the transmitted pulse can be obtained as follows :

$$E = \int P_2 . dx = \int P_2 . v_2 \, dt \qquad\qquad (11)$$

v_2 is the partical velocity given by Eqn. 9. Thus energy,

$$E = \frac{A}{(\rho c)} \int (\sigma_1^2 - \sigma_3^2) . dt \qquad\qquad (12)$$

where A and (ρc) are constant with time.

3.4.4 Details of Bridge Circuit

The bridge circuit converts the change in resistance of the strain gauges bonded to the load bar into a potential diffe rence. This potential difference is in turn, recorded on the oscilloscope. Fig. 3.16 shows the configuration of the bridge circuit used in this study. R_1, R_2, R_3 and R_4 are four strain gauges each having a resistance value of 120 $\pm$ 0.3 Ω. R_1 and R_3 represent the strain gauges bonded to the load bar. R_2 and R_4 are the dummy gauges. These dummy strain gauges are bonded on a steel plate which acts as a heat sink to the heat generated in the coils of the strain gauge when current flows through it. The bridge circuit is balanced to give zero voltage output for no change in resistance of the active strain gauges. This is done by connecting a 1.0 Ω resistance in series and
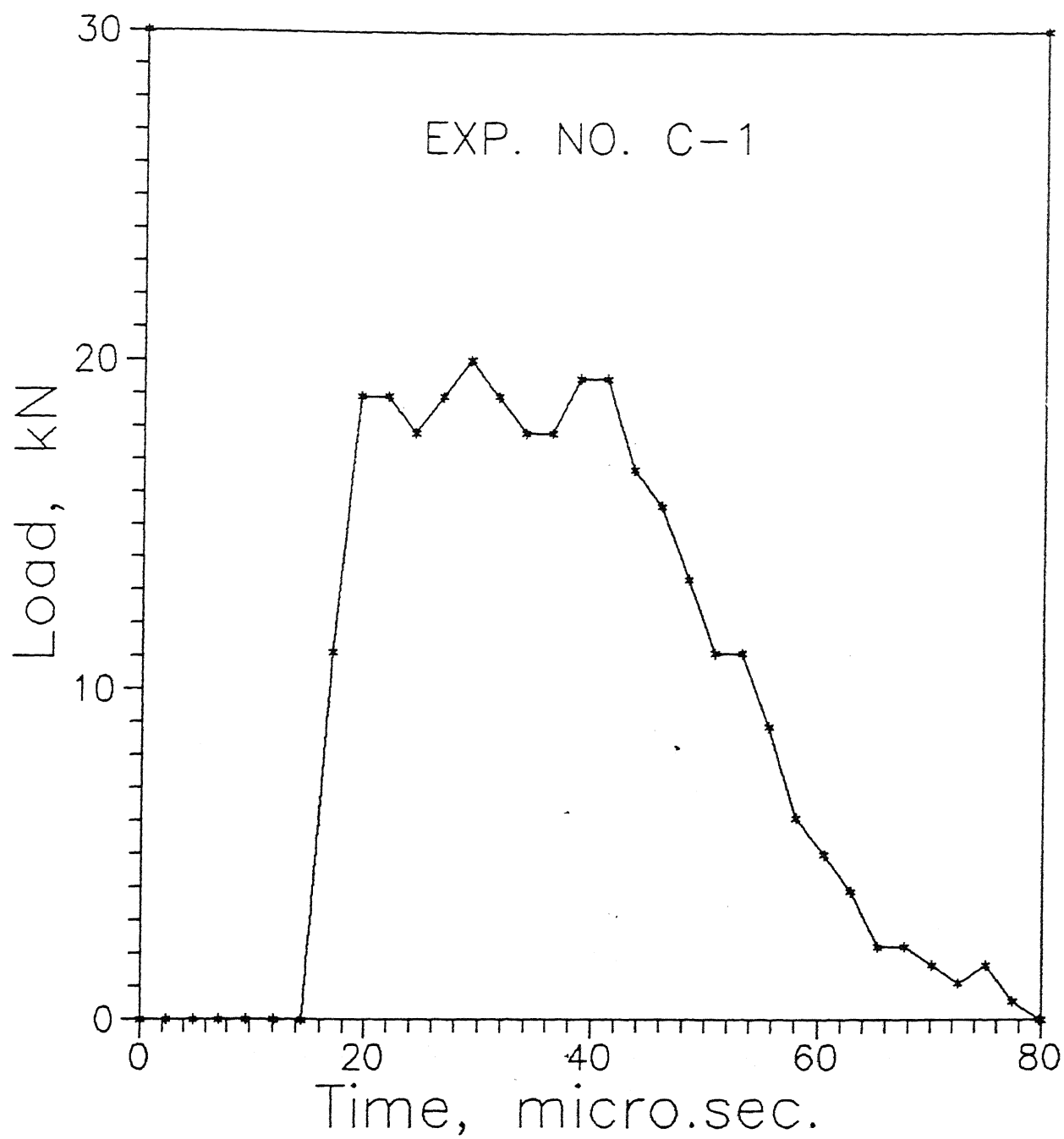
FIG. 3.15   LAOD PULSE IMPARTED TO THE SPECIMEN CORRESPONDING TO THE STRESS PULSES OF FIG. 3.13

36

R$_1$, R$_3$: ACTIVE GAUGES

R$_2$, R$_4$: DUMMY GAUGES
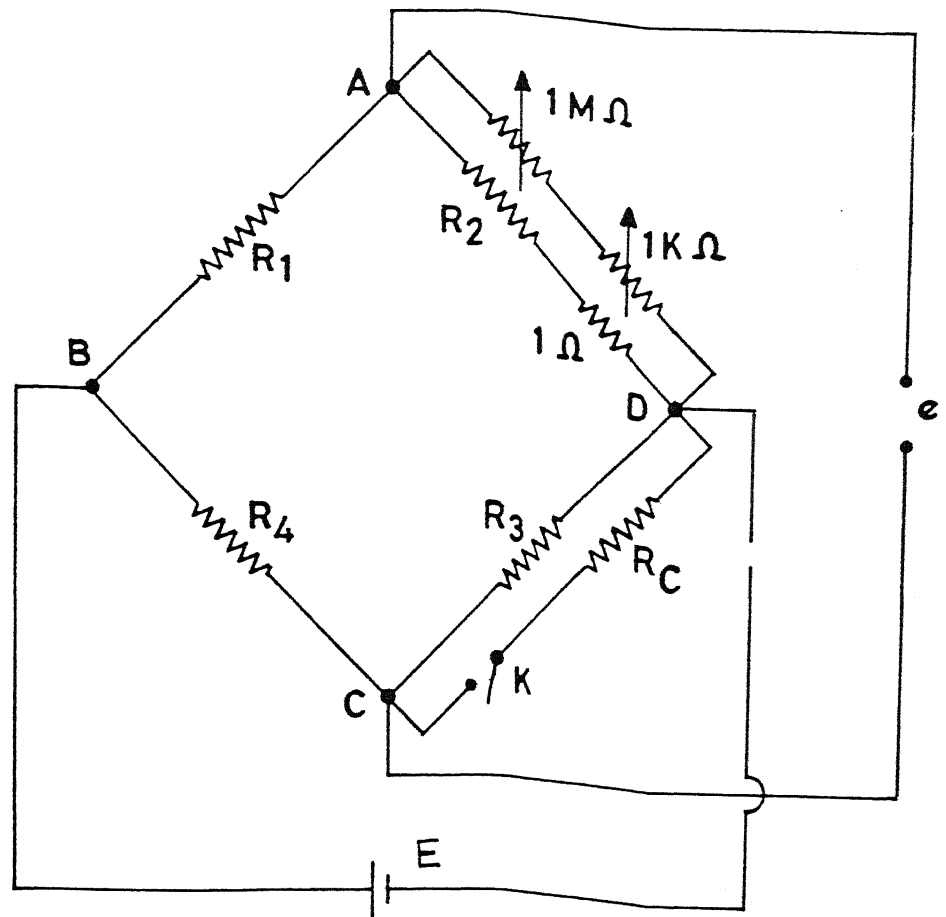
FIG. 3.16   BRIDGE CIRCUIT

two variable resistors (1.0 MΩ and 1.0 kΩ) parallel to one of the dummy strain gauges (R_2 in the shown circuit). To calibrate the the bridge circuit a calibration resistance R_c is connected parallel to one of the active gauges (R_3 in the diagram) through a switch (K). The value of the calibration resistance is 47.0 kΩ. The equations involving the calibration of the bridge circuit are as follows.

For a balanced bridge circuit the output voltage (Δe) is given by

$$\frac{\Delta e}{E} = \frac{R_1 \cdot R_2}{(R_1 + R_2)^2} \left[\frac{\Delta R_1}{R_1} - \frac{\Delta R_2}{R_2} + \frac{\Delta R_3}{R_3} - \frac{\Delta R_4}{R_4} \right] \qquad (13)$$

where E is the input voltage. It can be seen from the equation that similar (both positive or both negative) changes in resistance of opposite arms of the bridge circuit are added up and dissimilar (one positive and other negative) changes are canceled out. Thus by having the active strain gauges at the opposite arms only compressive pulse is recorded and bending effect is neglected.

The relation between the strain in the strain gauge and corresponding change in its resistance is governed by the following equation :

$$G.F. = \frac{\Delta R/R}{\Delta L/L}$$

$$\Delta L/L = \frac{\Delta R/R}{G.F.} \qquad (14)$$

where G.F. is the gauge factor and $\Delta L/L$ is the strain recorded by the strain gauge . The change in resistance of the arm CD after connecting R_c is given by

$$\Delta R = R - \left(\frac{R \cdot R_c}{R + R_c} \right)$$

leading to

$$\Delta R/R = \frac{R}{R + R_c} \qquad (15)$$

Corresponding to this change in resistance a voltage difference (Calibration Voltage, V_c) will occur between terminals A and C. This resistance change will also correspond to the strain (Eqn. 14), in the strain gauge R_3. From Eqns. 14 and 15 this strain will be

$$\varepsilon_c = \Delta L/L = \frac{R}{2.(R + R_c).G.F.} \qquad (16)$$

The strain value ε_c will thus correspond to the Calibration Voltage, V_c. A factor of 1/2 is introduced to average out the strains recorded by the two strain gauges R_1 and R_3 which are at the opposite arms of the bridge circuit. By the linearity of the relation (Eqn. 13 and Eqn. 14) between voltage drop across AC and strain in the strain gauges bonded to the load bar, the strain in the load bar corresponding to a voltage V recorded on the oscilloscope can be given as

$$\varepsilon = \frac{\varepsilon_c}{V_c} . V \qquad (17)$$

In previous works BNC connectors were used in the bridge box. But available BNC connectors were not of good quality. They did not provide reliable connection. These BNC connectors were replaced by specially designed cap and stud arrangement (Fig. 3.17a) to have press contact at the terminals. Four to six studs were screwed to a brass plate. They were provided with holes for the wires. The wires inserted in these holes were pressed against the plate by the cap. Fig. 3.17b shows the photograph of the cap and stud assemly. Fig. 3.18a shows the photograph of the interior of the bridge box, showing bridge connections, dummy strain gauges and battery and Fig. 3.18b shows a close view of the bridge connections. Direct contact between brass plates and the bridge box is avoided using a wooden block between them.

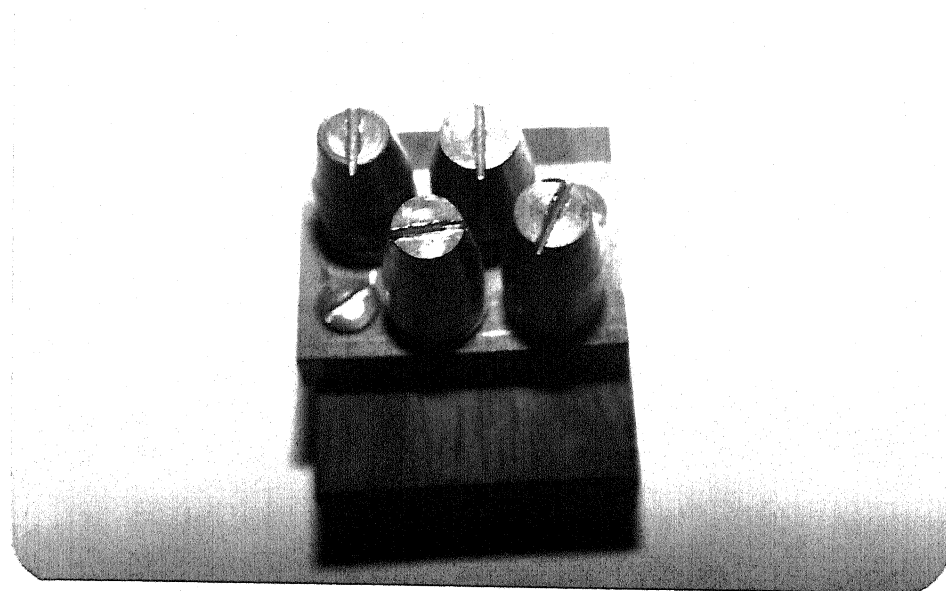FIG. 3.17a CAP, STUD AND WASER FOR PRESS CONTACT IN BRIDGE TERMINALS

FIG. 3.17b CAP AND STUD ASSEMBLY FOR PRESS CONNECTION IN BRIDGE BOX
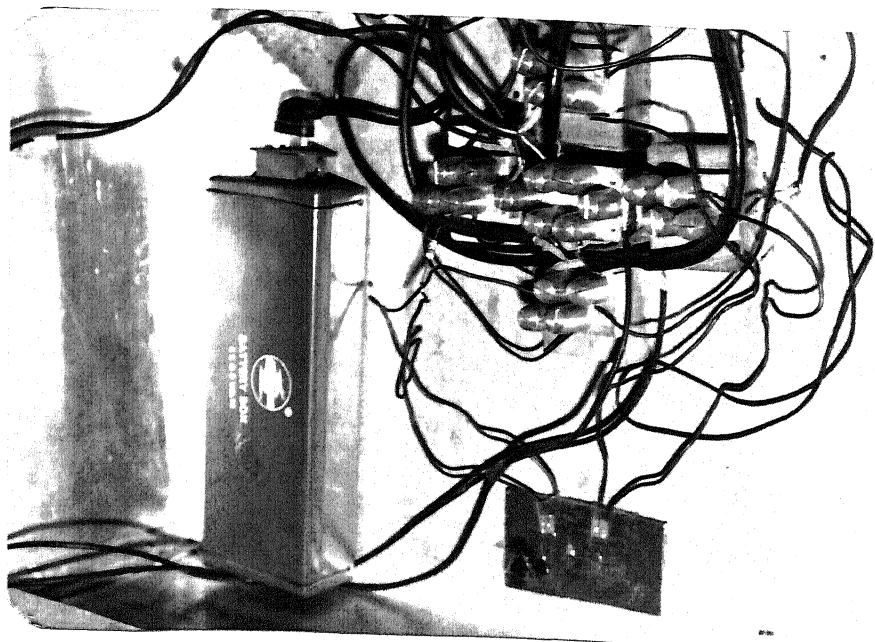
FIG. 3.18a INTERIOR OF THE BRIDGE BOX SHOWING BRIDGE
CONNECTIONS, DUMMY STRAIN GAUGES AND THE BATTERY
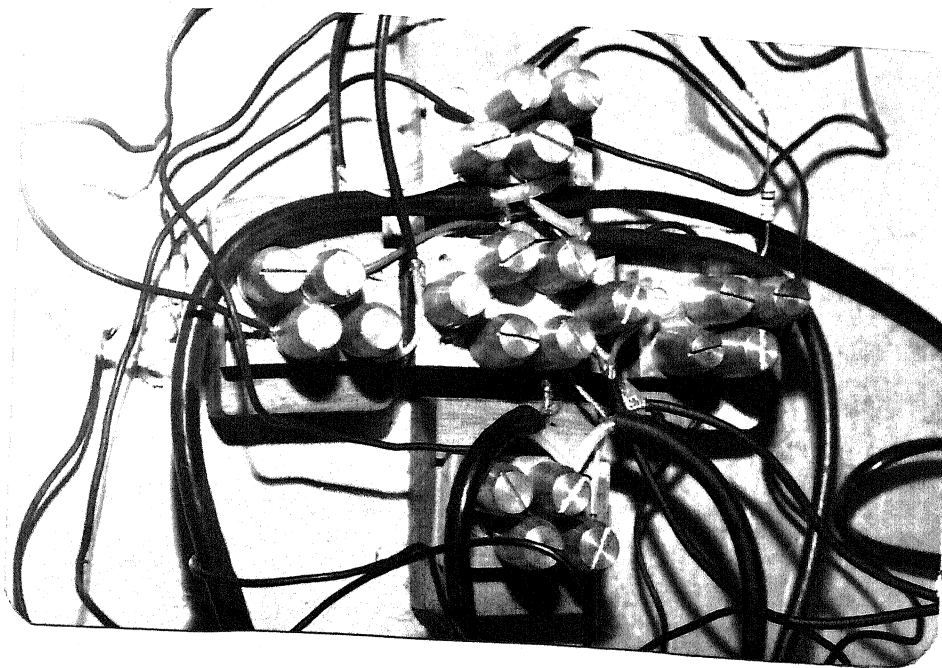
FIG. 3.18b CLOSE VIEW OF THE BRIDGE CONNECTIONS

3.4.5 Load Element

To impart greater amount of energy to the specimen some experiments were conducted in which a cylindrical bar (Load Element) of length 25-50 mm was screwed to the rear cantilever at the point of loading. The diameter and the material of the load element was same as that of the load bar. Special care was taken to align the load element with the load bar before applying the load pulse. Fig. 3.19 shows the photograph of the load element along with the DCB specimen. With the use of load element the energy input to the specimen increased by more than 10 times. The principle behind the higher energy transfer to the DCB specimen with the use of load element is as follows :

The stress pulse enters the rear cantilever of the specimen as a compressive pulse. This is reflected back as a tensile pulse from the other face of the rear cantilever. Since the thickness of the cantilever is small and the tensile pulse cannot enter the load bar from the cantilever, the cantilever flies off. With the use of load element the effective thickness of the cantilever is increased thus more energy is given to the specimen before it flies off.

3.4.6 Oscilloscope

Two different kinds of oscilloscopes Nicolet and Philips were used for recording the pulses. The salient features of each oscilloscope are given below.

NICOLET

This is a digital storage oscilloscope. Its data can be stored in the memory and can be recalled till the power supply is not switched off. It has 12 bit resolution (i.e. 2^{12} points on the screen) in both horizontal and vertical direction. The maximum sensitivity in the vertical direction is 0.05 mV and that in the horizontal direction is 0.5 μs. This oscilloscope is provided with differential input facility. It can record potential difference between two
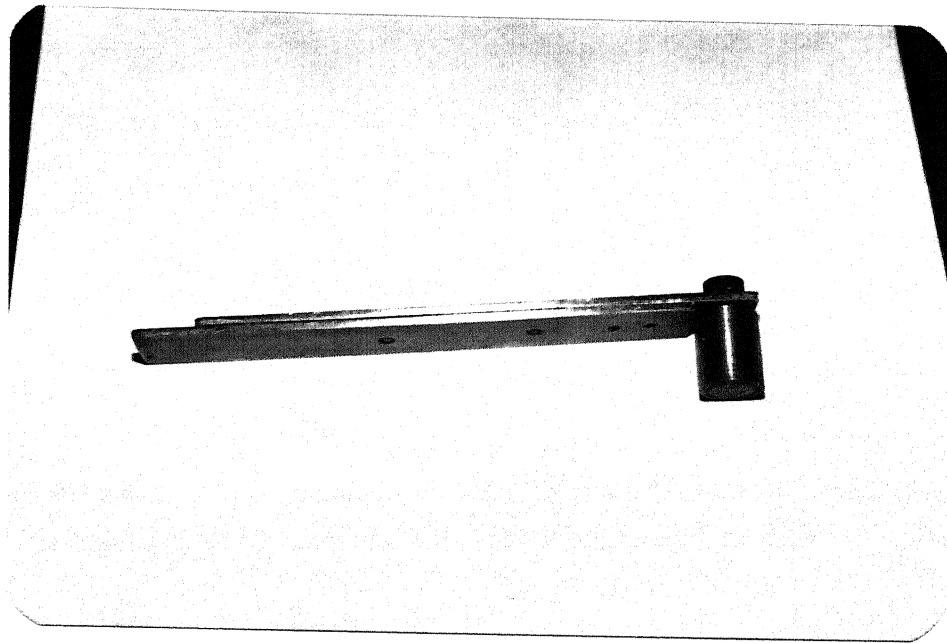
FIG. 3.19 LOAD ELEMENT SCREWED TO THE SPECIMEN

points as well as the voltage of a point with respect to the ground. It has a band width of 2 MHz which means it can record signals of upto 2 MHz frequency.

There is one malfunction occasionally developed in the present oscilloscope. Its screen goes off after about 20 to 30 minutes of power supply to it. Also its storage facility is not backed by any battery, thus once the screen is off the data stored can not be retrieved.

PHILIPS

This is a storage osilloscope with battery backup and the data stored in the oscilloscope remains in the memory even if the power is switched off. It has 8 bit resolution in vertical direction and 12 bit resolution in horizontal direction.   Its maximum vertical sensitivity is 0.0625 mV and maximum horizontal sensitivity is 1.2 ns. This oscilloscope is provided with only single ended (float) input facility and not with differential input.Thus, by itself, it can not record a potential difference between two points.   This oscilloscope has a maximum band width of 50 MHz.

While conducting the experiments with Philips ocilloscope the differential input facility of Nicolet was used.   There is one drawback assciated with Philips oscilloscope.   Although this oscilloscope has a band width of 50 MHz, it is greatly affected by the time window selected.   With the selected time window of 2 μs between two consecutive points on the oscilloscope, a voltage drop corresponding to the shearing of propagation gauge takes 8 to 12 μs on Philips oscilloscope whereas it takes only 2 μs on Nicolet oscilloscope for the same time window.   Thus for the time window selected for recording the experimental pulses the Philips oscilloscope has a poor frequency responce and it can not record very high frequency pulses.

44

3.5 CRACK PROPAGATION

The dynamic load pulse imparted to the rear cantilever of the DCB specimen travels as a flexural wave in that cantilever. As the front cantilever is held tight by the hinge, and if the load pulse is high enough the crack between the two strips of the DCB specimen starts propagating. Propagation gauges along with a electronic circuit unit help in obtaining the velocity of crack propagation.

3.5.1 Propagation Gauges

The propagation gauges consist of four thin strips of aluminum foil which are connected to each other at one end and are free at the other end (Fig. 3.20). The width of the strips vary from 1.0 mm to 2.5 mm. Extreme care is taken in cutting these strips from the aluminum foil.

All the strips of the gauge are bonded slightly ahead of the crack tip at the side face of the DCB specimen (Fig. 3.21). The gauge strips are successively numbered as 1, 2, 3, and 4 with gauge 1 being nearest to the crack tip. The distance between the outer edge of the bonded gauge strips and their position from the load application point are measured carefully under a travelling microscope with an accuracy of ± 0.01 mm. When the crack passes under a gauge strip they shear off. The shearing of each propagation gauge is recorded as a voltage drop on the oscilloscope with the help of an electronic circuit unit. On the oscilloscope screen a voltage drop starts as soon as the shearing of a propagation gauge completes. The time of of starting of a voltage drop is recored as the time of crack passing under the outer edge of the particulart gauge. On Nicolet oscilloscope this time is recoded within an accuracy of ± 0.5 μs and on Philips within an accuracy of ± 2.0 μs. By dividing the distance between the outer edge of two gauge strips by the time interval of their shearing the average crack velocity at the mid-point of thei gauges can be obtained.

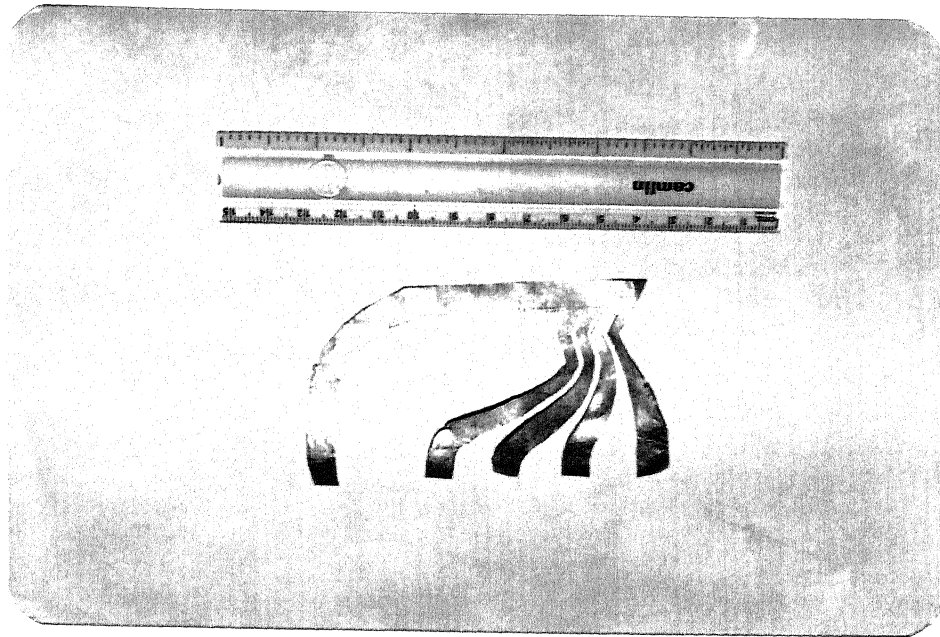The magnitude of voltage drops is different for each gauges. The
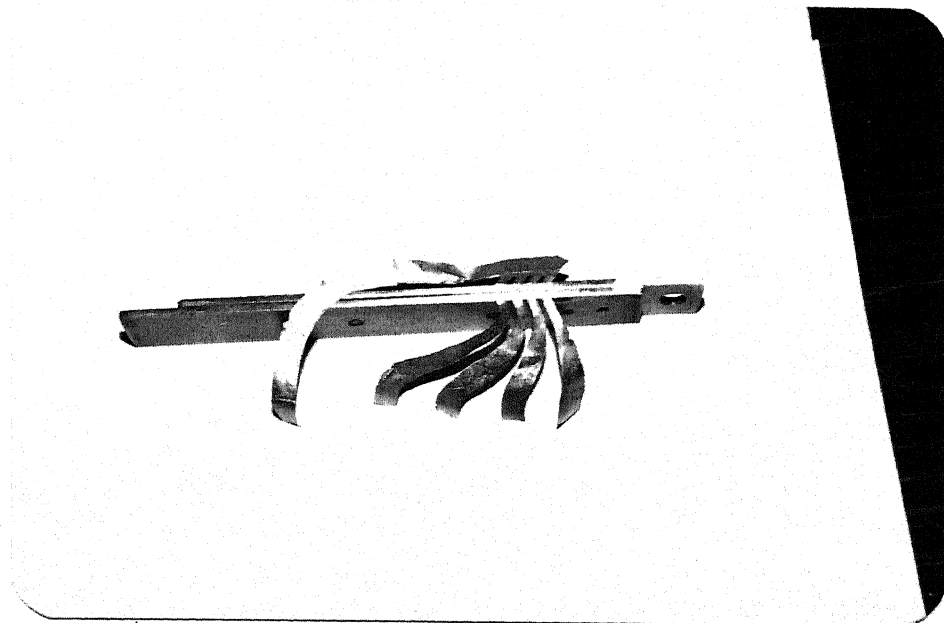
FIG. 3.20 PROPAGATION GAUGE

FIG. 3.21 PROPAGATION GAUGE BONDED TO THE SPECIMEN

46

ratio of the magnitude of voltage drop for gauges strips 1, 2, 3 and 4 is approximately 8:4:2:1 with the magnitude of voltage drop for gauge 1 being 800 mV. The ratio of voltage drops is such that the sum of no two (or three) voltage drops can be equal to the other drops or sum of other two drops. Thus if the shearing of two or more gauges is recorded in a single voltage drop they can be identified. Electronic circuit unit used for the propagation gauges is shown in Fig. 3.22.

Four kinds of propagation gauges were used. Three of them were used with steel DCB specimen and fourth was used with GFRP specimen. All the gauges were cut from thin aluminum foils. These aluminum foils are available in the market as food wrappers or in cigarette packs.

A. Propagation Gauges on Steel DCB Specimen

Shearing of propagation gauges is recorded as a voltage drop on the oscilloscope because of the discontinuity in the electrical contact between the two halves of sheared gauge strip. Since steel DCB specimen is electrically conductive the shearing of a gauge may not necessarily accompany a discontinuity in electrical contact. This requires a insulating layer between the gauge and the specimen. Three different kinds of insulating layer were tried. The gauges along with the insulating layer may be listed as :

    (a) Aluminum foil gauges with paper backing
    (b) Anodized aluminum foil gauges
    (c) Aluminum foil gauges with Kevlar fiber backing

Cigarette foils were used as paper backed aluminum foil gauges. These gauges are easy to use because the paper backing gives the thin gauge strips added strength. Also they bond well to the steel DCB specimen. The problem with this gauge could be due to fibrous nature of the paper backing. This might lead to fiber pullouts in the paper backing and hence not a claen shearing of the propagation gauges. Due to this factor the two halves of the gauge strip might remain in electrical contact even though the crack would have passed under
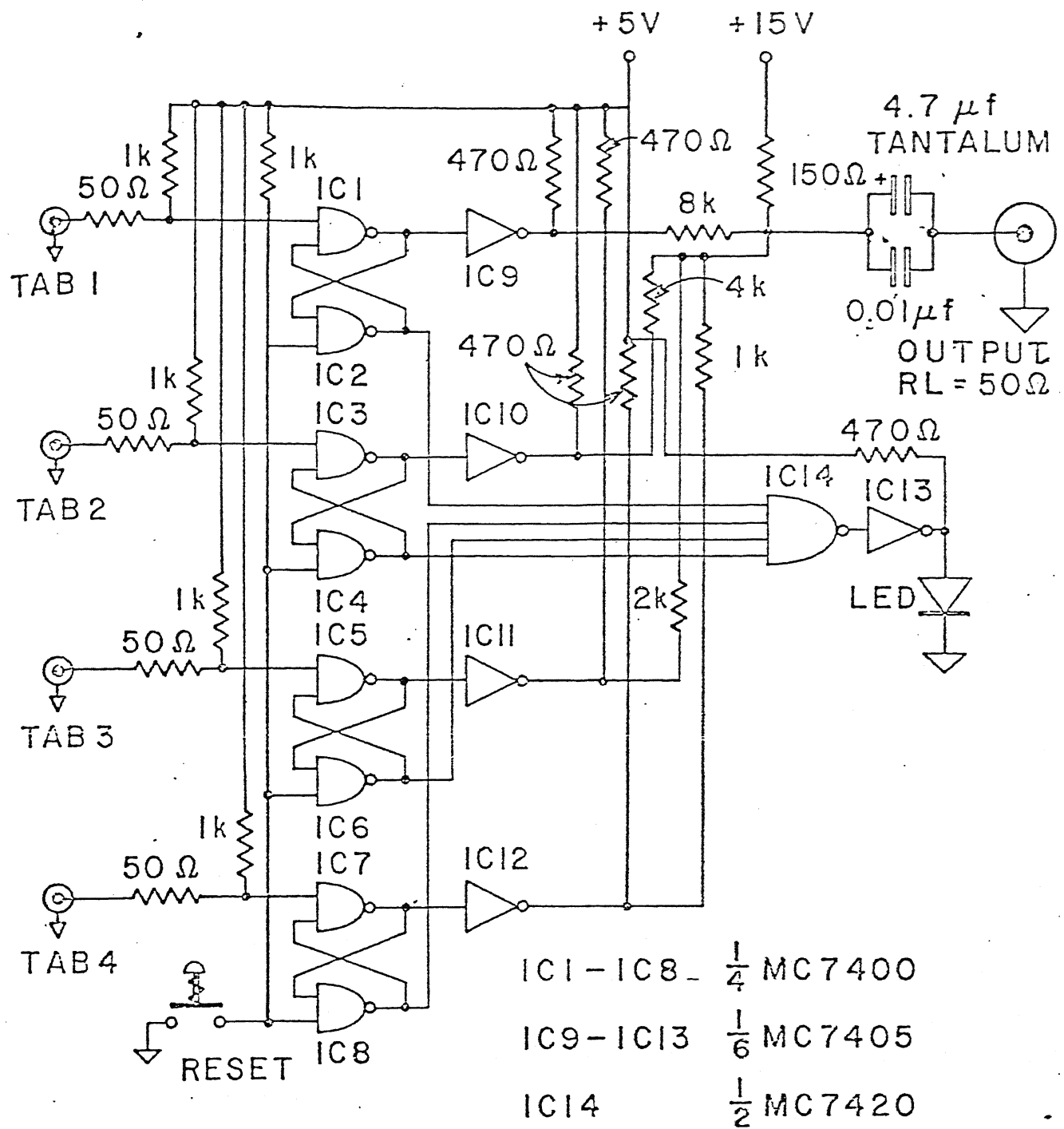
FIG. 3.22 ELECTRONIC CIOCUIT UNIT FOR PROPAGATION GAUGES

them.

In the second kind of propagation gauge the aluminum foils are anodized on the surface upto a depth of 15 to 20 μm. The core of the foil remains conductive. The anodizing was done with the help of AVM Udyog, Kanpur. The anodized coating (Al_2O_3) on the foil surface, which is nonconductive in nature, eleminated the need of any external insulatig layer. But these gauges were not very successful mainly because of two reasons : (i) the alumina (Al_2O_3) coating on the foil surface, which is a ceranic material, does not bond well to the steel specimen and (ii) the anodized foils become very brittle and it is very difficult to cut gauge strips from them.

In the third kind a layer of Kevlar fibers aligned along the crack of the specimen were used as the insulating layer between the gauge foilm and the steel specimen. Use of aligned Kevlar fibers as insulating layer eliminates the possibility of fiber pullouts during shearing of the gauges which is probably the main drawback of the paper backed aluminum foil gauges. The problem with these gauges is related to thier preparation. It is very difficult to align the fibers exactly along the crack. Also the fiber layer is thick and hence the shearing of gauge strip may not match with the propagation of the crack.

B.   Propagation Gauge on the DCB Specimen of GFRP

Since GFRP is non-conductive there is no need of any insulating layer between the gauge and the specimen. The aluminum foil is directly used as propagation gauge.

3.5.2 Bonding of Propagation Gauges

Extreme care is taken in bonding propagation gauge to the side face of the DCB specimen as the gauge strips are very thin (1.0 mm to 2.5 mm) and break very easily. Epoxy LY 556 and hardener HY 951 are used in bonding. Two are mixed well in the ratio of 10:1 by weight. The

ambient temperature is kept at 55° C to 60° C with the help of an infra-red heater. Localised pressure is applied while the curing takes place.

3.5.3 Crack Velocity

Figure 3.23 shows a typical record of voltage drops corresponding to the shearing of propagation gauges along with the stress pulses in the load bar. The starting time of the voltage drop corresponds to the completion of the shearing of a specific propagation gauge. The reference time is taken as the time when the incident pulse in the load bar reaches the specimen end of the bar. On the experimental trace it is at the mid point of the beginning of the incident pulse and that of the reflected pulse. Position of each gauge strip with respect to load application point is measured very carefully with the help of a travelling microscope.

Propagation gauge position (crack length) are plotted against the time of their shearing (Fig. 3.24). A first order best fit to this curve (shown in the figure by dashed lines) gives the idea about the advancement of the crack with time. The slope of this best fit curve gives a mean crack velocity. The equations governing this first order best fit curve is given by

$$a = 20.66 + 0.187.t$$

where a is the crack length (mm) and t is time (μs). Thus the crack velocity, v_{cr} would be :

$$v_{cr} = da/dt = 0.187 \ mm/\mu s \ (\ or \ 187 \ m/s \ )$$

3.5.4 Monitoring Crack Propagation with Strain Gauges

Two preliminary experiments were conducted using strain gauges instead of propagation gauges to monitor the stress pulses travelling along the rear cantilever of the DCB specimen. The strain gauges used in these experiments have a gauge length of 0.2 mm and a gauge
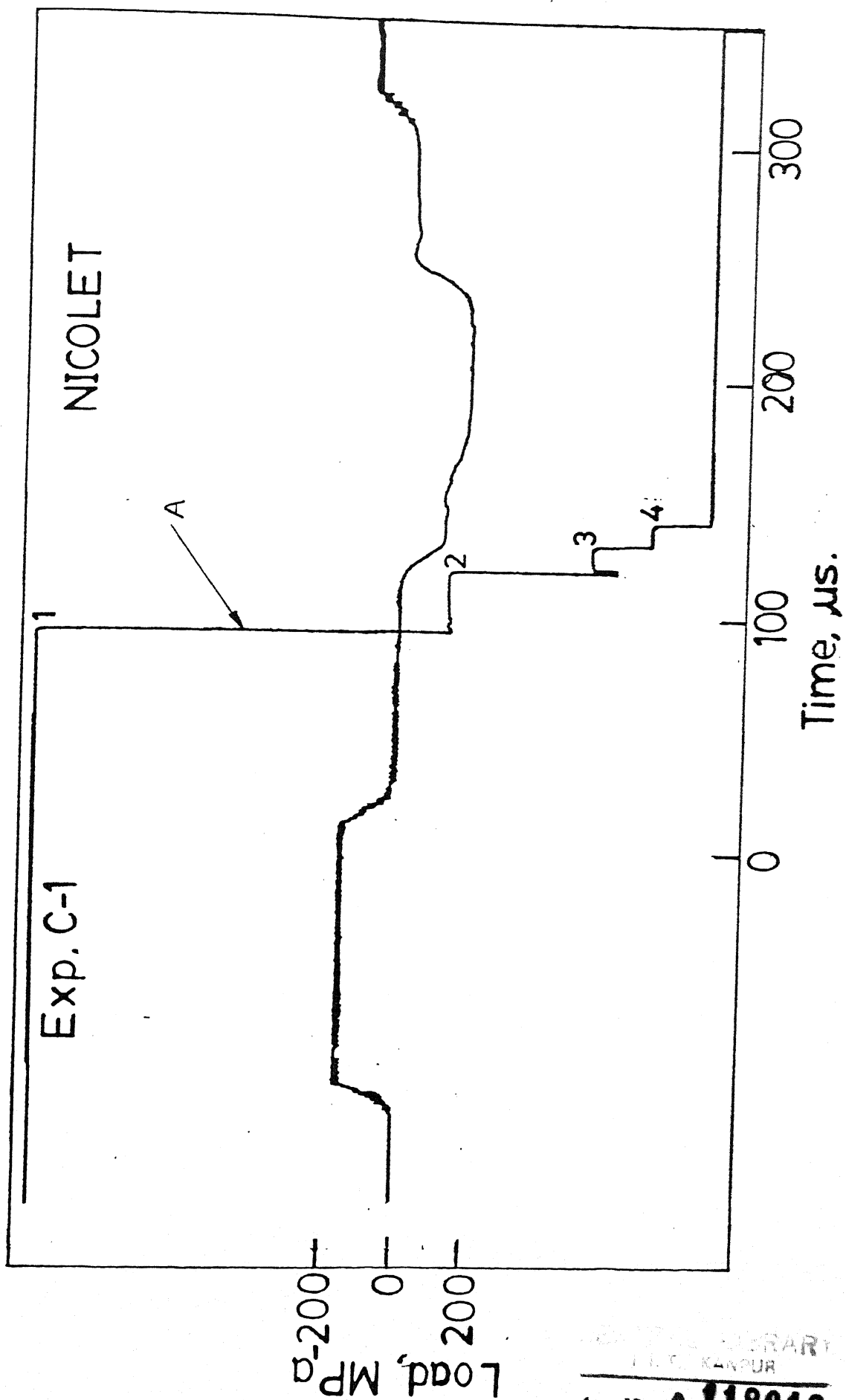
FIG. 3.23 A TYPICAL RECORD OF VOLTAGE DROPS (TRACE A) CORRESPONDING TO THE SHEARING OF PROPAGATION GAUGES AND STRESS PULSES IN THE LOAD BAR

51
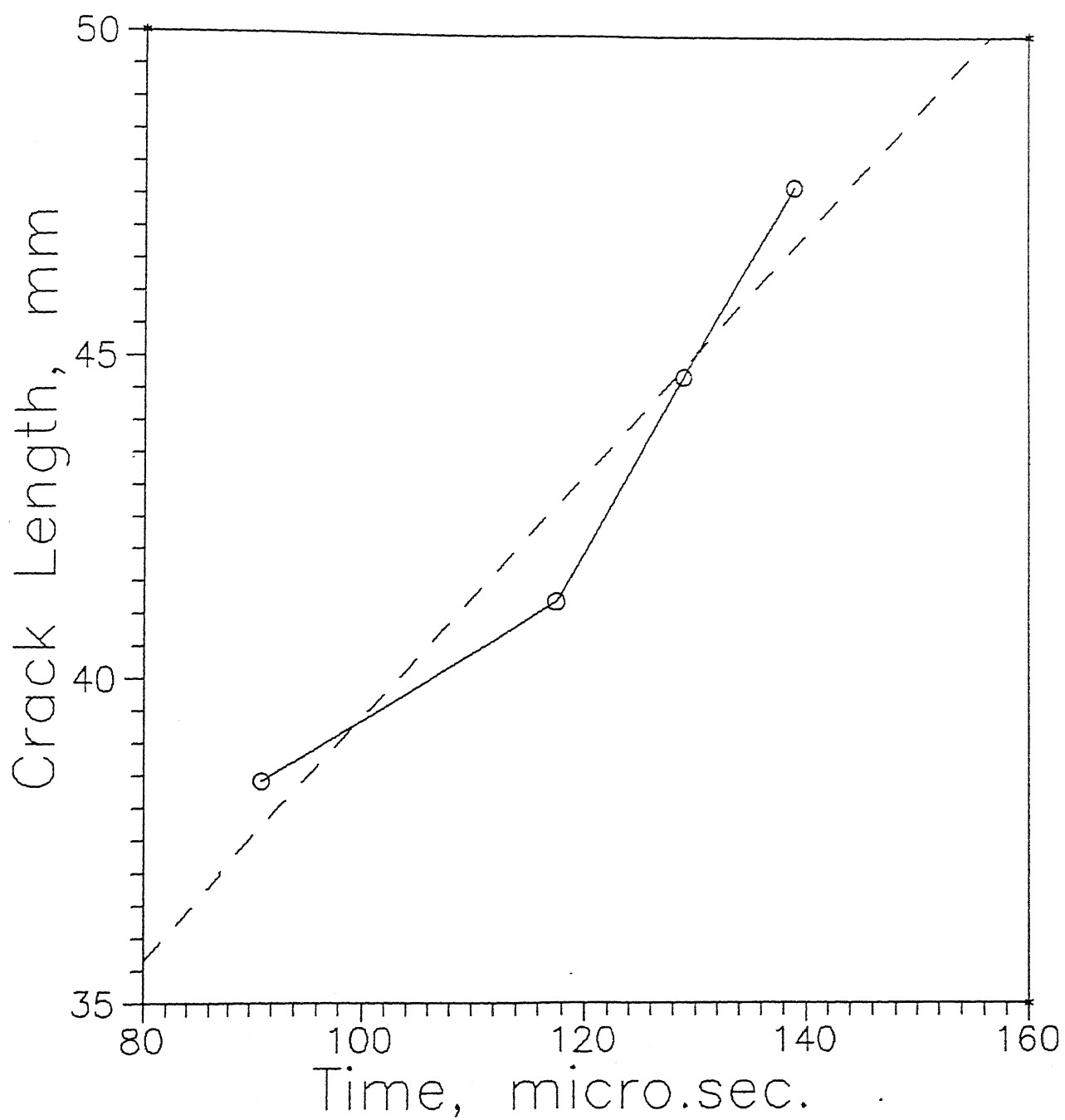
FIG. 3.24   CRACK LENGH VS. TIME PLOT FOR THE EXPERIMENTAL
RECORD OF FIG. 3.23

width of 1.5 mm.   The base of the strain gauge is rectangular with dimensions 3.5 mm x 2.5 mm.   Its resistance is 120$\pm$0.3 Ω and gauge factor (G.F.) is 2.07.   Fig 3.25 shows the details of the strain gauge.These strain gauges are supplied by Tokyo Sokki kenyujo Co. Ltd., Japan.

In the first experiment only one strain gaugewas used.   The strain gauge was bonded on the outer face of the rear cantilever at 3.8 mm from the crack tip.   This was done to find the time taken by flexural wave, in the rear cantilever, to reach the crack tip.   In the second experiment two strain gauges were used.   They were bonded on the outer face of the rear cantilever near the location of propagation gauges.   The first gauge was bonded at 3.7 mm from the crack tip and second gauge 1.3 mm further than that.   Since only two channels were available on the oscilloscope for recording, the stress pulses in the load bar were not recorded.   The purpose of doing this experiment was to find out the speed with which the flexural wave travels beyond the crack tip.
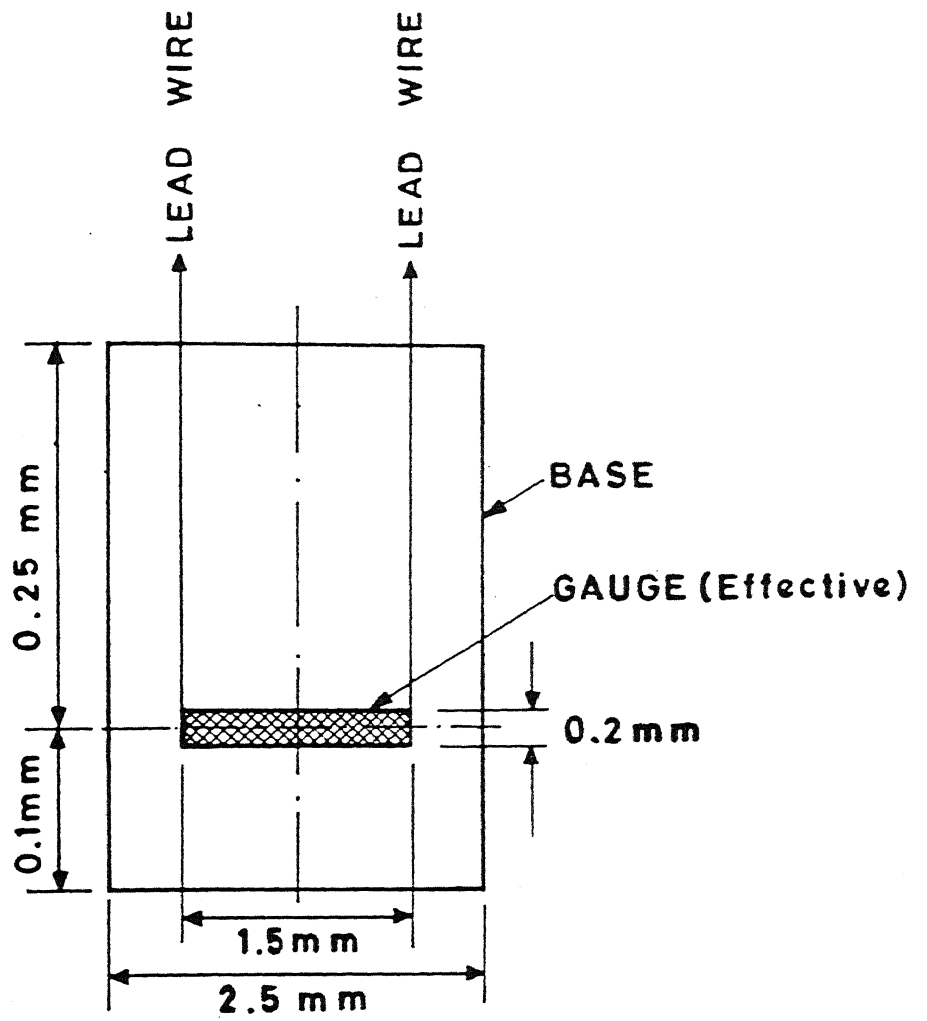
FIG. 3.25 DETAILED FIGURE OF THE STRAIN GAUGE

4. EXPERIMENTAL RESULTS AND DISCUSSION

4.1 INTRODUCTION

This chapter deals with experimental results needed to evaluate the dynamic interlaminar fracture toughness of DCB specimen through experimental-cum-numerical technique. In the impact set up the load bar imparts impact energy to one cantilever of the DCB specimen and propagation gauges monitor crack velocity (Chapter 3).

Four kinds of propagation gauges and two kinds of DCB specimen were tried in this study. Various combinations used are :

A. Steel DCB specimen with paper backed aluminum foil propagation gauges,

B. Steel DCB specimen with anodized aluminum foil propagation gauges,

C. Steel DCB specimen with paper backed aluminum foil propagation gauges and the load element,

D. Steel DCB specimen with Kevlar fiber backed aluminum foil propagation gauges and the load element,

E. DCB specimen of GFRP with aluminum foil propagation gauges and the load element.

Experimental results of above mentioned combinations have been discussed in the following sections.

4.2 STEEL DCB SPECIMEN WITH PAPER BACKED ALUMINUM FOIL GAUGES

In this combination the steel DCB specimen were prepared by bonding

two steel strips with epoxy. Aluminum foil strips backed with paper (Sec. 3.5.1) as insulating layer between the specimen and the gauge were bonded on one of the two side faces of the specimen to determine the crack velocity. Nine experiments were conducted in this category. The results of Exp. A-1 has been discussed extensively giving details of data processing.

Experiment A-1 to A-5.

Fig 4.1a shows experimentally recorded stress pulses in the load bar and the voltage drops corresponding to shearings of propagation gauges for experiment A-1. Trace A in Fig 4.1a shows the incident and reflected stress pulses and trace B the voltage drops. The incident pulse is compressive and reflected pulse is tensile in nature. The reference for time varying experimental records is taken as the time when the incident stress pulse reaches the specimen end of the load bar. On the oscilloscope trace it lies at the mid-point of the beginning of the incident pulse and the beginning of reflected pulse.

The incident stress pulse has a magnitude of 202.4 MPa for a duration of 101.5 μs. It has a rise time of 16.5 μs and a fall time of 28.5 μs. Thus the total duration of the pulse is 146.5 μs. As explained in Sec. 3.4.4 load transfer to the rear cantilever of the DCB specimen is obtained by superposing the incident and the inverted reflected pulse, taking their difference and multiplying with the area of cross-section of the load bar. The shaded area in Fig. 4.1b corresponds to the difference of magnitude between the incident and the reflected pulses. The load pulse imparted to the specimen, hence obtained, has a duration of 44.8 μs and a peak value of 11.8 kN. This is shown in Fig. 4.2. Energy corresponding to this load pulse is 0.267 J. Since this load pulse is the difference of two large quantities namely incident and reflected stress pulses in the load bar it is approximate and so is the energy associated with it.

Voltage drops in trace B of Fig. 4.1a show the time of the breakages

(a)

EXP. A-1   PHILIPS

B

A

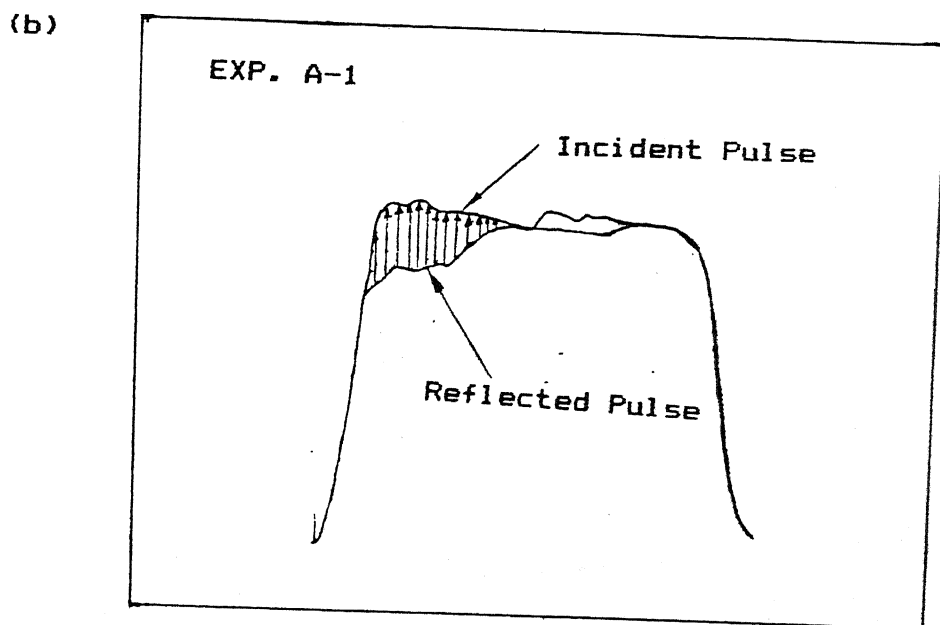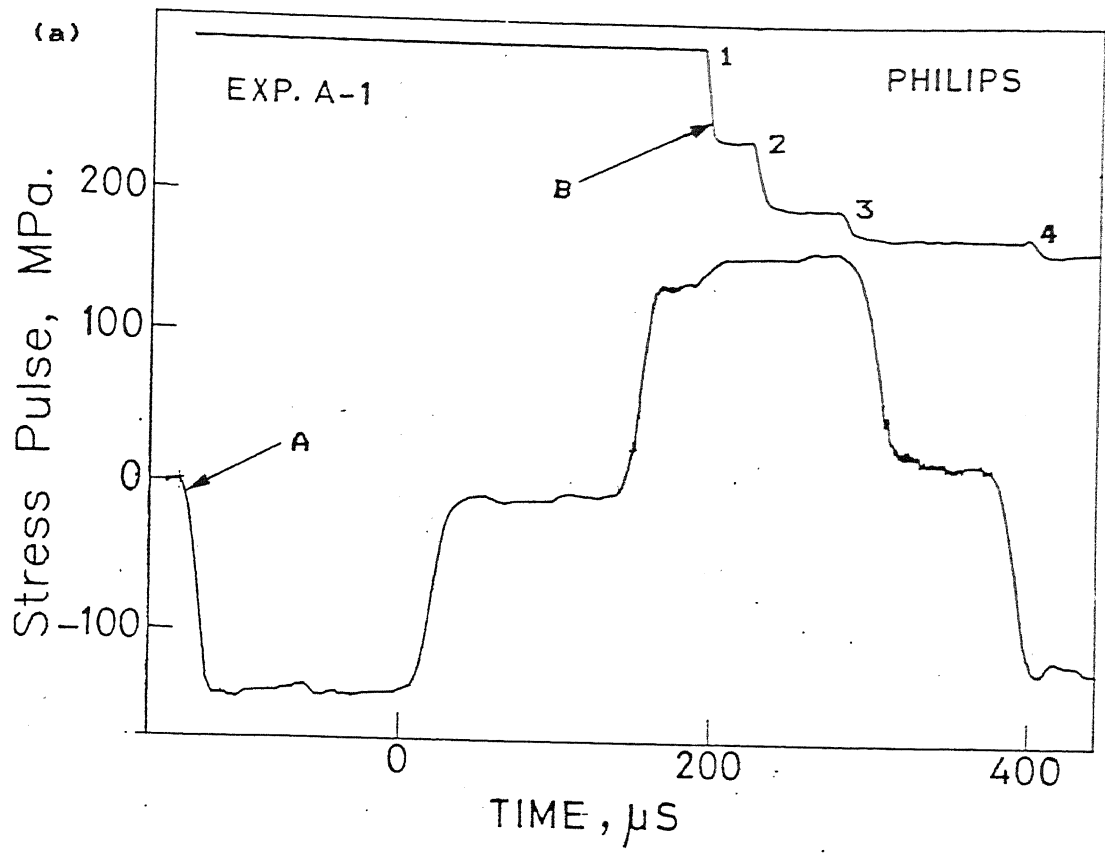TIME, μS

(b)

EXP. A-1

Incident Pulse

Reflected Pulse

FIG. 4.1 — (a) Experimental records, and (b) superposed
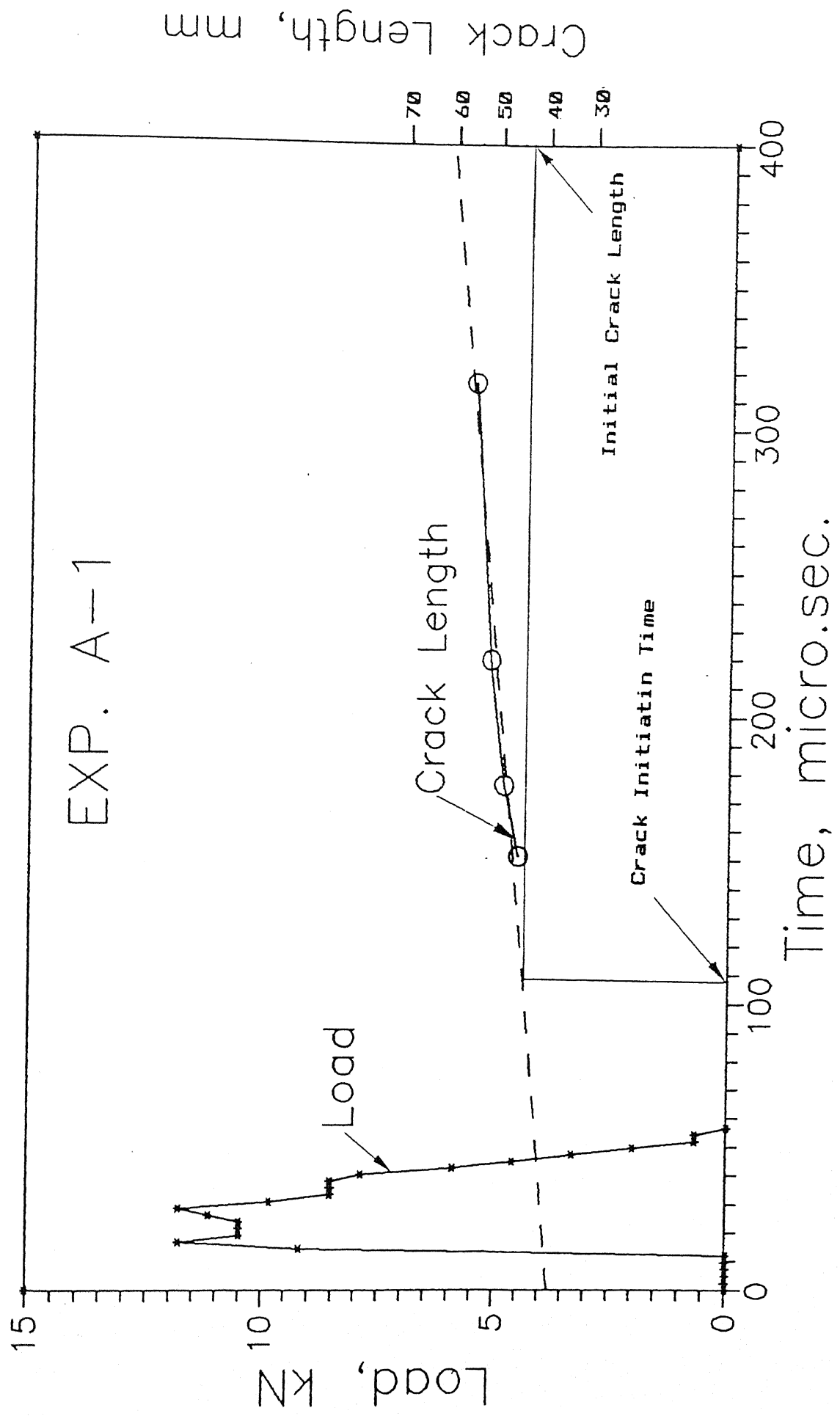incident and reflected pulses for Exp. A-1.

FIG. 4.2 - Load pulse imparted to the specimen and crack length vs. time plot for Exp. A-1.

of propagation gauges. Each drop corresponds to the breakage of specific propagation gauge indicated in the figure. Propagation gauges 1, 2, 3 and 4 were bonded successively in front of the crack tip, with gauge 1 being nearest to the crack tip. The magnitude of voltage drop for gauges 1, 2, 3 and 4 has a ratio of 8:4:2:1. As the crack grows and passes under gauge 1 the gauge shears off. This causes a drop of 0.8 V in trace B. This voltage drop starts when far edge of the gauge strip shears off causing discontinuity in electrical contact. Similar voltage drops with different magnitude take place when the crack passes under other gauge strips causing them to shear. It can be noted that two different oscilloscopes were used for different experiments. Some experiments were conducted using Philips oscilloscope and others using Nicolet oscilloscope. The relative advantages and disadvantages of the oscilloscopes have been discussed in detail in Sec. 3.4.6. Philips oscilloscope had one major disadvantage against Nicolet oscilloscope. On Nicolet digital oscilloscope the voltage drop after shearing of a propagation gauge took 0.5 μs equivalent to two consecutive points on the time axis. Whereas on Philips this sharp voltage drop changed into a ramp which took 8 to 12 μs, equivalent to five to seven consecutive points on the time axis even though the time interval between two consecutive points was only 2 μs. Because of this drawback of Philips oscilloscope, it could not record the voltage drops distinctly if they occurred within a time interval of 8 μs.

By knowing the position of each propagation gauge and time of their breakage, the crack velocity distribution can be obtained. Trace of instantaneous crack length vs. time along with the load pulse has been shown in Fig. 4.2. The dashed line in Fig. 4.2 is the first order best fit of crack length vs. time plot. Approximate crack initiation time can be obtained from this best fit curve as shown in Fig. 4.2. Also the slope of this best fit curve gives a mean value of crack velocity.

The experimental record of incident and reflected stress pulses in the load bar and the time of breakage of propagation gauges for

experiments A-2, A-3, A-4 and A-5 have been shown in Fig. 4.3.
These records have been processed in the same way as those for
experiment A-1 to get the load transfer to the rear cantilever of
the DCB specimen, the crack velocity distribution and the crack
initiation time. Crack length plotted against time along with the
load pulse imparted to the DCB specimen for experiments A-2, A-3,
.A-4 and A-5 has been shown in Fig. 4.4. Table 4.1 gives the
initial crack length, position of propagation gauges, their breakage
time and crack initiation time, obtained from the first order best
fit of the crack length vs. time plot, for experiments A-1, A-2,
A-3, A-4 and A-5.

TABLE 4.1. Initial crack length, location of propagation gauges and
their breakage time for experiments A-1 to A-5.

EXP. No.	Initial Crack Length (mm)	Position of Propagation Gauges from the Load Application Point. (mm)				Breakage Time of Propagation Gauges. (μs)				Crack Initiation Time. (μs)
		1	2	3	4	1	2	3	4	
A-1	43.4	45.2	48.4	51.5	55.2	151.0	175.8	219.4	316.2	106.6
A-2	47.0	50.7	53.6	56.9	59.6	142.0	159.0	241.0	248.0	86.7
A-3	42.8	51.0	61.2	71.1	81.3	264.0	352.2	455.0	513.0	198.7
A-4	49.9	51.6	55.0	57.8	60.6	215.5	231.0	235.5	245.5	211.6
A-5	42.0	49.4	52.6	55.8	59.2	33.0	35.5	44.0	59.0	10.3

In Exp. A-5 the breakage time of first gauge is much early, 33 μs,
as compared to those for other experiments. After the experiment
was completed and cracked surface observed, it was found that the
bonding material used for this experiment was not of good quality.

Flexural waves take about 8 to 10 μs to start loading the crack tip
whereas the crack initiation time for experiments A-1 to A-4 range
from approximately 85 μs to 200 μs. This can be explained by
assuming that the crack initiation takes place after the crack tip
is loaded again by the load pulses reflected either from the loading
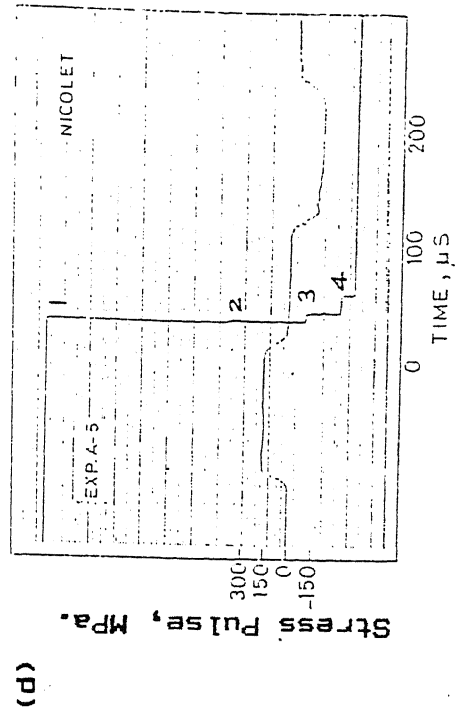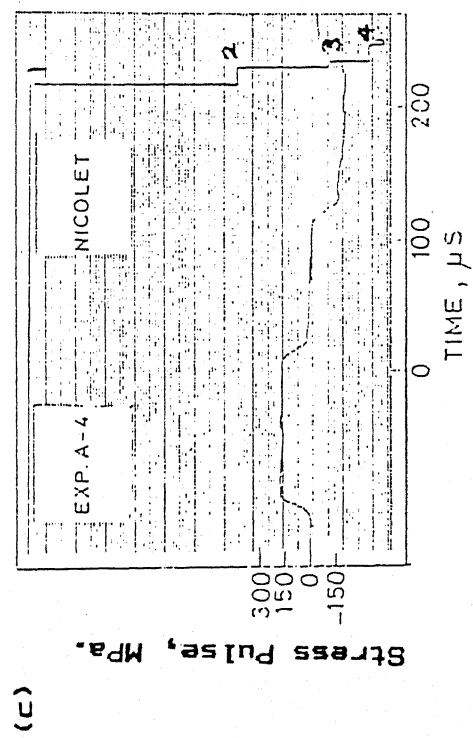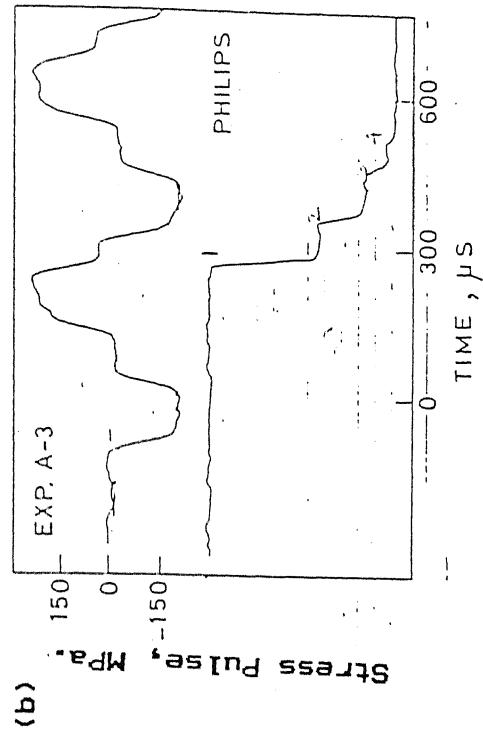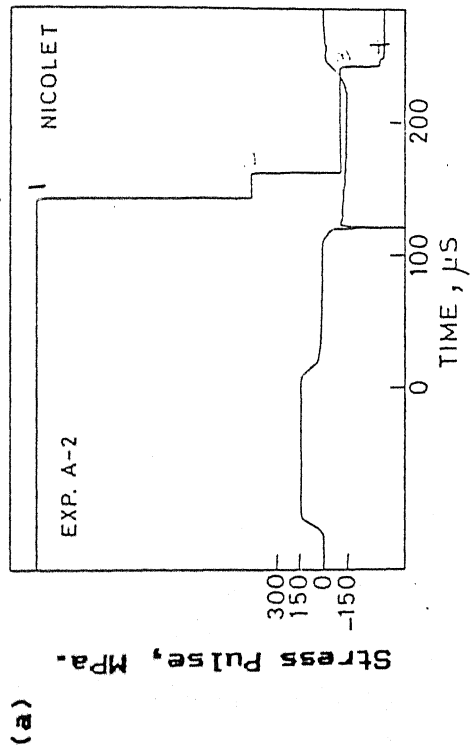end of the cantilever or from the far end of the specimen. Table

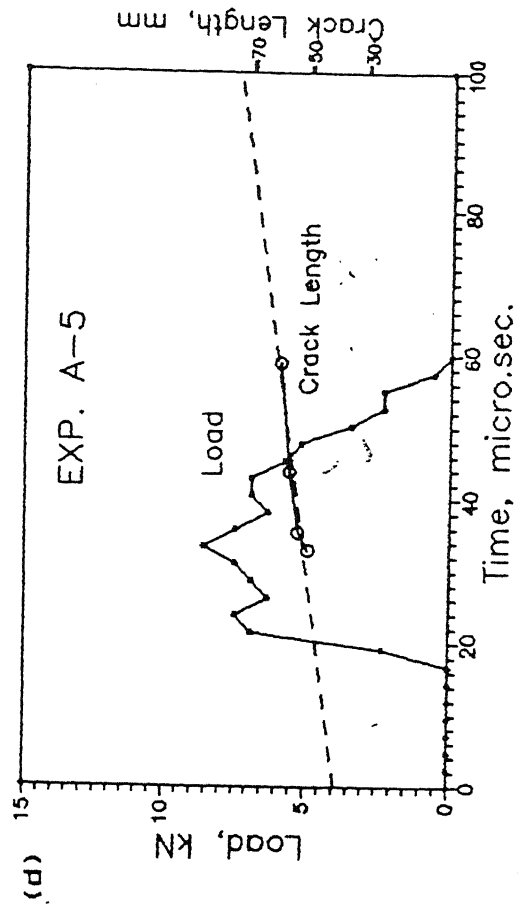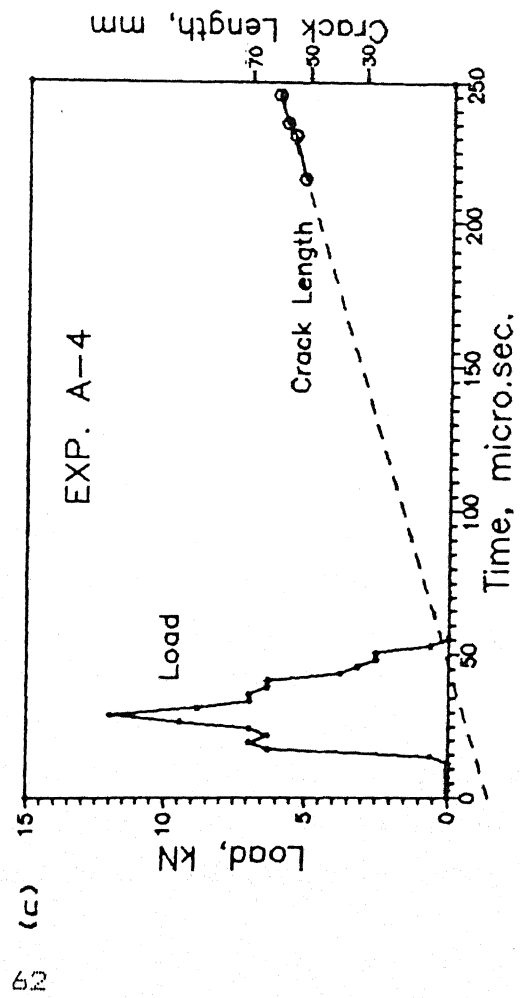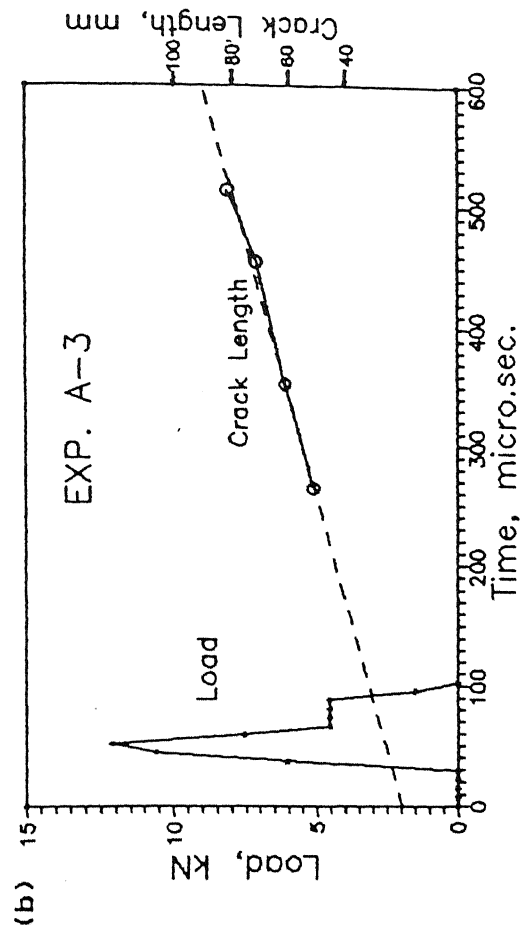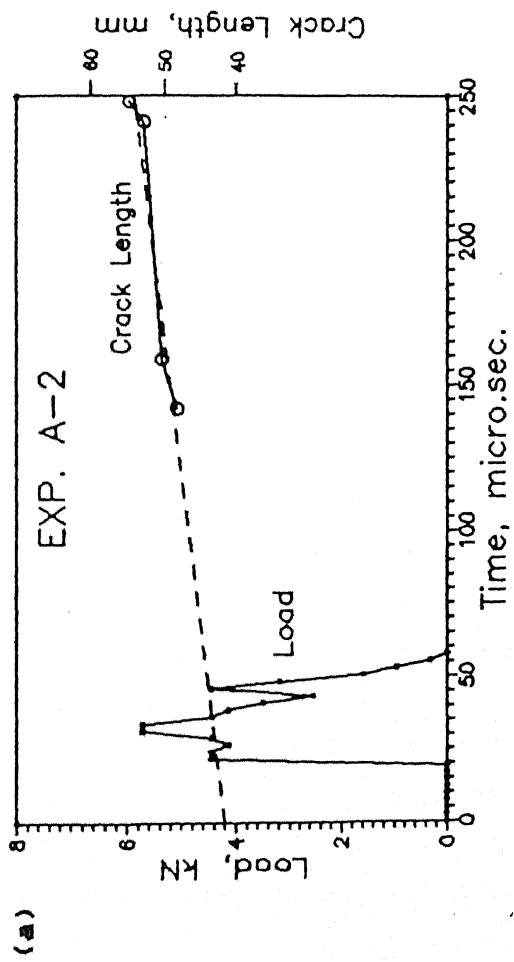FIG. 4.3 — Experimental records of Exp. A-2, A-3, A-4, and A-5.

FIG. 4.4 - Load pulse imparted to the specimen and crack length vs. time plot for Exp. A-2, A-3, A-4 and A-5.

62

4.2 gives the magnitude of the incident pulse in the load bar; the peak value, the duration and the energy associated with the load pulse imparted to the specimen; and the crack velocity obtained from the slope of the first order best fit of crack length vs.time plot for experiments A-1 to A-5.

TABLE 4.2. Magnitude of incident pulse in the load bar, details of load pulse imparted to the specimen and the crack velocity for experiments A-1 to A-5.

EXP. No.	Magnitude of Incident pulse in the Load Bar. (MPa)	Imparted Load pulse.			Best Fit Crack Velocity (m/s)
		Peak Value (kN)	Duration (μs)	Energy (J)	
A-1	202	11.8	44.8	0.27	57
A-2	146	5.7	38.5	0.05	74
A-3	203	12.1	73.4	0.29	117
A-4	173	12.0	43.5	0.15	303
A-5	166	8.6	43.0	0.13	342

There is no direct correspondence between the crack velocity obtained from best fit curve and the energy or the peak value of the load pulse imparted to the impact face of specimen cantilever.   A load pulse with high peak value and high energy associated with it can cause a high or low crack velocity.

Crack velocity, at the mid-point of two gauge strips,can be obtained by dividing the distance between the gauge strips by the time interval in their breakage. This gives three crack velocity values at three different crack lengths.   These crack velocities are plotted against the crack length for experiments A-1, A-2, A-3 and A-4 and are shown in Fig. 4.5. It can be observed that the crack velocity is very high ranging from 2.0 % to 20.0 % of the Rayleigh wave velocity. From the figure it can also be observed that the crack velocity variation over the crack length does not follow any
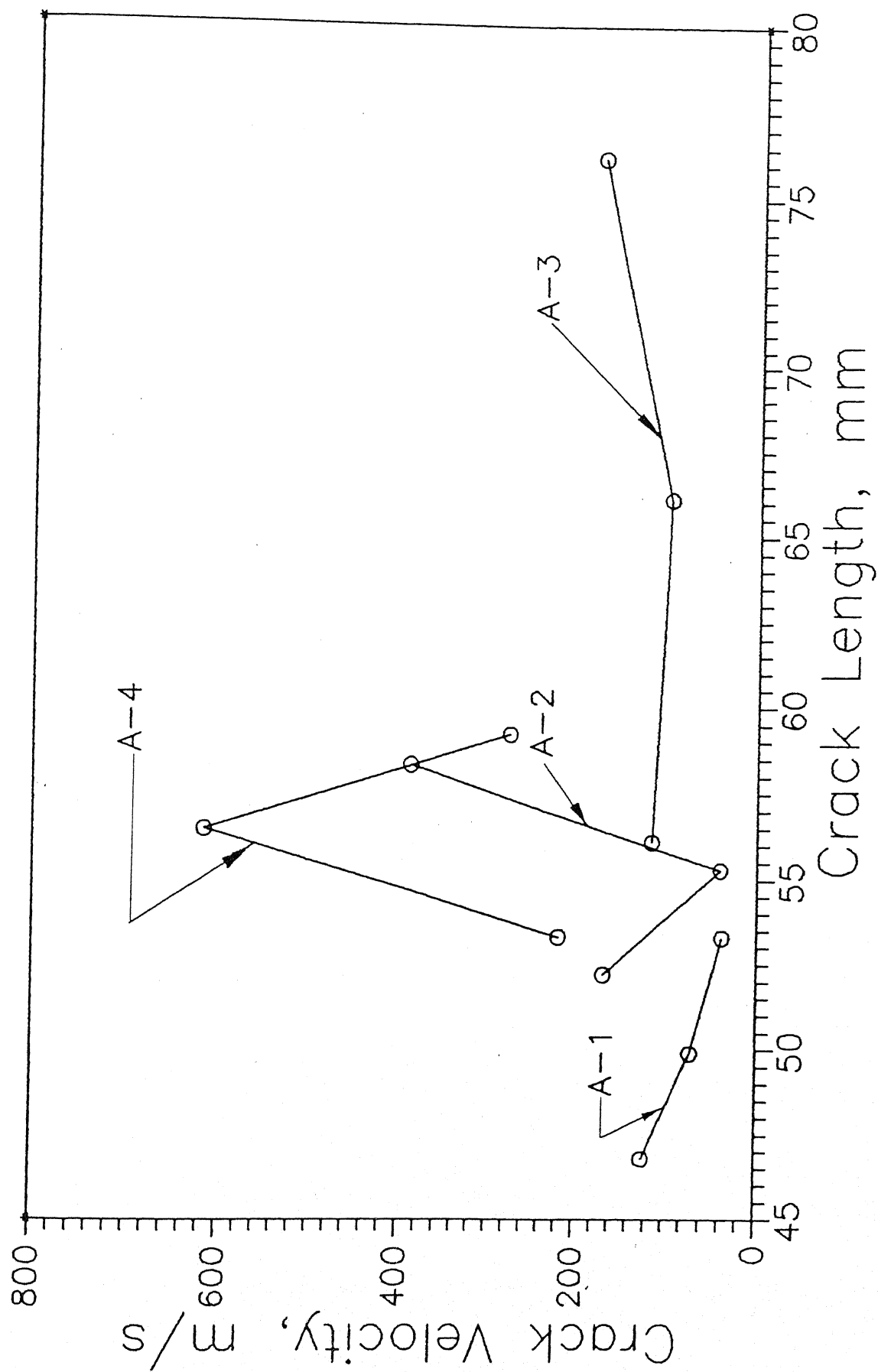
FIG. 4.5 - Crack velocity at the mid-point of propagation gauges vs. crack length plot for Exp. A-1, A-2, A-3 and A-4.

fixed pattern. In experiment A-1 the crack velocity decreases with increasing crack length, in experiments A-2 and A-3 first it decreases and then again increases and in experiment A-4 the crack velocity increases first and then decreases.

Experiment A-6 to A-9.

In all of these four experiments the propagation gauges either did not shear in the expected sequence or shearing of two or more gauges were not distinguishable. The experimental record of the shearing of propagation gauges and the incident and reflected pulses in the load bar for experiments A-6 to A-9 are shown in Fig. 4.6.

Normally as the crack advances, the propagation gauges should shear in the sequence of 1, 2, 3 and 4. But in experiments A-6, A-7, and A-9 there is a change in this normal sequence of shearing of propagation gauges. Also in experiments A-6 and A-9 the shearing of two propagation gauges are indistinguishable. In experiment A-8 only three gauges were used and shearing of all these three gauges were recorded in a single voltage drop and hence indistinguishable. The initial crack length, position of propagation gauges and their breakage time are given in Table 4.3.

TABLE 4.3. Initial crack length, location of propagation gauges and their breakage time for experiments A-6 to A-9.

EXP. No.	Initial Crack Length (mm)	Position of Propagation Gauges from the Load Application Point. (mm)				Breakage Time of Propagation Gauges. (μs)			
		1	2	3	4	1	2	3	4
A-6	42.7	49.4	54.6	60.4	64.7	233.0	277.0	254.0	254.0
A-7	42.7	46.6	51.8	56.8	62.1	152.2	288.2	240.2	310.2
A-8	42.5	44.5	51.0	54.6	—	87.0	87.0	87.0	—
A-9	42.9	47.0	51.8	55.2	59.7	202.4	202.4	161.4	234.0

All these experiments were conducted using Philips oscilloscope. As
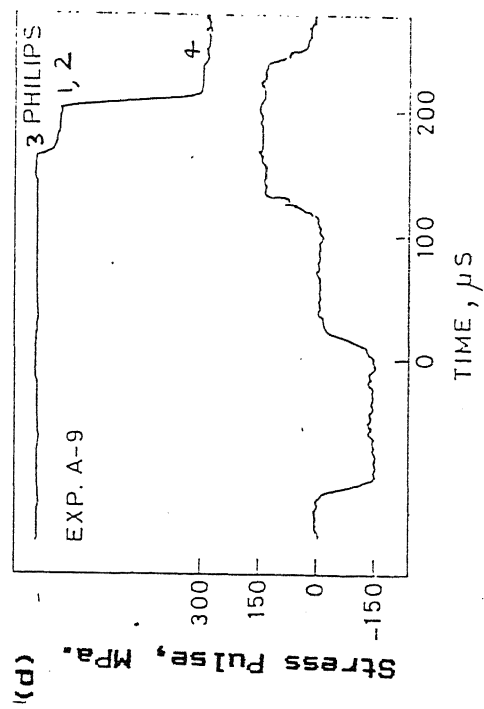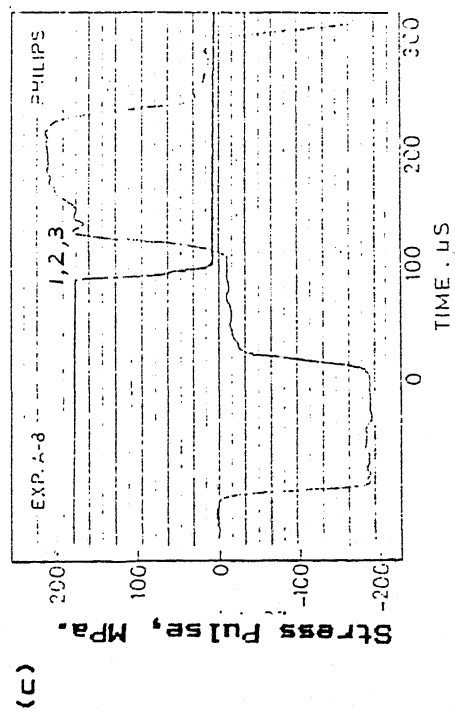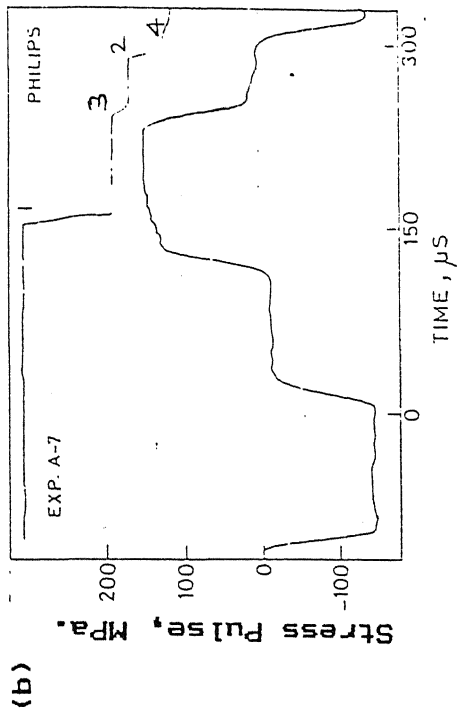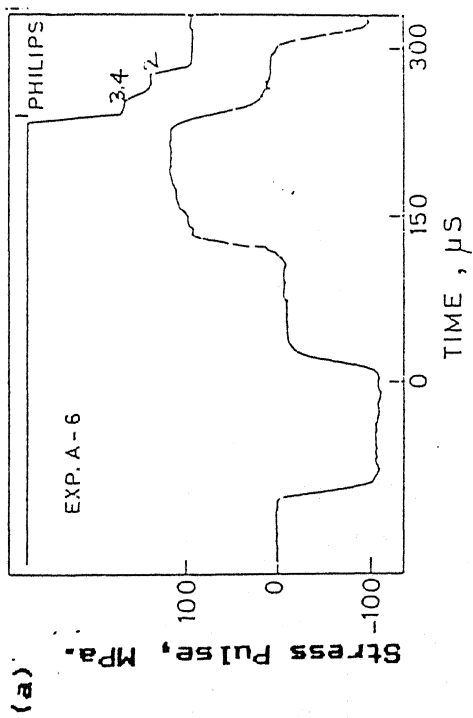
FIG. 4.6 – Experimental records of Exp. A-6, A-7, A-8 and A-9.

explained earlier in this section, a sharp voltage drop, corresponding to the shearing of a propagation gauge, changed into a ramp which took 8 to 12 μs involving five to seven consecutive points. If two gauges shear within an interval of 8 μs they will be recorded in a single drop and hence cannot be distinguished. This explains the indistinguishable drops of two or more propagation gauges.

As far as change in the order of shearing of propagation gauges is concerned it is not fully understood. Still a plausible explanation for this might be as follows. The flexural load pulse applied to the specimen might travel along the impacted cantilever of the specimen as a series of pulses with positive or negative curvature. The pulse of positive curvature has a tendency to open the crack whereas the pulse with negative curvature has a closing tendency. This is supported by the numerical analysis. As in the case of experiments A-1 to A-4 the breakage time of propagation gauges is late in this set of experiments also. There is a possibility that the crack propagation starts, when the flexural pulses reflected from the ends of the specimen reach the crack tip. This might create a situation in which there is compression between two cantilevers of the DCB at a gauge nearer to the crack tip and tension at a propagation gauge away from the crack tip. Due to this kind of distribution of flexural load pulse a new crack might open up away from the tip of pre-crack. Then the propagation gauge which is away from the crack tip would shear before the one which is nearer to the crack tip.

Table 4.4 gives the magnitude of the incident pulse in the load bar and; the peak value, the duration and the energy associated with the load pulse imparted to the specimen for experiments A-6 to A-9.

TABLE 4.4. Magnitude of incident pulse and details of load pulse imparted to the specimen for experiments A-6 to A-9.

EXP. No.	Magnitude of Incident pulse in the Load Bar. (MPa)	Imparted Load pulse.		
		Peak Value (kN)	Duration (μs)	Energy (J)
A-6	110	5.9	55.0	0.07
A-7	145	7.9	47.0	0.10
A-8	185	11.5	50.8	0.26
A-9	150	6.25	35.2	0.06

The crack velocity for none of these four experiments could be computed because of the change in the order of the shearing of propagation gauges. Experimental records of all the four experiments were processed for the load transferred to the specimen. Fig 4.7 shows the load pulse imparted to the specimen for this set of experiments.

4.3 STEEL DCB SPECIMEN WITH ANODIZED ALUMINUM FOIL GAUGES

Although a plausible reason for the non sequential shearing of propagation gauges has been given in Sec. 4.2, it was felt that the fibrous paper backing of the propagation gauges might be the reason behind the change in order of the shearing of propagation gauges (Sec. 3.5.1). Considering this factor it was decided to replace the paper backed aluminum foil propagation gauges by anodized aluminum foils (3.5.1) to make their surface electrically nonconductive. Since the foil was anodized only up to 15 to 20 μm under the surface, their core remained conductive and also the need of any insulating layer between the gauge and the specimen was eliminated. The drawback with the anodized aluminum foil was that it became very brittle and the gauges sheared during the setting up of the experiments. Three experiments were conducted in this category but only once could all four strips of the propagation gauge be bonded to the specimen edge. Also the anodized foils did not bond very well to the specimen.
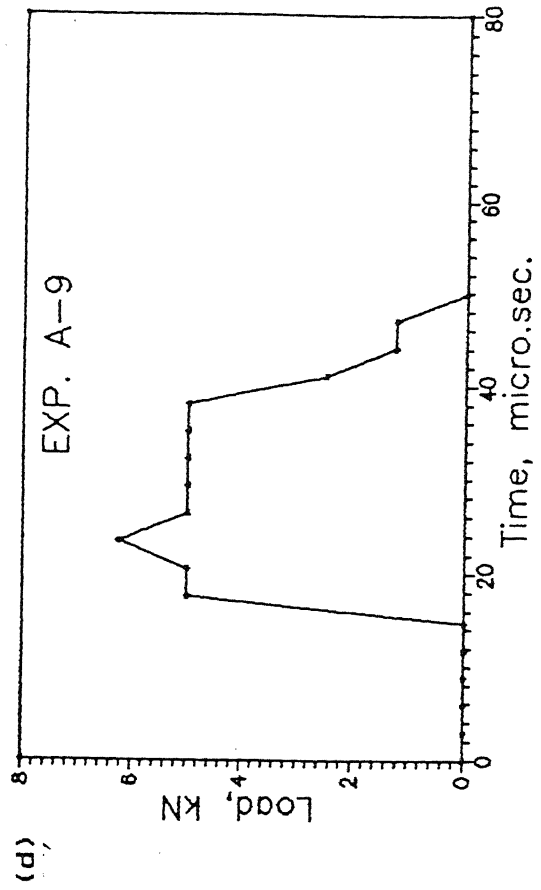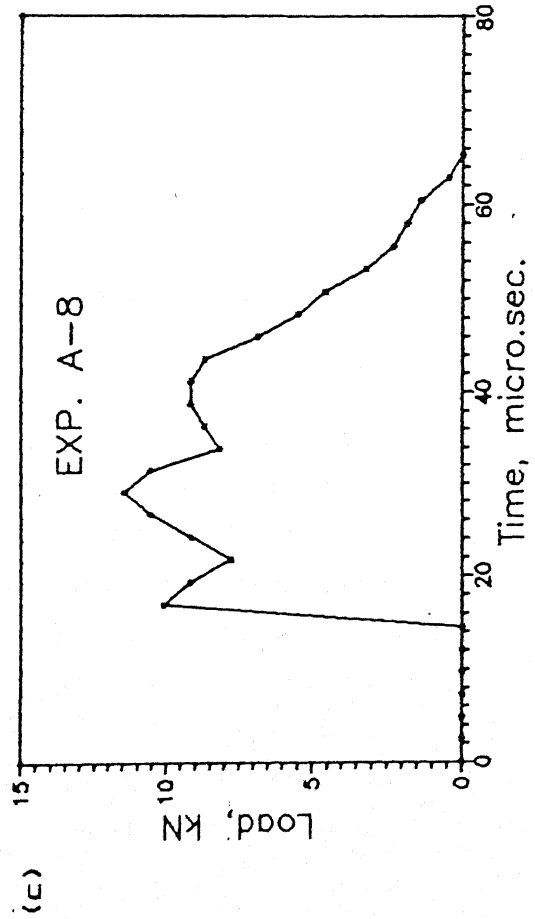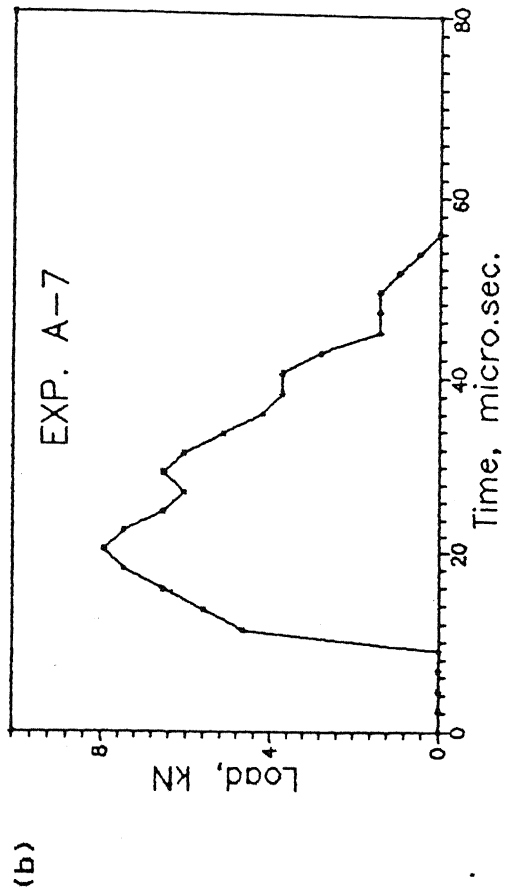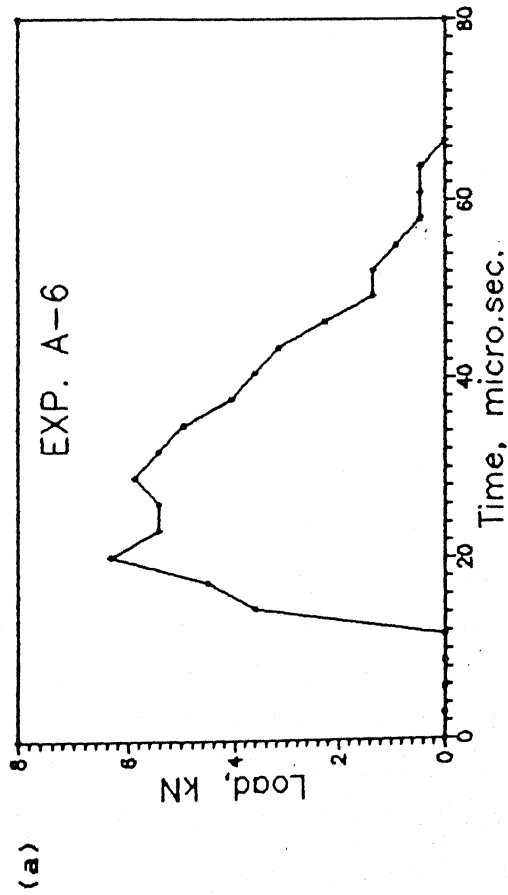
FIG. 4.7 - Load pulse imparted to the specimen for Exp. A-6, A-7, A-8 and A-9.

Experiment B-1 to B-3.

In all these three experiments the shearing of gauge 1 did not show up on the oscilloscope screen. Also in one of the experiments there was a change in the normal sequence of shearing of propagation gauges.

Figure 4.8 shows the experimental record of stress pulses in the load bar and the voltage drops corresponding to the shearing of propagation gauges for experiments B-1, B-2 and B-3. Table 4.5 gives the position of propagation gauges, their breakage time and the initial crack length.

TABLE 4.5. Initial crack length, location of propagation gauges and their breakage time for experiments B-1, B-2 and B-3.

EXP. No.	Initial Crack Length (mm)	Position of Propagation Gauges from the Load Application Point. (mm)				Breakage Time of Propagation Gauges. (μs)			
		1	2	3	4	1	2	3	4
B-1	42.6	48.2	53.4	57.8	61.5	—	824.0	358.0	506.0
B-2	42.5	47.6	52.0	—	59.5	—	89.7	—	261.7
B-3	42.6	43.1	47.3	—	—	—	201.0	—	—

As seen in Fig 4.8 shearing of gauge 1 is not recorded on the oscilloscope for any of the three experiments of this set. This might have been because gauge 1 did not shear within the taken time window. In experiment B-1 there is a change in sequence of shearing of gauges. In experiment B-2 only three gauges could be used and shearing of only two gauges were recorded. In experiment B-2 only two gauges could be bonded to the specimen and shearing of only one gauge was recorded on the oscilloscope. The experimental record of these experiments was processed for the load pulse imparted to the specimen which are shown in Fig. 4.9. The magnitude of the incident stress pulse in the load bar and details of the load pulse imparted to the specimen for this set of experiments are given in Table 4.6
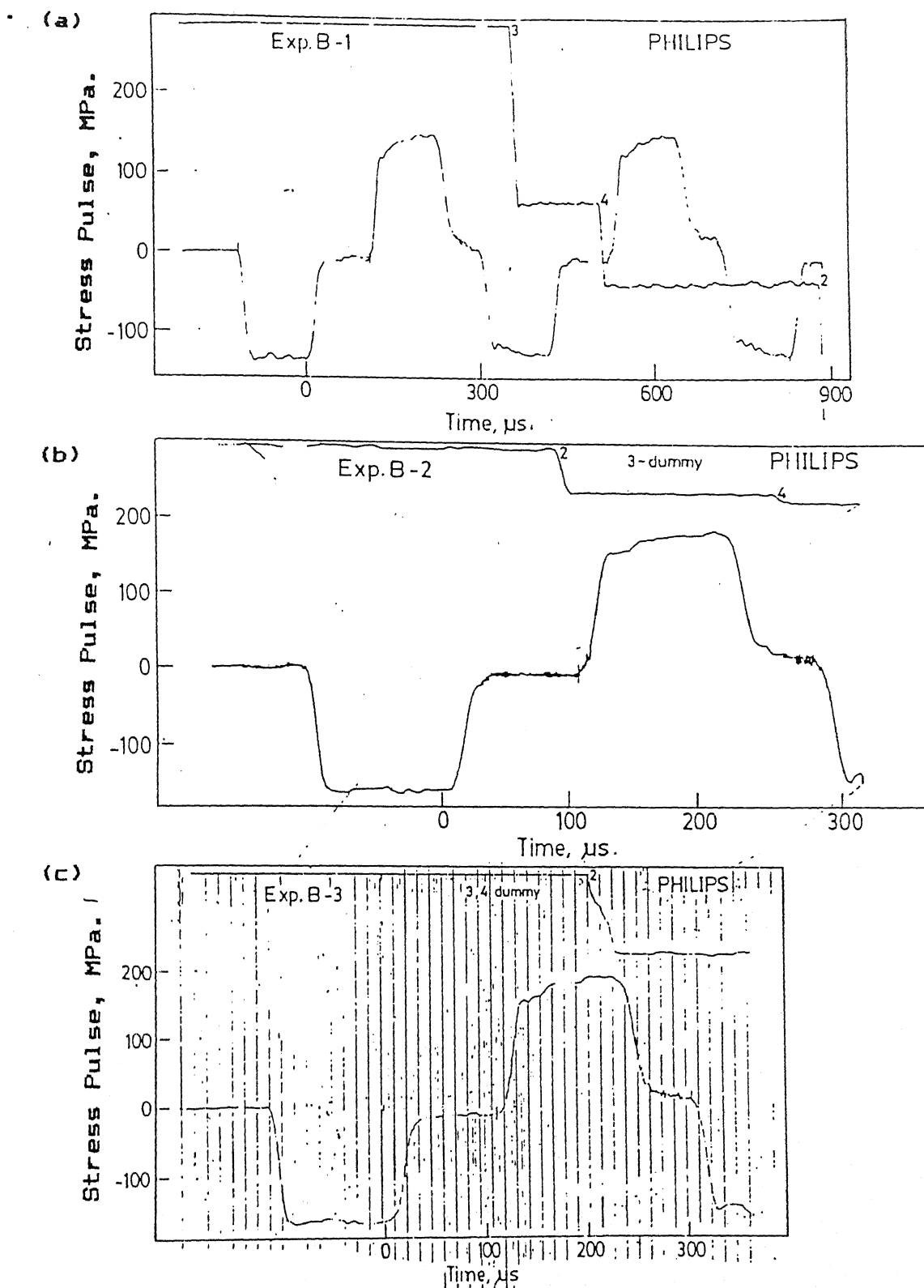
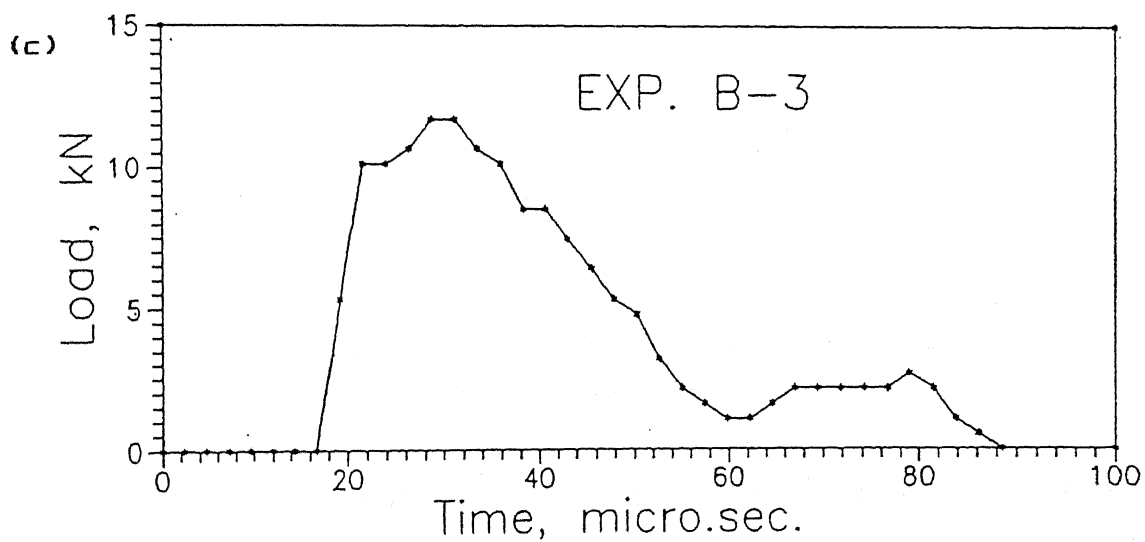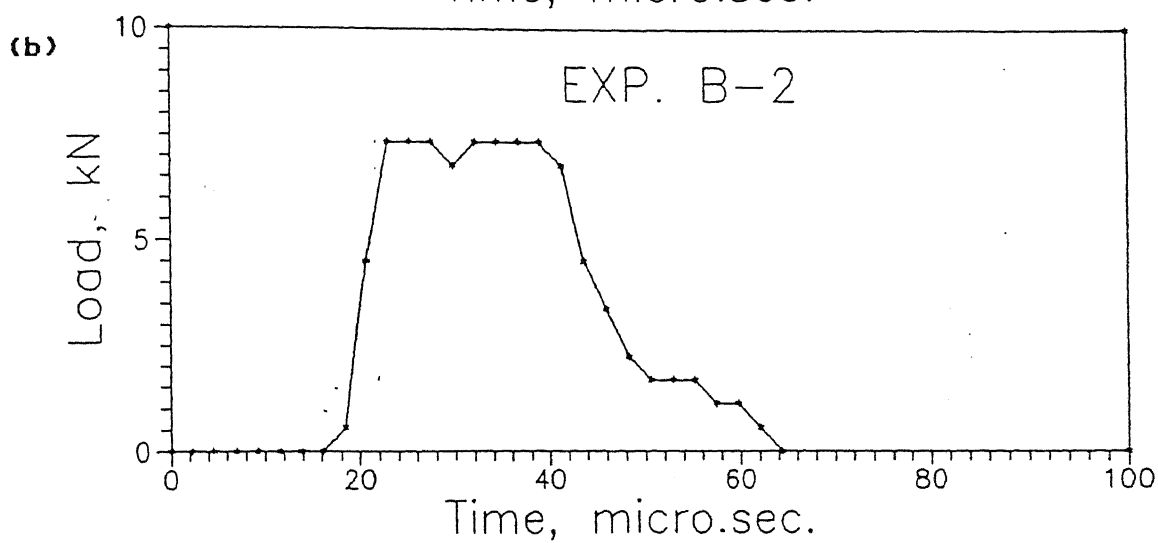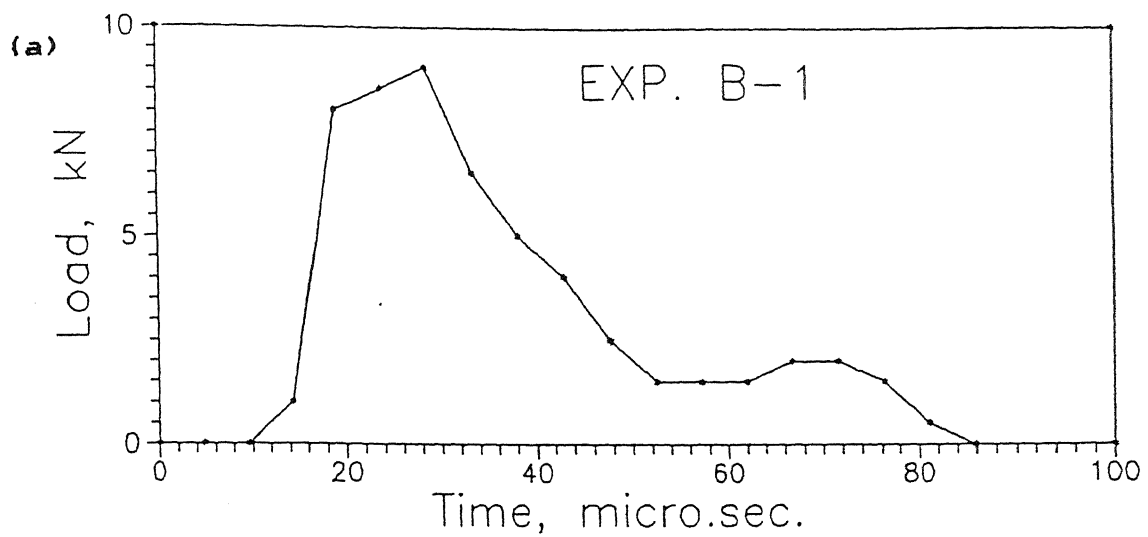FIG. 4.8 – Experimental records of Exp. B-1, B-2 and B-3.

71

FIG. 4.9 — Load pulse imparted to the specimen for Exp. B-1, B-2, and B-3.

72

TABLE 4.6. Magnitude of incident pulse in the load bar and details of load pulse imparted to the specimen for experiments B-1, B-2 and B-3.

EXP. No.	Magnitude of Incident pulse in the Load Bar. (MPa)	Imparted Load pulse.		
		Peak Value (kN)	Duration (μs)	Energy (J)
B-1	134.5	9.0	76.4	0.14
B-2	167	7.4	46.0	0.11
B-3	169	11.7	71.8	0.25

On comparing this set of experiments with the previous experiments it is observed that the breakage duration of the gauges are very large even though the the peak value, duration and energy associated with the imparted load pulse has similar values. It was also observed that the anodized aluminum foil gauges did not bond very well to the specimen. It could be peeled out easily in spite of taking all precautions. Also because of brittleness the anodized foils posed some difficulty in preparing the gauge strips. Because of all these drawbacks the experiments of this category were not very successful and hence were discontinued.

4.4 STEEL DCB SPECIMEN WITH PAPER BACKED ALUMINUM FOIL GAUGES AND LOAD ELEMENT

In all the previous experiments the crack propagation started after 80 μs of starting of loading. This happened probably because the crack propagation was initiated by the load pulses reflected from the ends of the specimen and not directly by the applied flexural wave. To initiate the crack propagation directly by the applied load pulse it was decided to increase the energy associated with the pulse. For this purpose a cylindrical bar was screwed to the specimen cantilever at the load application point as explained in detail in Sec. 3.4.5. Since the anodized aluminum foils did not work very well use of paper backed aluminum foil was resumed.

Experiment C-1 and C-2.

Figure 4.10 shows the experimental record of the incident and reflected pulses in the load bar and the voltage drops corresponding to the shearing of propagation gauges for experiments C-1 and C-2. In experiment C-1 the propagation gauges broke in the proper sequence. But in experiment C-2 there was a change in the order of shearing of propagation gauges . Table 4.7 shows the position and the breakage time of propagation gauges for these experiments. Processing of stress pulses show that the peak value of the imparted load pulse increased by 2 to 5 times and the energy associated with the pulse increased by 10 to 30 times.

TABLE 4.7. Initial crack length, location of propagation gauges and their breakage time for experiments C-1 and C-2.

EXP. No.	Initial Crack Length (mm)	Position of Propagation Gauges from the Load Application Point. (mm)				Breakage Time of Propagation Gauges. (μs)				Crack Initiation Time. (μs)
		1	2	3	4	1	2	3	4	
C-1	38.3	38.4	41.2	44.7	47.7	91.0	117.5	129.0	139.0	90.0
C-2	36.7	39.7	42.4	45.6	48.5	111.0	103.0	114.0	122.0	——

Initial crack length in both these experiments were smaller by 4 to 6 mm as compared to those for all the previous experiments. Also the spacing between the gauge strips was less. This is the reason behind shearing of all four propagation gauges well within 150 μs where as in previous experiments it took about 250 μs or more for the shearing of all the propagation gauges.

Table 4.8 gives the details of the load pulses for experiments C-1 and C-2. The imparted load pulse obtained after processing the experimental records have been shown in Fig. 4.10 along with the plots of experimental record.
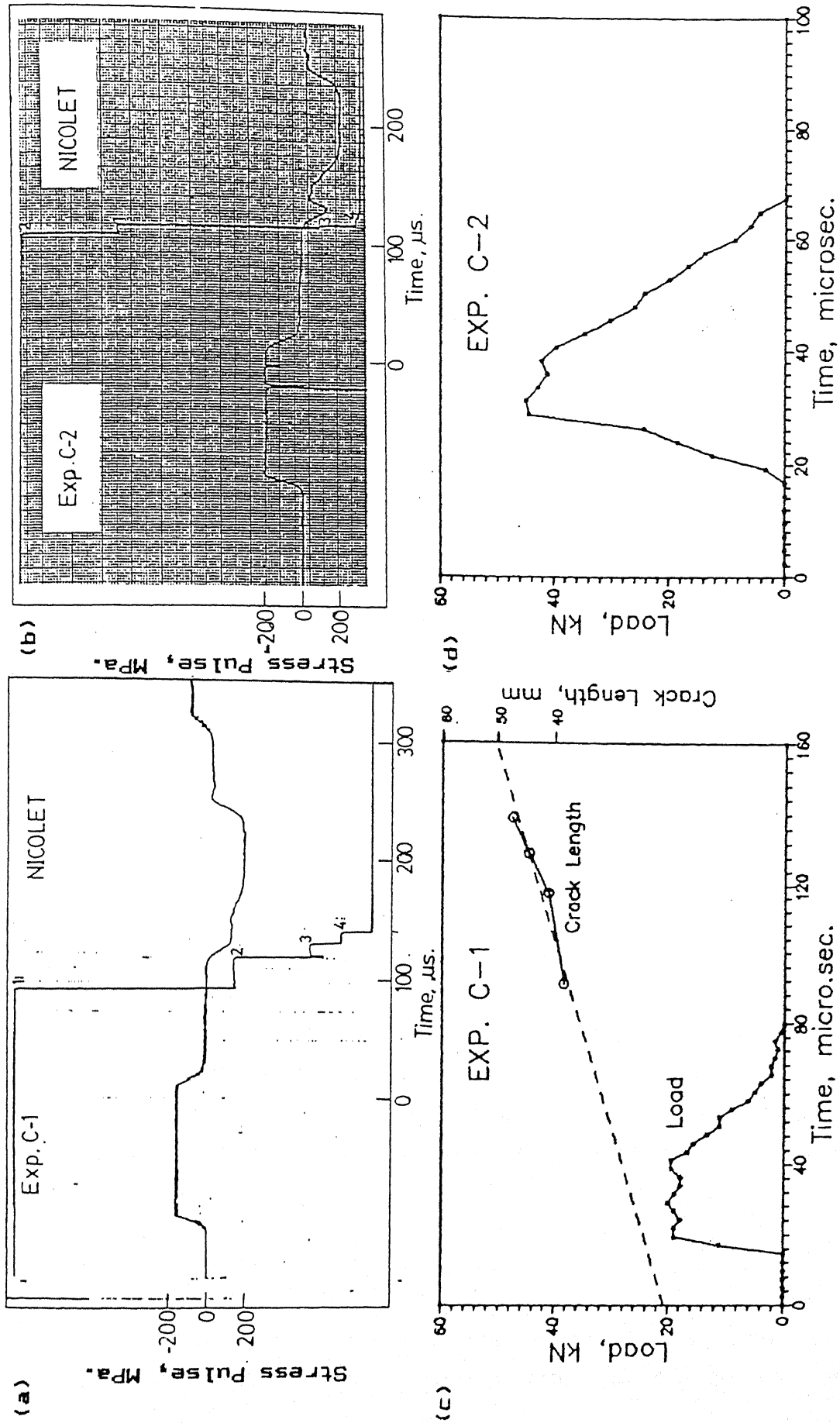
FIG. 4.10 - Experimental records and processed pulses for Exp. C-1 and Exp. C-2.

TABLE 4.8.   Magnitude of incident pulse, details of load pulse imparted to the specimen and the crack velocity for experiments C-1 and C-2.

EXP. No.	Magnitude of Incident pulse in the Load Bar. (MPa)	Imparted Load pulse.			Best Fit Crack Velocity (m/s)
		Peak Value (kN)	Duration (μs)	Energy (J)	
C-1	173	20.0	65.3	1.04	187
C-2	194	45.0	45.0	3.52	——

Crack velocities obtained at the mid-point of gauge strips as explained in Sec. 4.2 is plotted against time and is shown in Fig. 4.11.

It can be observed that although the energy input to the specimen increased many fold the crack initiation time did not have any perceptible change. Also the crack velocity was not very different either. This implies that with this set up also the crack was not initiated directly by the applied flexural wave but probably by the pulses reflected by the ends of the cantilever.

4.5 STEEL DCB SPECIMEN WITH KEVLAR BACKED ALUMINUM FOIL GAUGES AND LOAD ELEMENT

Another attempt was made to replace the paper backing of the gauge foils. The paper backing of the gauge foil was replaced Kevlar fibers aligned along the crack (Sec. 3.5.1). The load element i.e. the cylindrical bar attached to the specimen at the load application point was retained as it helped in increasing the energy input to the specimen cantilever. Following experiment was done in this category.

Experiment D-1.

Figure 4.12a shows the experimental record of stress pulses in the load bar and the voltage drops corresponding to the shearing of

Jropagation gauges. All four gauges were recorded to shear in the proper sequence. Position of all the propagation gauges, their breakage time and the initial crack length are given in Table 4.9.

TABLE 4.9. Initial crack length, location of propagation gauges and their breakage time for experiment D-1.

EXP. No.	Initial Crack Length (mm)	Position of Propagation Gauges from the Load Application Point. (mm)				Breakage Time of Propagation Gauges. (μs)				Crack Initiation Time. (μs)
		1	2	3	4	1	2	3	4	
D-1	40.0	41.8	44.6	47.0	50.7	112.0	117.0	148.0	173.0	93.8

In this experiment also since the crack propagation started very late it would not have started due to loading at the crack tip directly by the flexural wave but by the pulses reflected from the ends of the specimen. Experimental records were processed for the imparted load pulse and crack velocity and is shown in Fig. 4.12b. Table 4.10 gives the magnitude of incident pulse, details of the imparted load pulse and best fit crack velocity.

TABLE 4.10. Magnitude of incident pulse, details of load pulse imparted to the specimen and the crack velocity for experiment D-1.

EXP. No.	Magnitude of Incident pulse in the Load Bar. (MPa)	Imparted Load pulse.			Best Fit Crack Velocity (m/s)
		Peak Value (kN)	Duration (μs)	Energy (J)	
D-1	153	29.6	45.9	1.15	137

Crack velocities obtained at the mid-point of gauge strips has been plotted against time and is shown in Fig. 4.11.
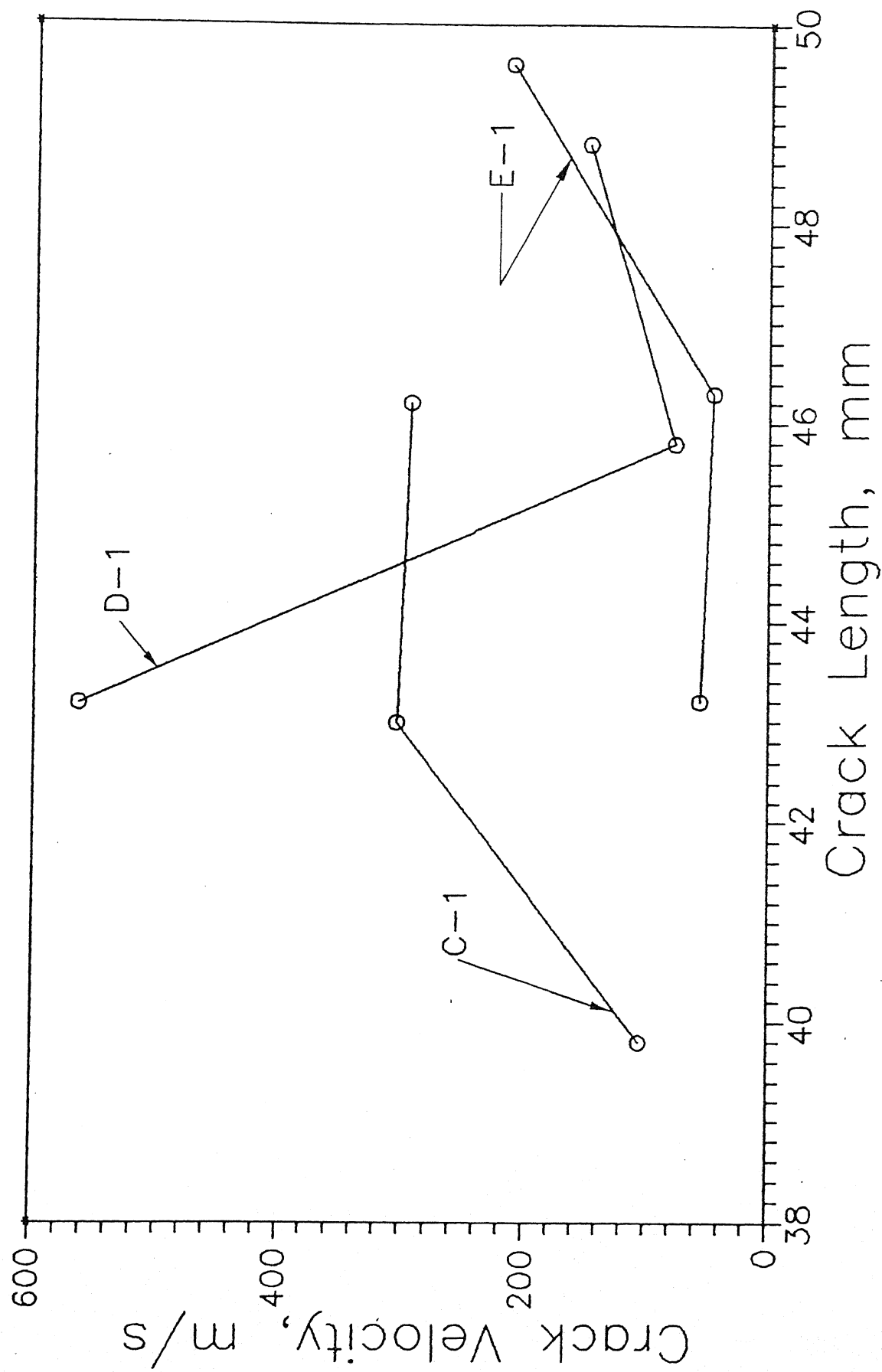
FIG. 4.11 - Crack velocity at the mid-point of propagation gauges vs.
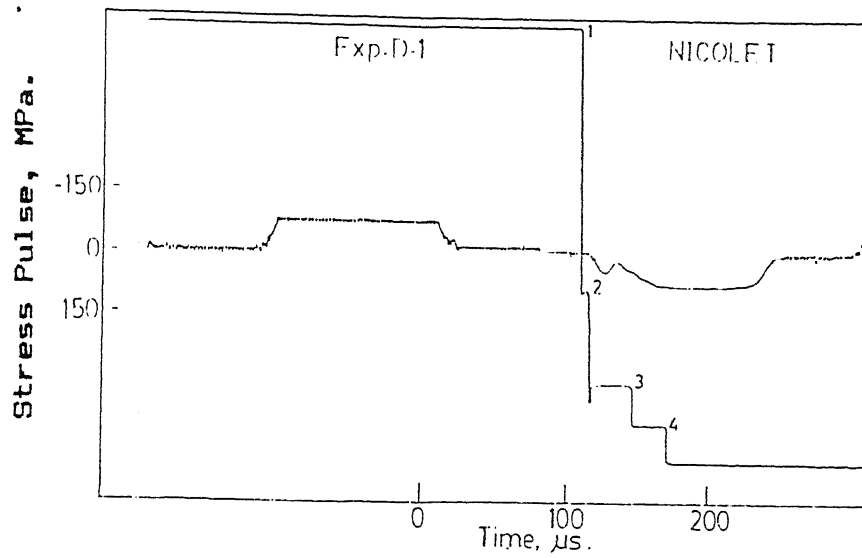crack length plot for Exp. C-1, D-1 and E-1.

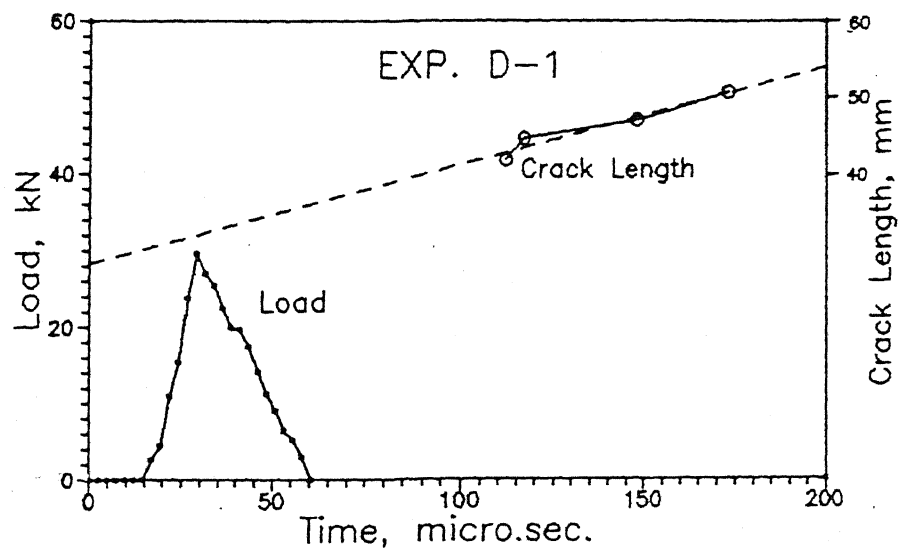FIG. 4.12a - Experimental records of Exp. D-1.

FIG. 4.12b - Load pulse imparted to the specimen and crack length vs. time plot for Exp. D-1.

4.6 DCB SPECIMEN OF GFRP WITH ALUMINUM
FOIL GAUGE AND LOAD ELEMENT

One experiment was conducted using glass fiber reinforced plastic (GFRP) specimen instead of steel DCB specimen. Unidirectional glass fibers were used to reinforce the plastic. Orientation of fiber layers is given in Sec. 3.2.2.

Since GFRP is electrically nonconductive its use as the specimen eliminated the need of any insulating layer between the propagation gauge strips and the DCB specimen. Aluminum foil gauges were directly bonded to the side face of the specimen. Thus any uncertainty regarding shearing of gauges due to the use of a insulating layer was eliminated. Results of this experiment are as follows.

Experiment E-1.

Figure 4.13a shows the experimental record of incident and reflected stress pulses in the load bar and the voltage drops corresponding to the shearing of propagation gauges. All the gauges sheared in the same order in which they were bonded. The experimental records were processed to get load pulse imparted to the specimen, the crack propagation rate and the crack initiation time. The imparted load pulse and the crack length plotted against time are shown in Fig. 4.13b. Table 4.11 gives the initial crack length, propagation gauge position from the load application point and time of their shearing. The crack velocities, for experiment E-2, obtained at the mid-point of the gauge strips are plotted against the crack length and is shown in Fig. 4.11 along with the crack velocity plots for experiments C-1 and D-1.
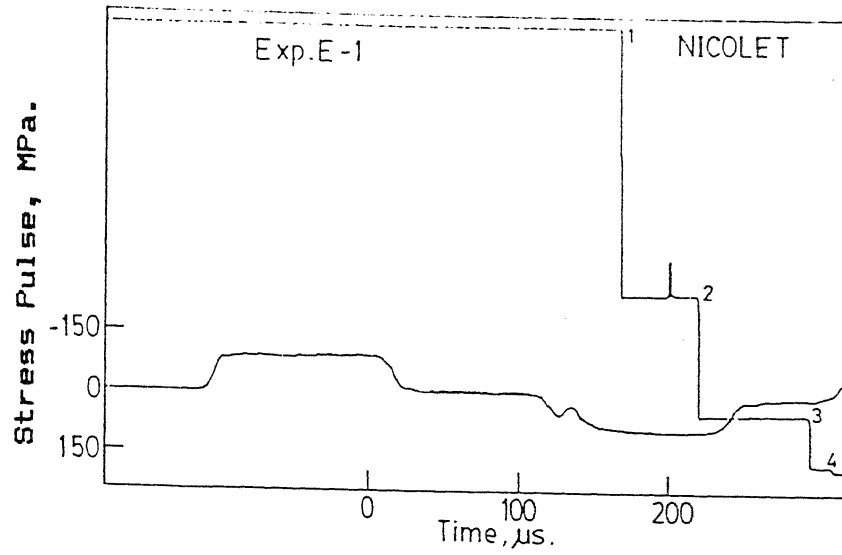
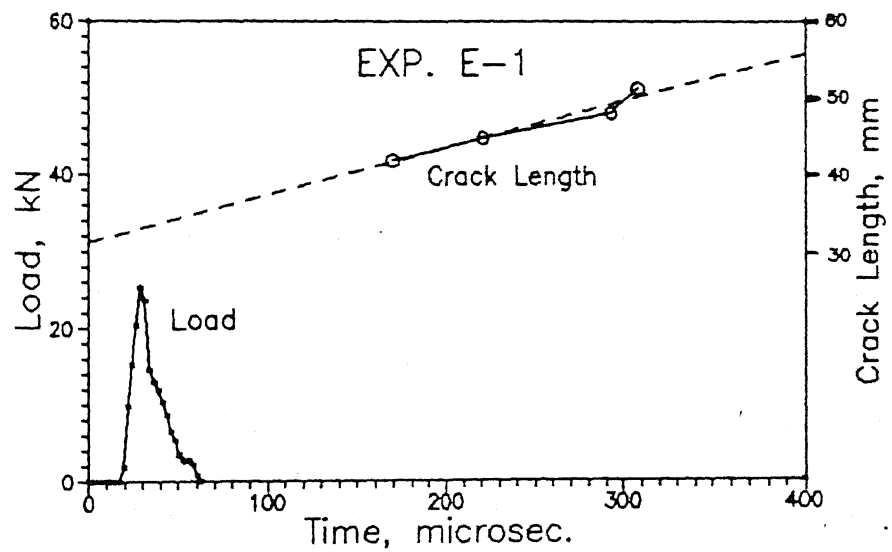FIG. 4.13a - Experimental records of Exp. E-1.

FIG. 4.13b - Load pulse imparted to the specimen and crack length vs. time plot for Exp. E-1.

TABLE 4.11. Initial crack length, location of propagation gauges and their breakage time for experiment E-1.

EXP. No.	Initial Crack Length (mm)	Position of Propagation Gauges from the Load Application Point. (mm)				Breakage Time of Propagation Gauges. (μs)				Crack Initiation Time. (μs)
		1	2	3	4	1	2	3	4	
E-1	39.6	41.8	44.7	48.0	51.2	169.0	220.5	292.5	307.5	142.0

The shearing of all four propagation gauges took more than 300 μs even though the position and spacing of propagation gauges is similar as those for experiments C-1 and D-1. Approximate crack initiation time, obtained from the first order best fit of the crack length vs. time plot, is also about 140 μs which is very late as compared to those for experiment C-1 and D-1. Table 4.12 gives the magnitude of incident pulse, details of imparted load pulse and the best fit crack velocity.

TABLE 4.12. Magnitude of incident pulse, details of load pulse imparted to the specimen and the crack velocity for experiment E-1.

EXP. No.	Magnitude of Incident pulse in the Load Bar. (MPa)	Imparted Load pulse.			Best Fit Crack Velocity (m/s)
		Peak Value (kN)	Duration (μs)	Energy (J)	
E-1	183	25.2	45.8	0.60	64.7

It can be observed that the crack in GFRP propagated with a slower velocity as compared to that with steel specimen. Fig. 4.11 shows that the crack velocity is very low at the beginning and then rises sharply. Hear too the crack propagation was probably initiated by the pulses reflected from the ends of the specimen.

4.7 EXPERIMENTS WITH STRAIN GAUGES BONDED
TO THE SPECIMEN.

Propagation gauge, used to obtain the Crack velocity in a DCB specimen for a specific load pulse applied to the specimen, is a mechanical device. The gauges may take finite time to shear. Experiments with strain gauges were done to find out the time when the stress pulse reaches a point slightly beyond the crack tip.

Two experiments were done with the strain gauges. In both the experiments GFRP specimen were used. Glass fiber fabric was used to reinforce the plastic. The gauges were bonded to the DCB specimen slightly beyond the crack tip. In the first experiment only one strain gauge and in the second experiment two strain gauges were used.

4.7.1 Experiment with One Strain Gauge.

One experiment was done on a DCB specimen of GFRP with a strain gauge bonded on its surface at location 3.8 mm from the crack tip (Fig 4.14). This strain gauge was used only to get the shape of the stress pulse beyond the crack tip and hence not calibrated. Fig 4.15 shows the experimental record of the incident and the reflected pulses in the load bar (Trace A) and the stress pulse recorded by the strain gauge bonded to the specimen (Trace B).

From the experimental record it can be seen that a stress pulse reaches the strain gauge location 36 μs after application of the load. This pulse has a duration of 108 μs. The nature of the stress pulse (tensile or compressive) is not known, as the strain gauge was not calibrated. This pulse was chopped at the top due to flaw developed in the Nicolet oscilloscope. This pulse reverses its nature of curvature after 108 μs.

From this experiment it can be inferred that the load pules starts loading the the crack tip within expected time. But probably the propagation is not directly started by this pulse, but by the pulses
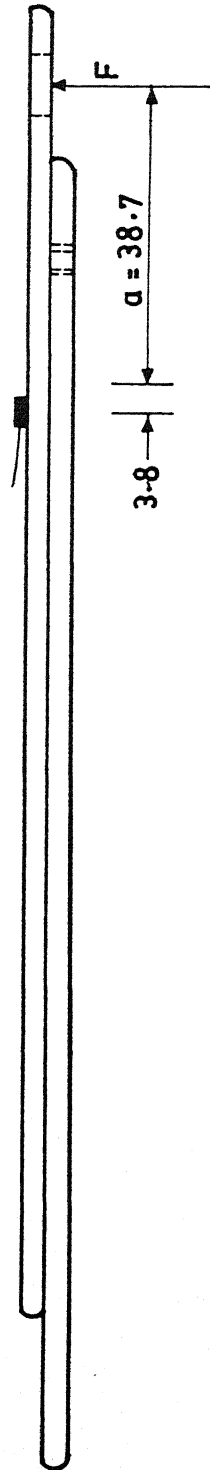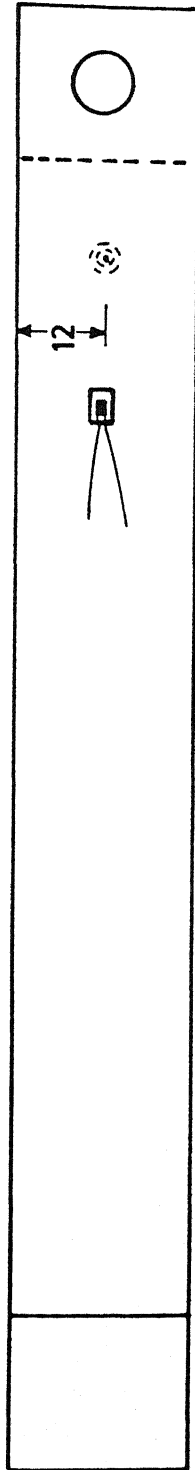
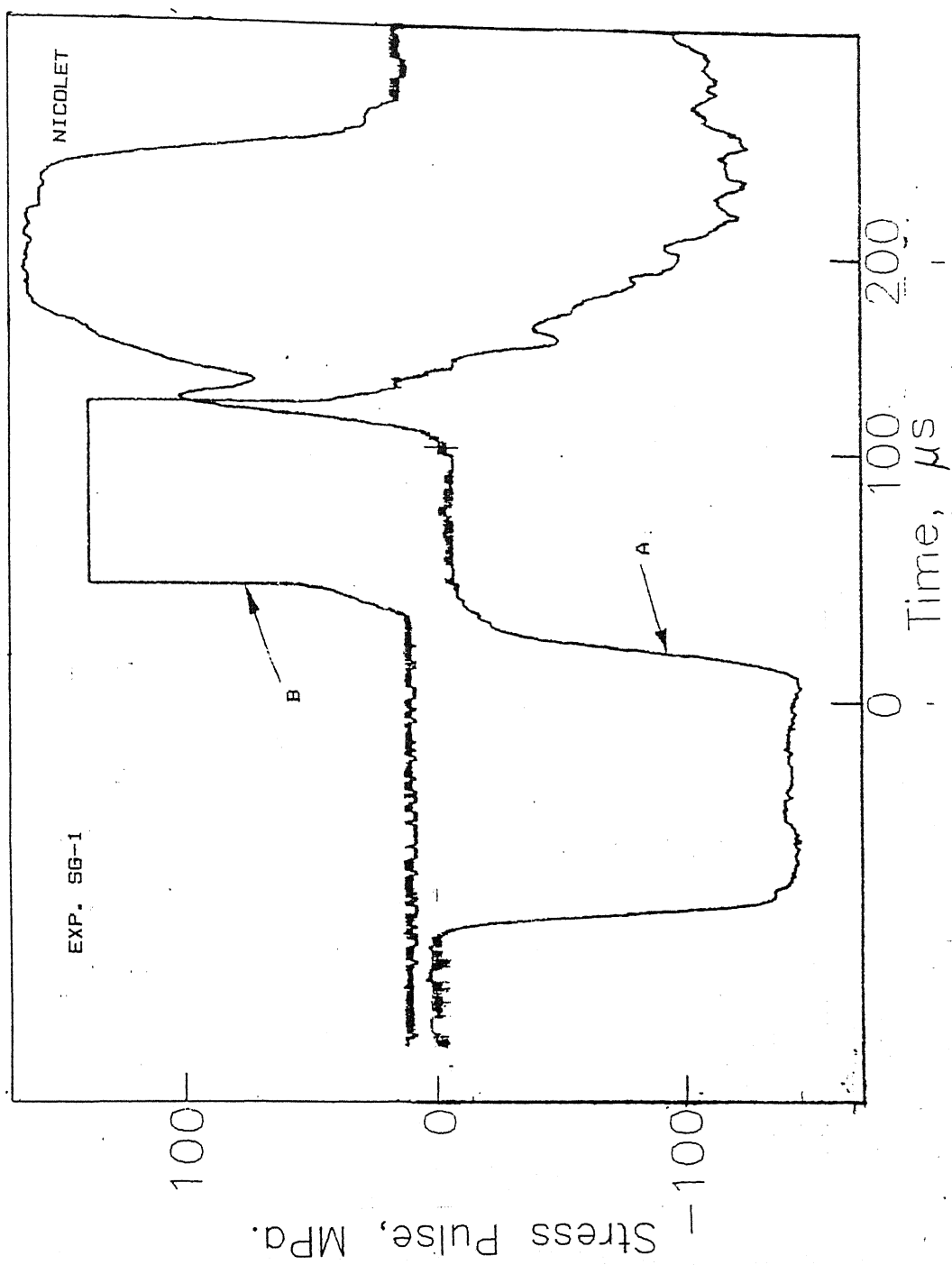FIG. 4.14 LOCATION OF STRAIN GAUGE IN EXP. SG—1

FIG. 4.15 STRESS PULSE AND STRAIN GAUGE RECORD FOR EXP. SG-1

reflected from the ends of the specimen.

4.7.2 Experiment with Two Strain Gauges

In this experiment two strain gauges were used. Fig. 4.16 shows the location of the strain gauges. These gauges are bonded near the location of propagation gauges. The spacing between two gauges was 1.3 mm. Both these gauges were calibrated to give magnitude and nature of the strain recorded. This experiment was conducted to know the nature of the pulse and the speed with which it moves beyond the crack tip. Since there were only two channels on the oscilloscope the pulses in the load bar were not recorded. Fig. 4.17 shows the experimental record of the pulses picked by the strain gauges bonded to the specimen. Trace A corresponds to the pulse recorded by the gauge nearer to the pre-crack tip and trace B is the pulse recorded by the later gauge.

Both the strain gauges first recorded a tensile strain on the surface of the specimen. Both the pulses have a duration of about 100 μs. It can be noted that the starting time and the peak time of both the pulses coincide with each other. Thus the pulse velocity could not be measured. Since the time interval between two points on the oscilloscope is 0.5 μs and the spacing between two strain gauges is 1.3 mm, it can be inferred that the speed of the pulse is more than 2 600 m/s. This is too large a speed for any crack. After about 100 μs the tensile strain on the surface of the specimen reverses into a compressive strain.

4.8 CONCLUSION

In the experiments done on steel DCB specimen without using the load element the crack initiation time ranged from about 85 μs to 200 μs. In two experiments on steel DCB with the load element attached to them the crack initiation time was 90 μs and 93.8 μs. In GFRP specimen with the load element the crack initiation time was 142 μs.

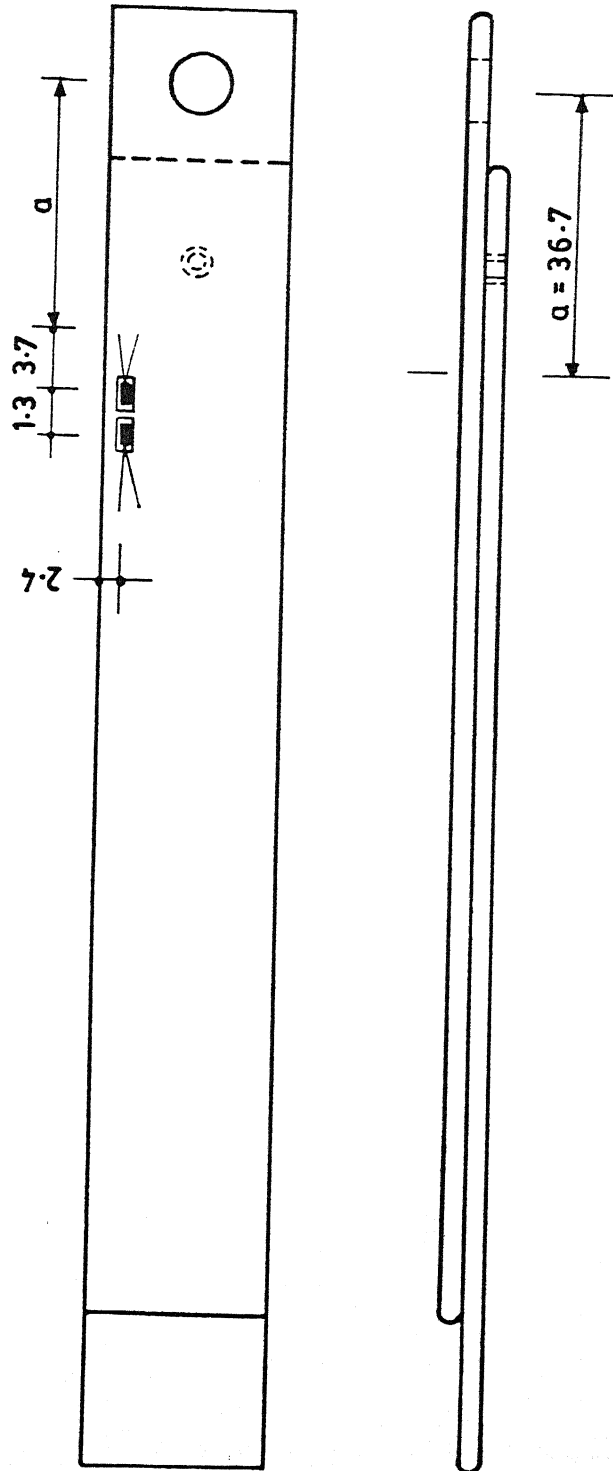The numerical program predicts the crack initiation time to be

FIG. 4.16 LOCATION OF STRAIN GAUGES IN EXP. SG-2
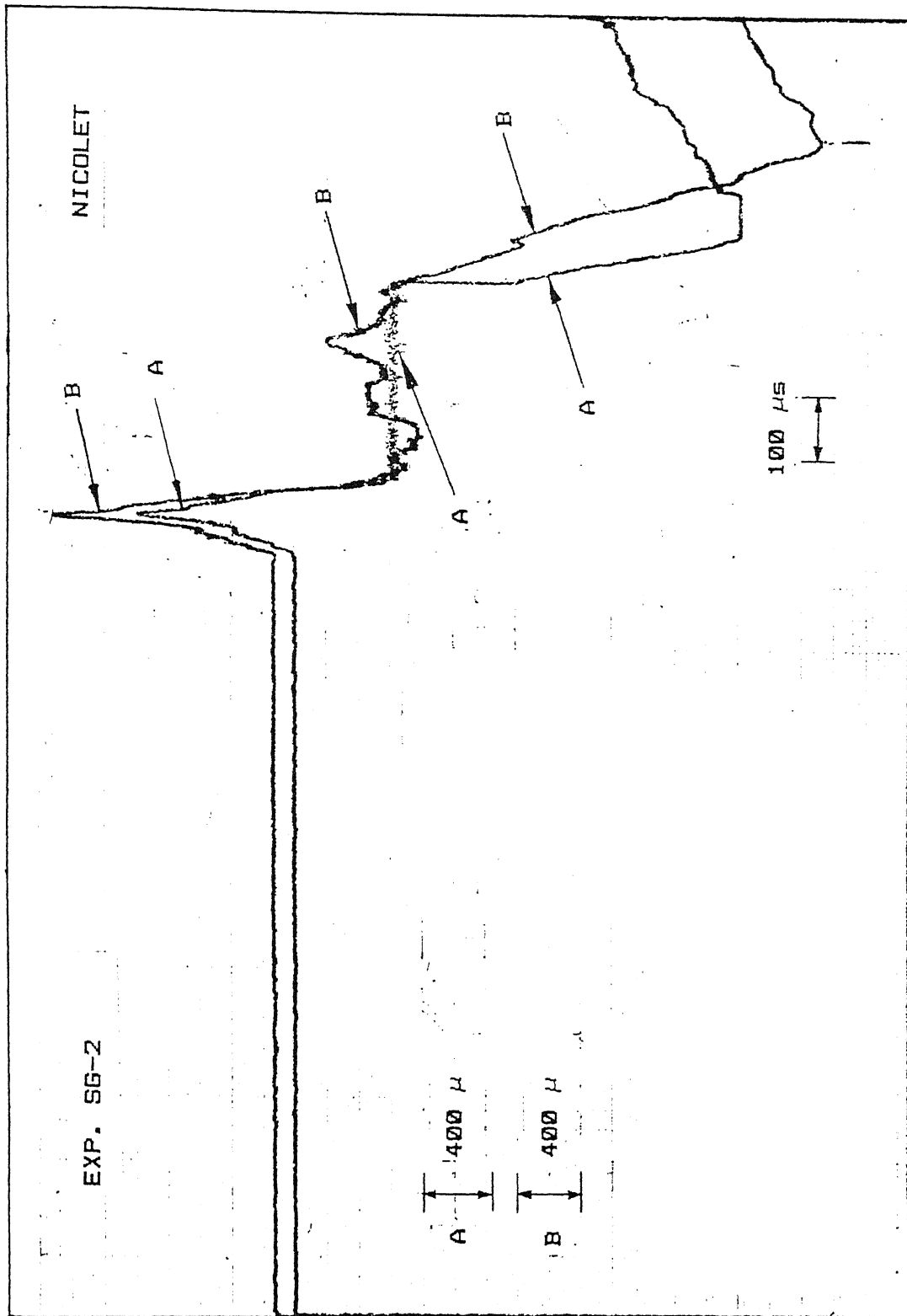
FIG. 4.17 STRAIN GAUGE RECORD FOR EXP. SG-2

within 30 μs. Thus the crack initiation time is much larger the
the expected value. It can be noted that in the experiments wit
the load element the range of crack initiation time was on the lowe
side of that for the experiments without the load element. It i
also known that the attachment of the load element to the specime
increases the energy imparted to the specimen. From this it can b
inferred that if the energy associated with the load pulse imparted
to the specimen is increased the crack initiation time can be
reduced. For further investigation it is therefore suggested that
the rear cantilever of the DCB specimen is screwed directly to the
load bar. This will increase the energy of the load pulse imparted
to the specimen by a much larger factor. Also it is suggested that
experiments should be conducted with the strain gauge(s) bonded at
the side face of the rear cantilever and near the crack tip so that
the stress field just near the crack tip can be monitored.

5 CONCLUSION AND SUGGESTIONS FOR FUTURE WORK

A technique has been developed to determine the dynamic interlamina
fracture toughness for slender laminates. This technique employs
combined experimental and numerical work. The aim of the presen
work has been to experimentally determine the crack velocity and th
corresponding dynamic load pulse applied to a slender DCB specime
for interlaminar crack propagation. These experimental data can b
used as input by the finite element code to obtain the dynami
interlaminar fracture toughness parameter for slender laminates.

Two kinds of DCB specimen are used. One is made by bonding two thir
strips of hardened alloy steel with epoxy and the other DCB specimer
is made of glass fiber reinforced plastic (GFRP). Most of the
experiments were conducted with steel DCB specimen.

A load bar technique has been developed to apply a dynamic load
pulse to one of the cantilevers of the DCB specimen. In this
technique a striker bar, accelerated in an air gun, impacts one end
of a long circular load bar which in is partially imparted to one of
the cantilevers of the specimen. The stress pulses in the load bar
are monitored by strain gauges. A few experiments were also
conducted wherein a small cylindrical bar was screwed to the
impacted cantilever at the load application point to increase the
energy input to the specimen.

Propagation gauges used to monitor the crack velocity consist of
four thin strips of aluminum foil which are bonded to the side face
of the DCB specimen. The position of each gauge strip is recorded
carefully. When the crack advances and passes under a gauge strip
it shears off. The time of the shearing of each gauge strip is
recorded on the oscilloscope as voltage drop with the help of an
electronic circuit unit. By knowing the position of each gauge
strip and the time of their shearing the crack velocity is obtained.

The load pulse imparted to the specimen has a duration of 40 to 60

μs and a peak value of 6 to 30 kN. The crack velocity achieved i
very high ranging from 100 to 600 m/s. However in some experiment
there is a change in the order of the shearing of the gauges i.e
the gauge nearer to the crack tip sheared after that of a gaug
farther from the crack tip.

The finite element analysis predicts that the load pulse takes abou
15 to 20 μs to reach the crack tip. It is thus expected that th
crack growth should initiate within 30 μs of the application of th
load pulse.   But the crack initiation time obtained fro
experimental data ranges from 80 to 150 μs. This late initiation o
the crack could not be fully understood. A plausible reason fo
this delay might be that the crack propagation is not directl
initiated by the applied direct load pulse but by the pulse
reflected from the ends of the cantilever. Other reason might be a
time lag in the shearing of propagation gauges.

For future continuation of the work following steps may be taken
into account.

    (i)   Experiments should be conducted by replacing the
            propagation gauges with strain gauges to monitor the
            flexural pulses beyond the crack tip.

    (ii)   High speed recording system can be used to monitor the
            crack propagation. With the help of high speed recording
            system 10 to 20 exposures within a short time interval
            (20 to 40 μs)can be taken, thus a better crack velocity
            distribution and reliable crack initiation time can be
            obtained.

REFERENCES

[1] P. Davies, C. Maulin, H. H. Kausch and M. Fisher, Measuremer of G_{IC} and G_{IIC} in carbon/epoxy composite, Composite Scienc and technology, 39, pp. 193-205 (1990)

[2] A. Shukla, B. D. Agarwal and B. Bhushan, Determination o stress intensity factor in orthtropic composite materials usin strain gauges, Engineering Fracture Mechanics, 32, pp. 469-47: (1989)

[3] K.Ravi Chander and W.G.Knauss, Dynamic crack tip stress under stress wave loading - a comparison of theory and experiment, Int. J. of Fracture, 20, pp. 209-222 (1982).

[4] K.Ravi Chander and W.G.Knauss, An experimental investigationinto dynamic fracture : mode I Crack initiation and arrest, Int. J. of Fracture, 25, pp. 247-262 (1984).

[5] K.Ravi Chander and W.G.Knauss, An experimental investigation into dynamic fracture : II Microstructural aspect, Int. J. of Fracture, 26, pp. 65-80 (1984).

[6] K.Ravi Chander and W.G.Knauss, An experimental investigation into dynamic fracture : III On steady state crack propagation and crack branching, Int. J. of Fracture, 26, pp. 141-154 (1984).

[7] K.Ravi Chander and W.G.Knauss, An experimental investigation into dynamic fracture : IV On the interaction of stress waves with propagating cracks, Int. J. of Fracture, 26, pp. 180-200 (1984).

[8] A. J. Rosakis, J. Duffy & L. B. Freund, The Determination of Dynamic Fracture Toughness of AISI, 4340 steel by the shadow spot method, *Journal of Phys. solids, Vol. 32, No. 4 (1984), pp*

443-60

[9]. A. Shukla, B. D. Agarwal & bharat Bhushan, Determination of Stress Intensity Factor in Orthotropic Composite Materials using strain gauges, *Engineering Fracture Mechanics, Vol. 32, No. 3, (1989), pp 469-77*

[10] G.Ravichandran and R.J.Clifton, Dynamic fracture under plane wave loading, Int. J. of Fracture, 40, pp. 157-201 (1989).

[11] J. R. Berger & J. M. Dally, A Spacially Overdetermined Analysis for Propagation Poughness Using Strain Gauges, *Mechanical Research Communications, Vol 17 (2), pp 93-9*

[12] T. Nishioka, T. Murakami, H. Uchiyama, K. Sakakura & H. Kittaka, Specimen Size Effects on Dynamic Crack Propagation and Arrest in DCB Specimens, *Engineering Fracture Mechanics, Vol 39, No. 4 (1991), pp 757-767*

[13] O. Kolenik, On the Physical Meaning of the J-Δa Curves,*Engineering Fracture Mechanics, Vol 38, No. 6 (1991), pp 403-412*

[14] Kesavan Potty P.K., M. Tech. thesis (1992), Mechanical Engg. Dept. IIT Kanpur.

[15] Lovi Raj Gupta, M. Tech. thesis (1993), Mechanical Engg. Dept. IIT Kanpur.

[16] N. N. Kishore, Prashant Kumar and Sanjay Verma, Numerical methods in dynamic fracture, Journal of The Aeronautical Society of India, Vol. 44, No. 4, pp. 323 to 333.

[17] Klauss-jurgen Bathe, Finite element procedure in engineering analysis, Prentice Hall of India, 1990.

[18] K. M. A. Jaleel, N. N. Kishore and V. Sunderarajan, Finite element simulation of elastic wave propagation in orthtropic composite materials, Material Evaluation, pp.830-838 (1993).

[19] A.S. Kobayashi and W.W. King, Fast fracture simulated by finite element analysis which accounts for crack tip energy dissipations, Numerical Methods in Fracture Mechanics, Eds. A.R. Luxmoore and D.R.J. Owen (Univ. College, Swansea), pp. 648-659 (1978).

[20] G. Rydhom, B. fredriksson and F. Nilsson, Numerical investigation of rapid crack propagation. Numerical Methods in Fracture Mechanics, Eds. A.R. Luxmoore and D.R.J. Owen (Univ. College, Swansea), pp. 660-672 (1978)

[21] A.S. Kobayashi, S. Mall, Y. Urabe and A.F. Emery, A numerical dynamic fracture analysis of three wedge load DCB specimen, Numerical Methods in Fracture Mechanics, Eds. A.R. Luxmoore and D.R.J. Owen (Univ. College, Swansea), pp. 673-684 (1978).

[22] Satya N. Atluri, Path independent integrals in finite elasticity and inelasticity with body forces, inertia and arbitrary crack face conditions, Engg. Fracture Mechanics, 16, No.3, pp. 341-364 (1982).

[23] T. Nishioka and S.N.Atluri, Path independent integrals, energy release rates and general solutions of near tip fields in mixed mode dynamic fracture mechanics, Engg. Fracture Mechanics, 18, No.1, pp. 1-22 (1983).

[24] K. Kishimoto, S. Aoki and M. Sakata, On the path independent integral $- \hat{J}$, Engg. Fracture Mechanics, 13, pp. 841-850 (1980).

[25] M.F. Kanninen C.H. Ppelar, Advanced Fracture Mechanics, Oxford University press, New York, 1985.

1994 - M - RAY - EXP